Doctoral Dissertation (Shinshu University)

Research on development of smart nanocomposites with shape memory and piezoelectric effects

September 2018

CHEN　HAIRONG

CONTENTS

Abstract

Piezoelectric materials and shape memory materials are the two classes of smart materials widely used in different fields such as aerospace, medical care, automobile and daily necessities. Over recent decades, their composites extra attract many researchers' attentions because the material performances are able to be remarkably improved by combining fillers and matrices, and the synthesis and applications of the composites have made great progress. However, the composites just have only one kind of smart effect, piezoelectricity or shape memory property. Here, we introduce a group of smart composites consisting of lead zirconate titanate (PZT) particles with the average diameters of 400 nm and shape memory polyurethane (SMPU) matrices, aiming to combine piezoelectric effect and shape memory effect into one composite. The resultant composites, PZT / SMPU composites, are prepared by the solution blending method, and three kinds of these composites, PZT 60% (%), PZT 70% (%) and PZT 80% (%), succeed in obtaining both the two smart effects. The above three composites all show recovery rates of above 94% in the third cycle. Compared with the pristine SMPU, PZT / SMPU composites show that the maximum recovery stresses are enhanced by at least 133%, elastic moduli are improved to more than 166% and yield stresses are increased by no less than 32%. Besides, the strong potential in nanopositioning is revealed by the results of nanoscale displacement measurements under step voltages because the displacements

with 1 nm resolution can be achieved in a common laboratory without any control of the environmental parameters. Taking the advantage of shape memory effect makes the film actuators made of PZT / SMPU composites easy to be deformed into a variety of designed shapes. As a consequence, the shaped actuators are capable of generating much more displacements which is several times, even dozens of times, more than that of the corresponding unshaped film actuators, while the positioning errors remain the same (still within ± 5 nm). This promising merit partly profits from the softness of SMPU matrices which, to some extent, could protect PZT particles from ambient noise. Thus, PZT / SMPU composites have the ability to output displacements with the positioning errors within ± 5 nm without the requirement for a controlled environment. This ability implies the possibility of reducing the costs of nanopositioning and, even, nanomachining and nanofabrication.

Although a large number of shape memory composites (SMCs) are reported, the variations in recovery rates of SMCs induced by fillers are also discovered and several simples reasons for the variations of recovery rates are also given, a thorough analysis, so far, has not been presented yet. To understand the essence of shape memory behaviors of SMCs, the molecular mechanism of SMCs is proposed on the basis of that of shape memory polymers (SMPs) by identifying the differences lying in the molecular motions of SMPs and SMCs. The analysis on molecular motions in consideration of the motions of fillers discloses the positive and negative effect of fillers on recovery rates and the decisive role of interfaces between fillers and matrices in the above two effects. Besides

PZT / SMPU composites, another group of SMCs, TiO_2 / SMPU composites, are tested likewise to make our conclusions more general. For directly verifying the role of interfaces, the recovery rates of SMCs with good interfaces are compared with that of SMCs with poor interfaces. The experimental results prove that interfaces are both benefit and harmful for recovery rates at the same time. Besides, the limit of programming ability of SMPs and SMCs are experimentally demonstrated too. Some conclusions on the relations between recovery rates and interfaces are given, and then are applied to explain the changes in recovery rates of other reported SMCs. Moreover, the conclusions are able to qualitatively predict the recovery rates of SMCs with more fillers or less fillers.

Besides recovery rates, the influences of interfaces on piezoelectric effect and relative permittivity are analyzed as well. As a result, PZT / SMPU composites with poor interfaces exhibit lower relative permittivity because of the existence of the free spaces between piezoelectric fillers and SMPU matrices, and the piezoelectric effect is critically dependent on whether the interfaces are good or poor. The experimental results testify that PZT / SMPU composites with poor interfaces are unable to produce any displacement. This inability of producing displacements could be explained by the microscopic mechanism for actuation behaviors of PZT / SMPU composites. Moreover, PZT fillers exhibit effective improvement in storage moduli, but very little effect on the glass transition temperature.

Interdigitated electrodes are made on the surfaces of PZT / SMPU composites to

utilize the piezoelectric effect along the longitudinal direction. PZT / SMPU composites with interdigitated electrodes demonstrate the ability to generate bending displacements and harvest energy from external vibrations. The experimental results of energy harvesting show that PZT / SMPU composites can produce electric voltages continuously which imply the potential for powering electric devices sustainably.

Finally, silver nano particles are added into PZT / SMPU composites and the resulting composites, Ag / PZT / SMPU composites, show an increase in piezoelectric charge constants. The values of piezoelectric constant of Ag / PZT / SMPU composites are at least twice as many as those of PZT / SMPU composites.

Chapter 1

General introduction

Chapter 1: General introduction

1.1. Shape memory materials

The phase transition resulting in shape memory effect was first observed in cadmium-gold (Cd-Au) alloys in 1938 [1]. However, the shape memory materials has not drawn the attentions of researchers until the shape memory effect of a nickel-titanium (Ni-Ti) alloy is reported [2,3]. Shape memory materials include shape memory alloys (SMAs), shape memory polymers (SMPs), shape memory ceramics and shape memory gels [4]. The shape memory effect is the ability to recover to the original shape from deformation by an external stimulus, so shape memory materials seem to "remember" or "memorize "their original shapes [5-7]. After the development in recent decades, the shape memory effect has been developed from the classical one-way shape memory effect to two-way shape memory effect, and dual shape memory materials have been improved to triple shape memory materials and even multiple shape memory materials [6, 8]. The one-way thermal shape memory materials retain a deformed state after the removal of an external force, and then recover to their original shapes upon heating; the two-way thermal shape memory materials can remember their shapes at both high and low temperatures [9,10]. SMAs and SMPs are the most famous two classes of shape memory materials.

1.1.1. Shape memory alloys

SMAs are capable of regaining their original shape after deformation via heating because of a reversible diffusionless transformation between the starting austenite and post-deformation martensite phases, which occurs at the transformation temperature [11, 12]. Over the past decades, a large number of SMAs have been reported, for instance, Ag-Cd, Cu-Al-N, Cu-Sn, Ni-Al, Fe-Pd, Mn-Cu and Fe-Mn-Si [13]. Because of high recovery stresses, high power density, solid state actuation, high damping capacity, durability and fatigue resistance, SMAs have been applied in many fields, such as aerospace engineering, civil engineering, medical care, micro-electromechanical systems and other applications [14-18]. In the most of applications, SMAs are used as actuators, but the development of SMA actuator devices has exhibited that the transformation to occur repeatedly in every actuation cycle would lead to the gradual accumulation of defects and the transformation temperatures, stresses and strains subsequently decline [11]. However, Christoph Chluba and co-workers succeed in an ultralow-fatigue shape memory alloy (TiNiCu) which allows at least 10 million transformation cycles without any change in load and strain [19].

1.1.2. Shape memory polymers

Before the item of "shape memory polymer" came up, the heat shrinkable ability of polyethylene was discovered in 1960s [20]. Then a lot works have been done and a variety of polymers with shape memory effect have been reported, like

polyurethane-based SMPs [21] and epoxy-based SMPs [22]. Because SMAs have obvious disadvantages, high manufacturing cost, limited recoverable deformation and appreciable toxicity, SMPs, up to now, have attracted much attention on account of the light weight, easy processing, low costs, good biodegradability and large deformation [23]. Because of the above advantages, SMPs have been widely utilized in many areas, as an example, biomedicine [24], damage self-healing [25], smart textiles [26], automobiles [27] and aerospace [28]. Thus, an increasing number of international researchers have focused on the development of SMPs.

Generally, SMPs consist of two phases, cross-linkers (hard phase) and polymer segments (soft phase) and, according to the type of cross-linkers and the way of phase transition of polymer segments, they are divided into four classes as following [29].

(1) Covalently cross-linked glassy thermoset networks as SMPs. This class of SMPs has attractive characteristics that include excellent degree of shape recovery afforded by rubbery elasticity because of the nature of permanent (or near permanent) cross-linkers, tunable work capacity during recovery garnered by a rubbery modulus that can be adjusted through the extent of covalent cross-linkers, and an absence of molecular slippage between polymer segments due to strong chemical cross-linkers. However, since the primary shape is covalently fixed, once processed (casting or molding) these SMPs are difficult to reshape thereafter.

(2) Covalently cross-linked semi-crystalline networks as SMPs. Similar to the first class, the permanent shapes are determined by chemical cross-linkers and can not be reshaped

after processing. Compared with glassy materials, this class of materials is generally more compliant below the transition temperature. Shape recovery speeds are also faster due to the sharper transition zone.

(3) Physically cross-linked glassy copolymers as SMPs. To some extent, This class of SMPs exhibit rheological characteristics so they are able to be easily processed with conventional thermoplastics technology.

(4) Physically cross-linked semi-crystalline block copolymers as SMPs. The lower transition temperature is an advantage of this class of SMPs, therefore, they are, similar to the third class, easy to be processed.

To suit new applications, novel SMPs are proposed in recent years. The stimulus to activate shape memory effect has been not limited to temperature, pH-responsive [30], light-responsive [31], solvent-responsive [32] and water-responsive [33] SMPs have been developed. Besides, dual shape SMPs are improved to triple shape and even multiple shapes SMPs due to several well separated phase transitions [34].

1.2. Piezoelectric materials

Piezoelectric materials are smart materials with the ability to generate electric voltages in response to applied mechanical pressure and, inversely, generate mechanical displacements resulting from applied electrical voltages [35,36]. The piezoelectricity was first discovered in by some natural crystals such as quartz, tourmaline etc. by Pierre and Jacques Curie in 1880 [37]. With the development over a century, piezoelectric

materials already have become a large family including three main groups as below.

(1) Piezoelectric ceramics. This group can be further classified into lead containing ceramics, like Lead zirconate titanate (PZT), and lead free ceramics containing three classes, $BaTiO_3$, (Na,Bi)Ti-$BaTiO_3$-(K,Bi)TiO_3 (BNBK) and (K,Na)NbO_3 (KNN) [38].

(2) Piezoelectric polymers. There two different polymer categories, bulk piezoelectric polymers and voided charged polymers (polymer materials that contain internal gas voids). The bulk piezoelectric polymers involve semi-crystalline piezoelectric polymers (PVDF and PVDF co-polymers) and amorphous piezoelectric polymers (amorphous polyimide) [39].

(3) Piezoelectric single crystals. Most of nature piezoelectric materials, like quartz, are belong to this group. Also, some piezoelectric single crystals are synthesized artificially like lithium niobate (LN). The distinction from the above two groups is that piezoelectric single crystals are born with piezoelectric effect without request for polarization [40].

(4) Piezoelectric composites. Generally piezoelectric composites are compound by piezoelectric ceramics and polymers or piezoelectric polymers. Piezoelectric ceramics as fillers could be particles, powders, fibers, rods and sheets [41].

The unique ability of mutual transformation of electric energy and mechanical energy makes piezoelectric materials become the smart material most widely used in practice. The applications of piezoelectric materials range from buzzers to biomedical

ultrasound, piezoelectric surgery, high frequency medical imaging ultrasonic transducers, civil engineering, automobile industry, nuclear industry, aerospace engineering, nanopositioners in scanning microscopes and even nanogenerators [42-48].

1.2.1. PZT ceramics

PZT ($Pb[Zr_xTi_{1-x}]O_3$) ceramics are able to represent the success of piezoelectric materials because of their utilizations almost cover all aspects of people's life, for instance, the drivers of hard disk in computers [49, 50], the valves of fuel injectors in engines of automobiles [51, 52], the active sensors of health monitoring of aging aerospace structures [53], the actuators of vibration isolation of aerospace structures to make passengers feel more comfortable in flight [54], the part of buzzer to make sounds [55], the ultrasonic generator of B-ultrasonic scanner [56] and even the squeeze igniters [57]. These are all benefit from the outstanding advantages of PZT ceramics, the strong and stable piezoelectric effect [58], high operating frequency [59], the large electromechanical coupling coefficients, temperature stability, and high resistance to depolarization from mechanical stress [60, 61]. In light of the great market potential of PZT, nowadays, a lot of companies supply commercial products with different piezoelectric performances to satisfy the various requirements for researchers and manufacturer of PZT related devices.

1.3. Composites

A composite is the material made from two or more constituent materials with different material properties. In general, after combination, the resultant composite would generate new characteristics different from the two components or enhance the original material properties. The history of composites can track back to at least 3000 BC when asphalt mortars were employed to joint bricks [62]. The concrete should be one of the most common composites at present. In fact, virtually all natural materials are composites, such as plant cell walls, animal tissues, wood, bamboo, horn, wool, hair and nail, and most of them are sustainable, recyclable and biodegradable [63]. Besides, thousands of alloys, like SMAs [13], aluminum alloys [64], titanium alloys [65], and fiber reinforced materials, for example, carbon fiber reinforced polymers (CFRPs), glass fiber reinforced polymers (GFRPs) [66], nature fiber reinforced polymers [67] , are all composites. Recently, nanocomposites gradually become the most attractive.

1.3.1. Nanocomposites

Nanocomposites are the composites containing fillers with at least one dimension in nanoscale. Over recent years, nanocomposites have become a hot topic very fast by the reason of the quick development of nano fillers (nanoparticles, nanotubes, nanowhiskers, nanofibers, nanolayers and nanosheets) as well as the excellent material performances resulted from the great specific surface area, high surface energy, small size effect, quantum benefit and macroscopic quantum tunneling of nano fillers. The

vinyl ester resin composites with fillers (glass beads with mean sizes from 500 to 6 μm in diameter and alumina particles with average sizes from 70 μm to 15 nm) reveal that the elastic modulus and tensile strength of resultant composites both increase as the filler sizes decrease [68]. Only 0.1% of graphene improve the elastic modulus, tensile strength and fracture toughness of the graphene / epoxy nanocomposite by 31%, 40% and 53% respectively [69]. The addition of 2% of nanoclay (montmorillonite) increases 3,3',4,4'-biphenyltetracarboxylic dianhydride (BPDA) / p-phenylenediamine (PDA) polyimide and pyromellitic dianhydride (PMDA) / 4,4'-oxydianiline (ODA) polyimide by 42% and 110% in elastic modulus, respectively [70]. The electrical conductivity of nanocomposite, which is a hierarchically porous structure intimately intertwined by carbon nanotubes (CNTs) in weight ratio of 18% and nanowires, is 80 times as much as that of pristine V_2O_5 nanowires. Besides, the charge transfer in V_2O_5 nanowires is also improved by CNTs nanowires which lead to greater capacity when the nanocomposites is charged at high rate [71]. CNTs are used to advance the hardness and wear resistance through combination with Cu matrix by the method of calcination [72]. Silica nanoparticles bring in conspicuous increase in elastic modulus, yield strength and fracture toughness of the epoxy / silica nanocomposite [73]. The thermal conductivity of graphite nanoplatelet (GNP) / ultra-high molecular weight polyethylene nanocomposite is enhanced by 9 times due to the 21.4 vol% of GNPs, and moreover the thermal stability increases with the increasing addition of GNPs [74].

Although nanofillers enable nanocomposites to acquire promising, even amazing,

properties, not all nanocomposites are successful due to a number of factors including poor dispersion, poor interfacial load transfer, process-related deficiencies, poor alignment, poor load transfer to the interior of filler bundles, and the fractal nature of fillers clusters [75]. Many literatures have reported the discussion on material performances influenced by the aggregation and homogeneous dispersion of nanofillers, the interfacial characteristics between nanofillers and matrices, the orientation of nanofillers, especially nanotubes or nanofibers (rob-like nanofillers) and the sizes of nanofillers [68, 76-79]. In order to disperse nanofillers more uniformly and strengthen the interfacial adhesion, surface modification is introduced into the synthetic methods of nanocomposites. For example, nanocomposites containing surface functionalized GNPs, compared with the ones with pristine GNPs, display an augment in thermal conductivities and mechanical properties [80]. Similarly, the modified CNT / poly vinyl alcohol (PVA) nanocomposite show significantly improved mechanical properties in contrast with the pristine CNT / PVA nanocomposite [81].

1.4. Purpose of this research

This research aims to develop a new kind of smart composites combining the piezoelectric effect and shape memory effect by compounding PZT particles with the average diameter of 400 nm and shape memory polyurethane (SMPU) matrices. As what we discussed above, not every nanocomposite would acquire expected property because a number of factors have effect on the final material performances. Particularly,

PZT / SMPU composites are intended to the combination of two smart effects. However, PZT is an excellent piezoelectric material with strong and stable piezoelectric effect that would not degrade because of the usage. Its applications nearly exist in all aspects of human life. SMPU we used is one of amorphous SMPs with pretty good shape memory effect and thermoplasticity. The vast potential for future development of SMPs has been investigated by a great many internal researchers over the past decades. Therefore, after the consideration of the dramatic advantages of PZT and SMPU, we attempt to challenge to synthesize PZT / SMPU composites with the expectation to make a kind of decent functional composites which could be used to explore some satisfying applications in view of the widespread applications of either piezoelectric materials or shape memory materials.

PZT / SMPU composites with diverse content of PZT particles are prepared by solution blending method, film casting and hot-pressing. The resulting composites, PZT 60% (wt%), PZT 70% (wt%) and PZT 80% (wt%), actually succeed in both piezoelectric effect and shape memory effect. The recovery rates are all above 95% in the third cycle and the maximum recovery stresses of PZT 80% are greatly increased by 330%. But the recovery rates decrease as the increasing PZT content. The similar phenomenon is found in other reported shape memory composites (SMCs) too, while there is no throughout analysis on the reason for the changes in recovery rates induced by fillers. Thus, we analyze the movements of SMP chain segments and the fillers, and point out the distinctions in the molecular motions of SMPs and SMCs. After taking the

movements of fillers into consideration, the molecular mechanism of SMCs is proposed. To make the mechanism more general, TiO_2 whiskers are brought in to prepare TiO_2 / SMPU composites. The experimental data of both two kinds of composites strongly support the molecular mechanism of SMCs which can also explain the variations in recovery rates of other reported SMCs.

Piezoelectric effect is tested by measuring the output displacements of PZT / SMPU composites because nanopositioning and MEMS are two of the main applications of pure PZT. What we surprised is that PZT / SMPU composites are capable of generating displacements of 1 nm resolution with positioning errors within ± 5 nm in a common laboratory condition without controlling any environmental parameter. Besides, the nanoscale displacements are measured under step voltage signals in open-loop, no control method is employed. It implies the possibility to lower requirements for implementing nanopositioning. What is more, the advantage of possessing shape memory effect enable PZT / SMPU composites to be deformed into designed shapes very easily, and the deformation are able to enlarge the displacement ranges to several times, even dozens of times. It is more interesting that the positioning errors would not be amplified by the deformation, and still remain ± 5 nm.

Besides the two smart effects, PZT / SMPU composites are enhanced in mechanical properties as well. The results of tensile tests present the elastic moduli and yield stresses of PZT / SMPU composites increase with the content of PZT particles. PZT 80%, compared with pristine SMPU, exhibits 166% and over 99% of enhancement

in elastic moduli and yield stresses, respectively. The dynamic mechanical analysis (DMA) reveal that PZT particles promote both storage moduli and loss moduli, but have little effect on the glass transition temperature (T_g).

Reference

1. A. Olander, An electrochemical investigation of solid cadmium-gold alloys, *Journal of Applied Physics*, 1932**,** 54: 3819–3833.

2. W. J. Buehler, J. V. Gilfrich, R. C. Wiley, Effect of low-temperature phase changes on the mechanical properties of alloys near composition TiNi, *Journal of Applied Physics***,** 1963, 34: 1475- 1477.

3. G. B. Kauffmant, I. Mayo, The story of nitinol: the serendipitous discovery of the memory metal and its applications, *The Chemical Educator*, 1997, 2: 1-21.

4. L. Sun, W. M. Huang, Z. Ding, Stimulus-responsive shape memory materials: a review, *Materials and Design*, 2012, 33: 577-640.

5. W. M. Huang, Z. Ding, C. C. Wang, Shape memory materials, *Materials Today*, 2010, 13: 54-61.

6. J. Hu, Y. Zhu, H. Huang, Recent advances in shape–memory polymers: structure, mechanism, functionality, modeling and applications, *Progress in Polymer Science*, 2012, 37: 1720-1763.

7. I. S. Gunes, S. C. Jana, Shape memory polymers and their nanocomposites: a review of Science and Technology of New Multifunctional Materials, *Journal of Nanoscience*

and Nanotechnology, 2008, 8: 1616-1637.

8. T. Pretsch, Review on the functional determinants and durability of shape memory polymers, *Polymers*, 2010, 2: 120-158.

9. J. M. Jani, M. Leary, A. Subic, A review of shape memory alloy research, applications and opportunities, *Materials and Design*, 2014, 56: 1078-1113.

10. H. Qin, P. T. Mather, Combined one-way and two-way shape memory in a glass-forming nematic network, *Macromolecules*, 2009, 42: 273-280.

11. D. Dye, Towards practical actuators, *Nature Materials*, 2015, 14: 760-761.

12. A. Cladera, B. Weber, C. Leinenbach, Iron-based shape memory alloys for civil engineering structures: an overview, *Construction and Building Materials*, 2014, 63: 21-293.

13. S. Barbarino, E. I. S. Flores, R. M. Ajaj, A review on shape memory alloys with applications to morphing aircraft, *Smart Materials and Structures*, doi:10.1088/0964-1726/23/6/063001.

14. D. J. Hartl, D. C. Lagoudas, Aerospace applications of shape memory alloys, *Proceedings of the Institution of Mechanical Engineers*, 2007, 221: 535-552.

15. G. Song, N. Ma, H.-N. Li, Applications of shape memory alloys in civil structures, *Engineering Structures*, 2006, 28: 1266–1274.

16. L.G. Machado, M.A. Savi, Medical applications of shape memory alloys, Brazilian Journal of Medical and Biological Research, 2003, 36: 683-691.

17. Y. Bellouard, Shape memory alloys for microsystems: a review from a material

research perspective, *Materials Science and Engineering A*, 2008, 481-482: 582-589.

18. J. C. Wilson, M. EERI, M. J. Wesolowsky, Shape memory alloys for seismic response modification: a state-of-the-art review, *Earthquake Spectra*, 2005, 21: 569-601.

19. C. Chluba, W. Ge, R. L. de Miranda, Ultralow-fatigue shape memory alloy films, *Science*, 2015, 348: 1004-1007.

20. W. C. Rainer, E. M. Redding, J. J. Hitov (W. R. Grace & Co.), Polyethylene product and process, *US3144398 A*, 1964.

21. H. Tobushi, H. Hara, E. Yamada, Thermomechanical properties in a thin film of shape memory polymer of polyurethane series, *Smart Materials and Structures*, 1996, 5: 483-491.

22. M. Souri, Y. C. Lu, A. Erol, Characterization of unconstraint and constraint shape recoveries of an epoxy based shape memory polymer, *Polymer Testing*, 2015, 41: 231-238.

23. D. Ratna, J. Karger-Kocsis, Recent advances in shape memory polymers and composites: a review, *Journal of Materials Science*, 2008, 43: 254-269.

24. A. Lendlein, M. Behl, B. Hiebl, Shape-memory polymers as a technology platform for biomedical application, *Expert Review of Medical Devices*, 2010, 7: 357-379.

25. G. Li, D. Nettles, Thermomechanical characterization of a shape memory polymer based self-repairing syntactic foam, *Polymer*, 2010, 51: 755-762.

26. J. Hu, H. Meng, G. Li, A review of stimuli-responsive polymers for smart textile

applications, *Smart Materials and Structures*, doi:10.1088/0964-1726/21/5/053001.

27. www.acemr.eu/uploads/media/Trendstudy ACEMR Designmaterials 01.pdf

28. Y. Liu, H. Du, L. Liu, Shape memory polymers and their composites in aerospace applications: a review, *Smart Materials and Structures*, doi:10.1088/0964-1726/23/2/023001.

29. C. Liu, H. Qin, P. T. Mather, Review of progress in shape-memory polymers, *Journal of Materials Chemistry*, 2007, 17: 1543-155.

30. H. Chen, Y. Li, Y. Liu, Highly pH-sensitive polyurethane exhibiting shape memory and drug release, *Polymer Chemistry*, doi: 10.1039/c0xx00000x.

31. A. Lendlein, H. Jiang, O. Junger, Light-induced shape-memory polymers, *Nature*, 2005, 434: 879-882.

32. H. Du, J. Zhang, Solvent induced shape recovery of shape memory polymer based on chemically cross-linked poly(vinyl alcohol), *Soft Matter*, 2010, 6: 3370-3376.

33. W. M. Huang, B. Yang, Water-driven programmable polyurethane shape memory polymer: Demonstration and mechanism, *Applied Physics Letter*, doi: 10.1063/1.1880448.

34. T. Xie, Tunable polymer multi-shape memory effect, Nature, 2010, 464: 267-270.

35. A. H. Rajabi, M. Jaffe, T. L. Arinzeh, Piezoelectric materials for tissue regeneration: a review, *Acta Biomaterialia*, 2015, 24: 12-23.

36. P. K. Panda, B. Sahoo, PZT to lead free piezo ceramics: a review, *Ferroelectrics*, 2015, 474: 128-143.

37. P. Curie, J. Curie, Développement, par pression, de l'électricité polaire dans les cristaux hémièdres à faces inclinées, *Comptes Rendus de l'Académie des Sciences*, 1880, 91: 294-295.

38. T. R. Shrout, S. J. Zhang, Lead-free piezoelectric ceramics: Alternatives for PZT?, *Journal of Electroceramics*, 2007, 19: 113-126.

39. K. S Ramadan, D. Sameoto, S. Evoy, A review of piezoelectric polymers as functional materials for electromechanical transducers, *Smart Materials and Structure*s, doi:10.1088/0964-1726/23/3/033001.

40. Q. Zhou, K. H. Lam, H. Zheng, Piezoelectric single crystal ultrasonic transducers for biomedical applications, *Progress in Materials Science*, 2014, 66: 87-111.

41. E. K. Akdogan, M. Allahverdi, A. Safari, Piezoelectric composites for sensor and actuator applications, *IEEE Transactions on Ultrasonics, Ferroelectrics, and Frequency Control*, 2005, 52: 746-775.

42. E. Aksel, J. L. Jones, Advances in lead-free piezoelectric materials for sensors and actuators, *Sensors*, 2010, 10: 1935-1954.

43. A. Manbachi, R. S. C. Cobbold, Development and application of piezoelectric materials for ultrasound generation and detection, *Ultrasound*, 2011, 19: 187–196.

44. K. K. Shung, J. M. Cannata, Q. F. Zhou, Piezoelectric materials for high frequency medical imaging applications: a review, *Journal of Electroceramics*, 2007, 19: 139-145.

45. N.-C. Tsai, C.-Y. Sue, Review of MEMS-based drug delivery and dosing systems, *Sensors and Actuators A*, 2007, 134 : 555–564.

46. J. Nuffer, T. Bein, Application of piezoelectric materials in transportation industry, *Global Symposium on Innovative Solutions for the Advancement of the Transport Industry*, 2006, San Sebastian, Spain.

47. Y. S. Dambatta, A. A. D. Sarhan, M. Sayuti, Ultrasonic assisted grinding of advanced materials for biomedical and aerospace applications - a review, *The Internal Journal of Advanced Manufacturing Technology*, 2017, 92: 3825-3858.

48. J. Briscoe, S. Dunn, Piezoelectric nanogenerators - a review of nanostructured piezoelectric energy harvesters, *Nano Energy*, 2015, 14: 15-29.

49. B. Hu, J. Wan, C. K. Pang, Head-on-media detection with PZT self-sensing actuation in dual-Stage hard disk drives, IEEE Transaction on Magnetics, doi**:** 10.1109/TMAG.2016.2617345.

50. R. Horowitz, Y. Li, K. Oldham, Dual-stage servo systems and vibration compensation in computer hard disk drives, *Control Engineering Practice*, 2007, 15: 291-305.

51. N. Jalili, J. Wagner, M. Dadfarnia, A piezoelectric driven ratchet actuator mechanism with application to automotive engine valves, *Mechatronics*, 2003, 13: 933-956.

52. H. Nouraei, R. Ben-Mrad, A. N. Sinclair, Development of a Piezoelectric Fuel Injector, *IEEE Transactions on Vehicular Technology*, 2016, 65: 1162-1170.

53. V. Giurgiutiu, Active sensors for health monitoring of aging aerospace structures, *Proceedings of SPIE*, doi: 10.1117/12.388833.

54. E. T. Falungas, A vibration isolation system using active PZT brackets, *American Control Conference*, 1994, doi: 10.1109/ACC.1994.751825.

55. T. Ogawa, H. Akaishi, Piezoelectric ceramic energy harvesting, *Journal of Chemical Engineering and Chemistry Research*, 2014, 1: 373-378.

56. K. H. Martin, B. D. Lindsey, J. Ma, Dual-frequency piezoelectric transducers for contrast enhanced ultrasound imaging, *Sensors*, 2014, 14: 20825-20842.

57. L. Eyraud, B. Guiffard, D. Audigier, Electron transfer mechanism in PZT ceramics - application to squeeze ignition, *Ferroelectrics*, 2008, 366: 37-44.

58. T. G. King, M. E. Preston, B. J. M. Murphy, Piezoelectric ceramic actuators: a review of machinery applications, *Precision Engineering*, 1990, 12: 131-136.

59. G. Park, H. H. Cudney, D. J. Inman, Impedance-based health monitoring of civil structural components, *Journal of Infrastructure Systems*, 2000, 6: 153-160.

60. W. J. Choi, Y. Jeon, J.-H. Jeong, Energy harvesting MEMS device based on thin film piezoelectric cantilevers, *Journal of Electroceramics*, 2006, 17: 543-548.

61. C. Lee, T. Itoh, T. Suga, Micromachined piezoelectric force sensors based on PZT thin films, *IEEE Transactions on Ultrasonics, Ferroelectrics, and Frequency Control*, 1996, 43: 553-559.

62. A. Moropoulou, A. Bakolas, S. Anagnostopoulou, Composite materials in ancient structures, *Cement & Concrete Composites*, 2005, 27: 295-300.

63. U. G. K. Wegst, M. F. Ashby, The mechanical efficiency of natural materials, *Philosophical Magazine*, 2004, 84: 2167-2181.

64. C. S. Kaira, V. De Andrade, S. S. Singh, Probing novel microstructural evolution mechanisms in aluminum alloys using 4D nanoscale characterization, *Advanced Materials*, 2017, DOI: 10.1002/adma.201703482.

65. B. Dutta , F. H. Sam, Froes The additive manufacturing (AM) of titanium alloys, *Metal Powder Report*, 2017, 72: 96-106.

66. D. Kumar, K. K. Singh, An approach towards damage free machining of CFRP and GFRP composite material: a review, A*dvanced Composite Materials*, 2015, 24: 49-63.

67. K. Srinivas, A. L. Naidu, M. V. A. R. Bahubalendruni, A review on chemical and mechanical properties of natural fiber reinforced polymer composites, *International Journal of Performability Engineering*, 2017, 13: 19-200.

68. J. Cho, M. S. Joshi, C. T. Sun, Effect of inclusion size on mechanical properties of polymeric composites with micro and nano particles, *Composites Science and Technology*, 2006, 66: 1941-1952.

69. M. A. Rafiee, J. Rafiee, Z. Wang, Enhanced mechanical properties of nanocomposites at low graphene content, *ACS Nano*, 2009, 3: 3884-3890.

70. T. Agag, T. Koga, T. Takeichi, Studies on thermal and mechanical properties of polyimide - clay nanocomposites, *Polymer*, 2001, 42: 3399-3408.

71. Z. Chen, V. Augustyn, J. Wen, High-performance supercapacitors based on intertwined CNT / V_2O_5 nanowire nanocomposites, *Advanced Materials*, 2011, 23: 791-795.

72. K. T. Kim, S. I. Cha, S. H. Hong, Hardness and wear resistance of carbon nanotube

reinforced Cu matrix nanocomposites, *Materials Science and Engineering A*, 2007, 449-451: 46-50.

73. G. Ragosta, M. Abbate, P. Musto, Epoxy-silica particulate nanocomposites: chemical interactions, reinforcement and fracture toughness, *Polymer*, 2005, 46: 10506–10516.

74. J. Gu, N. Li, L. Tian, High thermal conductivity graphite nanoplatelet / UHMWPE nanocomposites, RSC Advances, 2015, 5: 36334-36339.

75. D. W. Schaefer, R. S. Justice, How Nano Are Nanocomposites?, *Macromolecules*, 2007, 40: 8501-8517.

76. B. Fiedler, F. H. Gojny, M. H. G. Wichmann, Fundamental aspects of nano-reinforced composites, *Composites Science and Technology*, 2006, 66: 3115-3125.

77. S. C. Tjong, Structural and mechanical properties of polymer nanocomposites, *Materials Science and Engineering: R: Reports*, 2006, 53: 73-197.

78. Z. Han, A. Fina, Thermal conductivity of carbon nanotubes and their polymer nanocomposites: a review, *Progress in Polymer Science*, 2011, 36: 914-944.

79. H. Zou, S. Wu, J. Shen, Polymer / silica nanocomposites: preparation, characterization, properties, and applications, *Chemical Reviews*, 2008, 108: 3893-3957.

80. J. Gu, X. Yang, Z. Lv, Functionalized graphite nanoplatelets / epoxy resin nanocomposites with high thermal conductivity, *International Journal of Heat and Mass Transfer*, 2016, 92: 15-22.

81. M. C. Paiva, B. Zhou, K. A. S. Fernando, Mechanical and morphological characterization of polymer-carbon nanocomposites from functionalized carbon

nanotubes, *Carbon*, 2004, 42: 2849-2854.

Chapter 2

Preparation of PZT / SMPU composites

Chapter 2: Preparation of PZT / SMPU composites

2.1. Introduction

Polymeric composites are synthesized by adding fillers into polymer matrices via different preparation methods. Till now, a plenty of methods have been employed to prepare polymeric composites, and new methods are still continuously proposed. Whereas, the primary methods are approximately classified into five categories.

(1) Sol-gel method: the method most widely used for the preparation of organic-inorganic composite materials because sol-gel chemistry offers a versatile approach to design new organic-inorganic composite materials [1].

(2) Blending method: one of the most convenient and fundamental techniques for preparation of composites. Specifically, this method contains three different classes (solution blending [2], melt blending [3] and emulsion blending [4]) according to the approach to mix fillers and matrices.

(3) *in-situ* method: a useful and convenient technique to overcome the phase separation between organic and inorganic phases [1].

(4) Intercalation method: a method primarily towards nanolayers such as graphene and nanoclay [5]. The intercalation of the polymer from a solution and direct intercalation of the molten polymer are the commonly used to make intercalation composites or

polymer layered composites [6].

(5) Self-assembly method: a technique to prepare composite with the ability to form the isotropic structure in molecular level. At first, it is proposed to prepare nanostructures[7], but it also appropriated to synthesize composites [8,9].

In addition, fillers are sometimes functionalized before the preparation of composites through the above methods or other ways, because the surface modification is expected to enhance the interactions between fillers and matrices and result in more promising material performances [10-12]. However, some surface modification does not give rise to the improvement in wanted material property. The surfactant treatment on CNTs reduces the electric conductivity of nanocomposites [13], and even weakens the shape memory effect [14].

The first aim of our research is to develop a kind of functional composites which have both shape memory effect and piezoelectric effect, though we know that it is a great challenge after reviewing plenty literatures on composites and nanocomposites. To increase the possibility of success as much as possible, we decide to prepare PZT / SMPU composites in solution blending method without any surface modification. The reasons are given as following.

(1) Synthesizing PZT / SMPU composites in solution blending method only need bring one solvent in the preparation, no other chemical agents required. The smart effects of PZT particles and SMPU matrices could be kept without any loss.

(2) Surfactant treatment is probable to decrease the two smart effects.

(3) Solution blending method is a cheap and time-saving approach, because overcoming the challenge need a large amount of attempts.

2.2. Materials and methods

2.2.1. Synthesis of PZT / SMPU composites

PZT / SMP composites were respectively synthesized by PZT particles (DPZ-LQ2-P6, Dai Nippon Toryo Co., Ltd., Japan) and a kind of commercial shape memory polyurethane (MM6520, SMP Technologies Inc., Japan). Figure 2-1 illustrates the whole process of preparation of PZT / SMPU composites schematically. First, PZT particles, with the average equivalent diameter of 400 nm and density of 7.9 g cm^{-3}, were poured into tetrahydrofuran (THF) and an ultrasonic device (Sonifier 250, Branson Ultrasonics Corp., U.S.A.) was employed to disperse PZT particles for 15min at the level 3. After dispersion, shape memory polyurethane pellets (the weight was one seventh of THF), with the glass transition of 65 ^{o}C and density of 1.25 g cm^{-3}, were dissolved in the PZT / THF suspension and the mixture was stirred magnetically for 48h at a speed of 400 r/min. Then THF evaporated naturally when the mixture was still stirred until the weight ratio of shape memory polyurethane and THF became 1:5. After the mixture was put statically for 48h to remove air bubbles, it was casted on a teflon film with an auto film applicator (PI-1210, Tester Sangyo Co., Ltd., Japan). The resulting films cured after evaporating THF again for 3 days in nature. The obtained PZT / SMPU composite films were further dried at 65 ^{o}C for 3 days and then pressed for 8h under the pressure of 6 MPa

at 80 °C by a hot-press machine (SA-303, Tester Sangyo Co., Ltd., Japan).

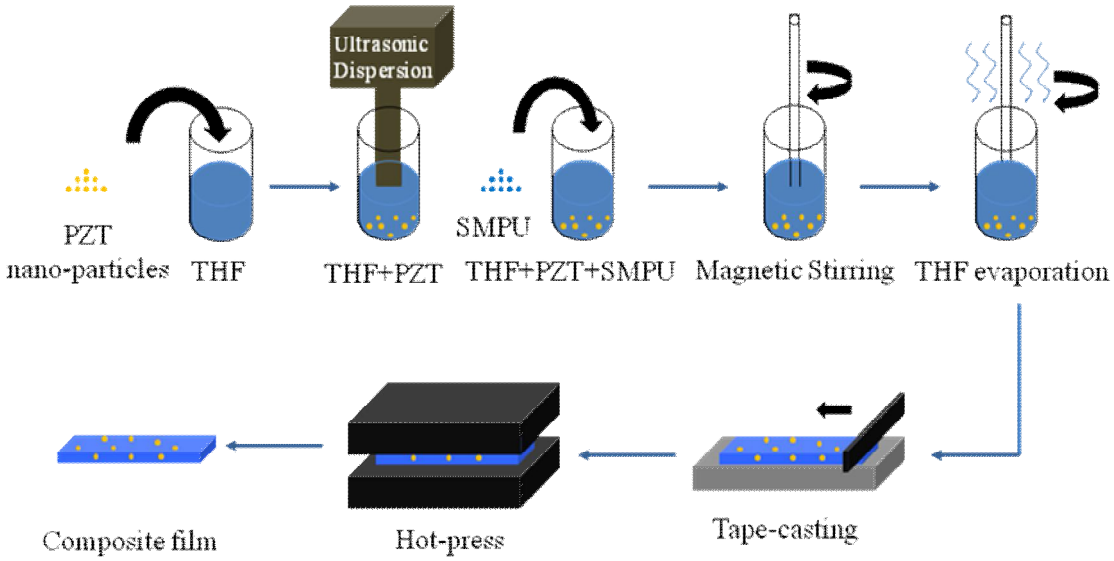

Figure 2-1. Schematic illustration for all the steps of preparation of PZT / SMPU composites.

2.2.2. Viscosity measurements

The viscosity of the solution of SMPU and THF is measured by a Cannon-Fenske viscometer (02611-025, Sibada Scientific Technology Ltd., Japan) at the temperature of 25 °C. The calculation of viscosity is according to the JIS Z8803. The equation is as following.

$$V_{dynamic} = A \times T$$

$$V = V_{dynamic} \times \rho$$

where, V is the viscosity, $V_{dynamic}$ is the dynamic viscosity, A is the calculated constant of viscometer, T is the time of all liquid flow out of the viscometer, ρ is the density of liquid.

2.2.3. Microscopic morphology

A field emission scanning electron microscopy (FE-SEM) (S-5000, HITACHI CO., LTD., Japan) was employed to observe the interfaces between PZT particles and SMPU matrices. The samples were all broken off in liquid nitrogen, and FE-SEM images showed the cryo-fractured surfaces.

2.3. Results and discussion

2.3.1. Protection for PZT particles from sedimentation

As we know, high density solids would settle down in low density liquid. The density of PZT particles is 7.9 g/cm^3 that is much higher than 1.25 g/cm^3 (SMPU) and 0.89 g/cm^3 (THF) because of the buoyancy much less than the gravity. Although the Brownian motion of liquid molecules would be helpful for PZT particles to suspend in liquid, the effect of Brownian motion is not enough and PZT particles would sink down. However, if SMPU pellets are added into THF to increase the viscosity of liquid to enough value, PZT particles are able to suspend in the solution of SMPU / THF because of the friction between PZT particles and solution. Figure 2-2 shows the experimental results of PZT particles in the solutions of SMPU and THF in different weight ratios. Until the weight ratio of THF and SMPU reaches to 7: 1, the corresponded viscosity (Table 2-1) is capable of preventing PZT particles from deposition. Figure 2-2a reveals two obvious separated layers whereas Figure 2-2b exhibits the PZT suspend in the mixture stably. The pale yellow layer (PZT particles are yellow) in Figure 2-2b is the

adhesion layer of the mixture caused by the surface tension of liquid.

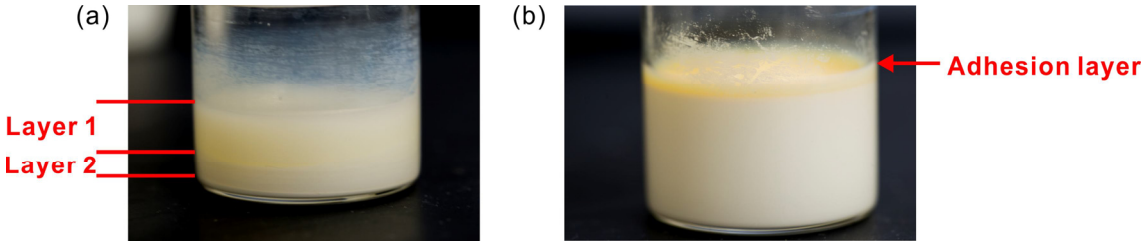

Figure 2-2. The mixture of PZT / SMPU / THF prepared 6 months ago. (a) The weight ratio of THF and SMPU is 8:1. (b) The weight ratio of THF and SMPU is 7:1.

Table 2-1. Viscosity of solutions of SMPU / THF at 25 °C

Weight ratio of THF and SMPU	10:1	9:1	8:1	7.5:1	7:1	6.5:1
Dynamic viscosity (cSt)	61.6[a)]	94.9	151.3	202.0	258.9	355.8
Viscosity (cSt)	56.8 [a)]	87.8	140.6	184.5	236.6	325.2

[a)] Dynamic viscosity and viscosity are the average value of five repeated experimental results.

Therefore, we choose the weight ratio of 7 : 1 (THF : SMPU) to prepare the initial mixture of PZT / SMPU /THF for the two purposes. First, dispersing PZT particles with ultrasonic device request adequate THF, otherwise the dispersion would be not good. The second one is to save the time of evaporating THF so as to increase the efficiency of material preparation.

2.3.2. Effect of hot-pressing on interfaces

Because the preparation of PZT / SMPU does not make use of any chemical agent and surface modification on PZT particles, the interfacial bonding between PZT particles and SMPU matrices is weak. Figure 2-3a exhibits the interfaces of PZT 60%

without hot-pressing. Obviously, lots of voids exist between PZT particles and SMPU matrices reveal the poor interfaces visually. According to the mechanisms of polymeric film formation, polymer chains would interpenetrate, go through a gel state and then form a film as the solvent evaporates [15]. However, with the evaporation of solvent, the polymer chains in composites would aggregate together and give rise to the formation of polymer phase by the polymer chain interpenetration, while the spaces of solvent molecules left by evaporation would be transferred to the regions between the fillers and matrices. In pristine polymeric films, all polymer chains would get together to form by the polymer chain interpenetration and the spaces of solvent molecules would be removed by being transferred to regions outside of polymer chains (here, regions outside of polymer chains means those outside of polymeric films). It is at the same in composites, but the difference is that regions outside of polymer chains means those between fillers and matrices. That's the main reason for the existed free spaces. The spaces left by the entrapped air are another reason.

Whereas, these free spaces are able to be eliminated by hot-pressing, because SMPU matrices above T_g are usually viscous fluids. If enough external pressure is applied, SMPU matrices above T_g would not only fill in the free spaces but also embrace PZT particles resulting in interfaces due to the high mobility. Figure 2-3b clearly shows the importance of hot-pressing for interfaces. After hot-pressing, the PZT particles are surrounded so tightly that no void is found at the interfaces of hot-pressed PZT 60%.

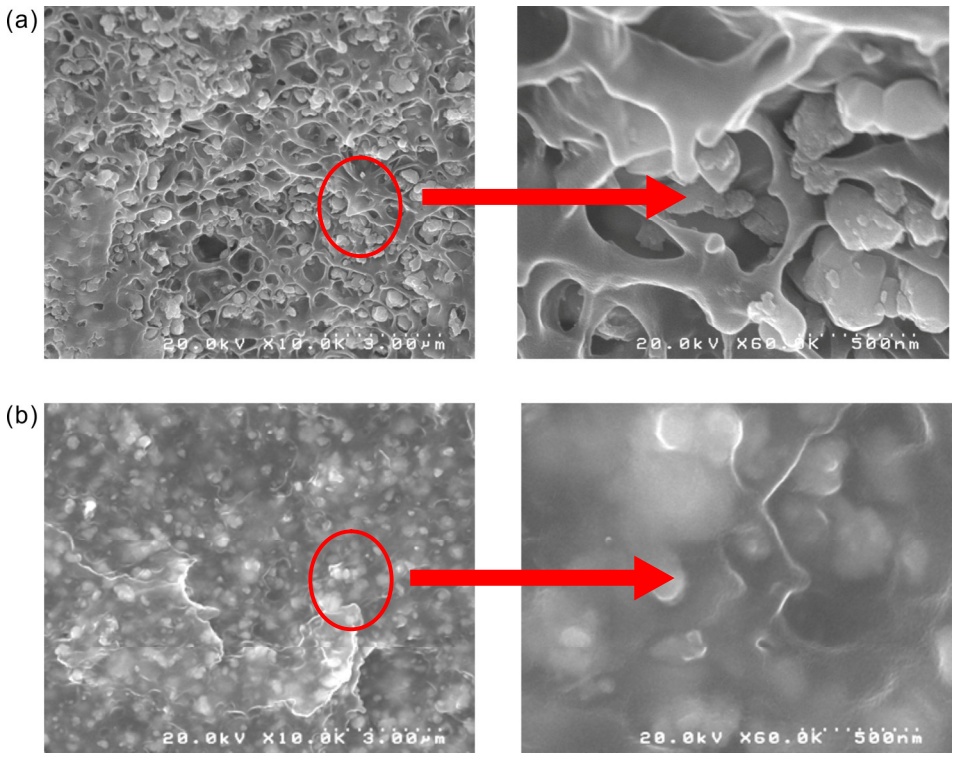

Figure 2-3. Comparison of the interfaces of PZT 60% before hot-pressing and the one after hot-pressing. (a) FE-SEM images of PZT 60% before hot-pressing. (b) FE-SEM images of PZT 60% after hot-pressing.

2.3.3. PZT particles compounding with another kind of SMPU

Besides SMPU (MM 6520), SMPU-90 (MM 9020), the products of the same series with MM 6520, is also used to prepare PZT / SMPU-90 composites with the same preparation method (hot-pressing is carried out at the temperature of 110 ^{o}C). But the FE-SEM image (Figure 2-4) displays the poor interfaces even after hot-pressing. The reason is that, compared with SMPU (T_g is 65 ^{o}C), SMPU-90 has more amount of hard segments (cross-linkers) to gain higher T_g (90 ^{o}C). More hard segments depress the mobility of chain segments of SMPU-90 at the temperature above T_g which results in the weak effect of hot-pressing on interfaces.

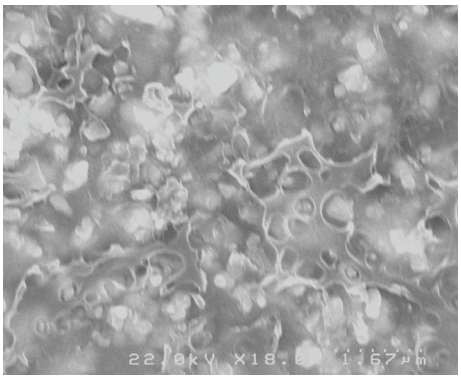

Figure 2-4. FE-SEM image of PZT 60% (SMPU-90) after hot-pressing.

2.3.4. Discussion on PZT / SMPU composites with different PZT content.

PZT / SMPU composites with PZT content, increasing from 40% (wt%) to 80% (wt%) by the step of 10% in weight, are synthesized for the sake of investigating the effect of PZT content on the material performances. But we find that PZT 80% already starts to show the brittleness (details would be discussed in the chapter 5), so the content of PZT particles should not be increased again for the flexibility of PZT / SMPU composites. Inversely, PZT 40% and PZT 50% are very flexible, whereas the PZT effect of them are too weak to be measured even with the laser sensor with 1 nm resolution. Therefore, our later work is focused on PZT 60% (Figure 2-5), PZT 70% and PZT 80%.

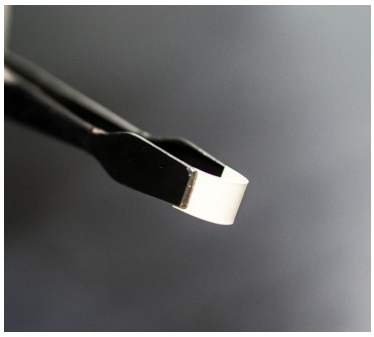

Figure 2-5. PZT 60% film with good flexibility.

2.4. Conclusions

In order to find out the optimal method to prepare PZT / SMPU composites, the viscosity of initial solution of SMPU / THF, how to get good interfaces and what content of PZT particles for decent material performances are discussed in this chapter. The results of experiments illustrate that the solution of SMPU / THF with the weight ratio of 1 : 7 is helpful for preparation by reason of effective dispersion of PZT particles, shorter time for evaporation of THF and insurance against the deposition of PZT particles. The significance of hot-pressing for good interfaces are proved by the FE-SEM images. Considering the piezoelectric effect and flexibility of PZT / SMPU composites, PZT 60%, PZT 70% and PZT 80% are the good choices. Besides, SMPU-90 also is utilized to synthesize PZT / SMPU-90 composites, unfortunately, their poor interfaces are difficult to be improved just by hot-pressing.

Reference

1. T. Ogoshi, Y. Chujo, Organic-inorganic polymer hybrids prepared by the sol-gel method, *Composite Interfaces*, 2005, 11: 539-566.

2. X. Zeng, J. Yang, W. Yuan, Preparation of a poly(methyl methacrylate)-reduced graphene oxide composite with enhanced properties by a solution blending method, *European Polymer Journal*, 2012, 48: 1674-1682.

3. Z. Jin, K. P. Pramoda, S. H. Goh, Poly(vinylidene fluoride)-assisted melt-blending of multi-walled carbon nanotube/poly(methyl methacrylate) composites, *Materials*

Research Bulletin, 2002, 37: 271-278.

4. M. Bertoldo, M.-B. Coltelli, T. Messina, An emulsion blending approach for the preparation of Gelatin/Poly(butylen succinate-co-adipate) films, *ACS Biomaterials Science & Engineering*, 2016, 2: 677-686.

5. M. Li, Z. Wu, A review of intercalation composite phase change material: Preparation, structure and properties, *Renewable and Sustainable Energy Reviews*, 2012, 16: 2094-2101.

6. M. Zanetti, S. Lomakin, G. Camino, Polymer layered silicate nanocomposites, *Macromolecular Materials and Engineering*, 2000, 279: 1-9.

7. G. M. Whitesides, J. P. Mathias, C. T. Seto, Molecular self-assembly and nanochemistry: a chemical strategy for the synthesis of nanostructures, *Science*, 1991, 254: 1312-1319.

8. T. Szaboa, A. Szeri, I. Dekany, Composite graphitic nanolayers prepared by self-assembly between finely dispersed graphite oxide and a cationic polymer, *Carbon*, 2005, 43: 87-94.

9. N. A. Kotov, I. Dekrany, J. H. Fendler, Ultrathin graphite oxide-polyelectrolyte composites prepared by self-Assembly: transition between conductive and non-conductive states, *Advanced Materials*, 1996, 8: 637-641.

10. L. Liu, A. H. Barber, S. Nuriel, Mechanical Properties of Functionalized Single-Walled Carbon-Nanotube/Poly(vinyl alcohol) Nanocomposites, *Advanced Functional Materials*, 2005, 15: 975-980.

11. J. Gu, X. Yang, Z. Lv, Functionalized graphite nanoplatelets / epoxy resin nanocomposites with high thermal conductivity, *International Journal of Heat and Mass Transfer*, 2016, 92: 15-22.

12. M. C. Paiva, B. Zhou, K. A. S. Fernando, Mechanical and morphological characterization of polymer-carbon nanocomposites from functionalized carbon nanotubes, *Carbon*, 2004, 42: 2849-2854.

13. Y. Geng, M. Y. Liu, J. Li, Effects of surfactant treatment on mechanical and electrical properties of CNT/epoxy nanocomposites, *Composites: Part A*, 2008,39: 1876-1883.

14. M. Raja, S. H. Ryu, A.M. Shanmugharaj, Thermal, mechanical and electroactive shape memory properties of polyurethane (PU)/poly (lactic acid) (PLA)/CNT nanocomposites, *European Polymer Journal*, 2013, 49: 3492-3500.

15. L. A. Felton, Mechanisms of polymeric film formation, *International Journal of Pharmaceutics*, 2013, 457: 423-427.

Chapter 3

Shape memory performances

Chapter 3: Shape memory performances and molecular mechanism of shape memory composites

3.1. Introduction

Shape memory polymers (SMPs) are a class of materials able to recover the shapes after deformation through an external stimulus [1, 2]. Therefore, SMPs seem to "memorize" [3] or "remember" [4] their original shapes. SMPs have been used in medical devices, smart structural repair, self-repairing, sensors, actuators and aerospace applications [4-6]. Compared with shape memory alloys, SMPs show attractiveness in primarily lying in the lower densities, easier processing, lower costs and larger deformation strains, whereas lower elastic moduli and recovery stresses are the main limitations [7]. To surmount these two shortcomings, various fillers have been employed to fabricate SMP composites. Carbon black [8], carbon nanofibers [9, 10], carbon nanopaper [11], graphene [12, 13] and CNTs [14-17] are added into SMPs to endow the SMCs with the new ability that can be actuated by the electric voltages as a result of the Joule's law. What is more, some remote controlled SMCs are successfully synthesized through adding CNTs (actuated by infrared [18] and microwave [19]) and graphene (actuated by infrared) [20], and consisting of a SMP / Fe_3O_4 region and a SMP / CNT

region (actuated by radiofrequency field) [21]. To make electric heating more efficient, 3D network structures of CNTs [22]and 3D scaffolds of CNTs / graphene aerogels [23] are proposed. Besides, sepiolite fibers are used to improve fixity rates [24], silk fibroins are utilized to enhance recovery rates [25] and graphene is employed to heighten self-healing property [26]. Although most of researchers focus on their desired performances, changes in recovery rates of SMCs are still reported. Not only the decreases in recovery rates are found [27-30], but also the increases in recovery rates are discovered [31, 32]. Some researchers respectively give simple reasons according to their own work, but the given reasons contradict others' work (detailed discussion on the reported reasons is the section 3.3.3). In fact, compared with the experimental researches on SMCs, theoretical analyses are very few. Two models for evaluating interfacial adhesion are introduced to attempt to find out a relationship between shape memory properties and interfacial bonding [33], but the conclusion is only based on SMCs with low percents of fillers. A bridging model is applied to predict recovery performances [34], whereas the predictions are just simulation without comparisons with recovery experimental data.

So far, a thorough analysis on the variations in recovery rates induced by fillers has not been presented yet, maybe because the molecular mechanism of SMCs is unclear. It is unlike the molecular mechanism of SMPs which has been discussed schematically [35-37]. Another possible reason may be that the mechanism of SMCs is considered to be

the same as that of SMPs (reference 32). As we know, a microscopic mechanism would be greatly helpful to understand material behaviors essentially and explore expected properties for promising applications. Moreover, with the rapid development in recent years [38], the molecular mechanism of SMCs become more and more important.

In this chapter, we challenge to combine piezoelectricity and shape memory property into one composite by adding a high percentage of PZT particles into shape memory polyurethane (SMPU) matrices. The resultant composites, PZT 60%, PZT 70% and PZT 80%, not only display decent shape memory property, but also indicate strong enhancements in the recovery stresses. Moreover, the molecular mechanism of SMCs is clarified by analyzing the distinctions between molecular motions of SMPs and SMCs. According to the molecular mechanism of SMCs, interfaces between fillers and matrices are the essential reason for variations in recovery rates of SMCs and the resultant effects of interfaces on recovery rates should be both positive and negative. To make clear the role of interfaces in shape recovery behaviors, another kind of fillers (TiO_2 whiskers) are also selected to synthesize SMCs and several experiments are specifically designed. The comprehensive conclusions are obtained on the basis of the experimental results. Besides, the limit on the programming ability of SMPs and SMCs is discovered. The conclusions are able to provide not only a common explanation for the varying recovery rates of other reported SMCs but also qualitative predictions for the trend of changes in recovery rates with adding more fillers.

3.2. Materials and methods

3.2.1. Preparation of hot-pressed TiO_2 / SMPU composites

Hot-pressed TiO_2 / SMPU composites were synthesized by TiO_2 whiskers (FT-3000, Ishihara Sangyo Kaisha, Ltd., Japan) and SMPU (MM6520, SMP Technologies Inc., Japan). TiO_2 whiskers are with the average diameter of 270 nm, the average length of 5.15 μm and the density of 4.3 g cm^{-3}. The synthetic procedures were the same as those of hot-pressed PZT / SMPU composites.

3.2.2. Preparation of Pristine SMPU films

Pristine SMP films were prepared in the same methods as those of hot-pressed PZT / SMPU composites but two steps (adding fillers and dispersing fillers).

3.2.3. PZT / SMPU and TiO_2 / SMPU composites without hot-pressing

This group of materials were compounded in the same methods as those of hot-pressed PZT / SMPU composites except the step of hot-pressing.

3.2.4. Recovery rate tests in three cycles

The shape recovery rates of PZT / SMPU composites were all measured by a thermo-mechanical analyzer (TMA / SS6100, Hitachi High-Tech Science Corp., Japan). Rectangle samples (the width of 2 mm, length of 10 mm and thickness between 127-150

μm) were tested for 3 cycles in the controlled force mode. Before the cyclic tests, the samples were heated from ambient temperature up to 71 ^{o}C with a stress of 0.025 MPa to protect samples from buckling. One experimental cycle was that firstly the stress was increased to 3.5 MPa at a speed of 0.139 MPa/min, then a fan was employed to quickly cool the samples down with the stress of 3.5 MPa, next the stress was unloaded from 3.5 to 0.025 MPa at a speed of - 0.695 MPa/min and finally the samples were heated up to 71 ^{o}C again while the stress was kept at 0.025 MPa. The strain of every sample was the quotient of the continuous displacement recorded by TMA device and its length.

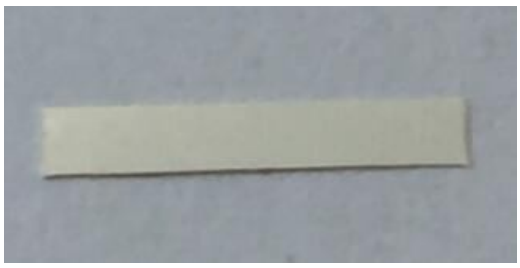

Figure 3-1. A rectangle sample for recovery rate measurements

3.2.5. Recovery rate tests in four cycles

The shape memory recovery rates of PZT / SMP composites and pristine SMPU were all measured by a thermo-mechanical analyzer (TMA / SS6100, Hitachi High-Tech Science Corp., Japan). Rectangle samples (similar to that in Figure 3-1) with the width of 2 mm, length of 10 mm and thickness between 120- 147 μm were tested in a designed four cycle method in the controlled force mode. To insure all samples were measured under the same stress state, the applied force for every sample was calculated in advance. Before the cyclic tests, the samples were heated from ambient temperature up to 71 ^{o}C

with a stress of 0.025 MPa to protect samples from buckling. The first two cycles were that the stress was increased from 0.025 to 2.5 MPa at a speed of 0.099 MPa/min, a fan was employed to quickly cool the samples down with the stress of 2.5 MPa, next the stress was unloaded from 2.5 to 0.025 MPa at a speed of - 0.495 MPa/min and then the samples were heated up to 71 ^{o}C again while the stress was kept at 0.025 MPa. The two later cycles were that the stress was increased from 0.025 to 3.5 MPa at a speed of 0.139 MPa/min, a fan was employed to quickly cool the samples down with the stress of 3.5 MPa, next the stress was unloaded from 3.5 to 0.025 MPa at a speed of - 0.695 MPa/min and then the samples were heated up to 71 ^{o}C again while the stress was kept at 0.025 MPa. The strain of every sample was the quotient of the continuous displacement recorded by TMA device and its length.

3.2.6. Recovery stress measurements

The shape memory recovery stresses of the PZT / SMP composites and pristine SMPU were all measured by a thermo-mechanical analyzer (TMA / SS6100, Hitachi High-Tech Science Corp., Japan). Rectangle samples with a width of 2 mm, length of 10 mm and thickness between 120 and 135 μm were tested for one cycle in the controlled displacement mode. First, the samples were heated from ambient temperature up to 71 °C while keeping the original strain. Second, the strain was increased to 2.5% (to protect the PZT 80% samples from plastic deformation) at 5 μm/min and then the samples were

naturally cooled down with a strain of 2.5%. Next, the strain was adjusted to make the stress 0 (release the stress caused by cooling) and finally the samples were heated up to 71 °C again while keeping the strain unchanged. The recovery stress of every sample was the quotient of the continuous force recorded by TMA device and its sectional area.

3.3. Results and discussion

3.3.1. Shape recovery rates and fixity rates

The recovery rates of pristine SMPU and PZT / SMPU composites were measured according to a three-cycle method described in section 3.2.4 (Figure 3-1). Recovery rates are calculated by $R_r(N) = \frac{\varepsilon_m(N) - \varepsilon_f(N)}{\varepsilon_m(N) - \varepsilon_f(N-1)} \times 100\%$, where R_r is the recovery rate, ε_m is the maximum under loading conditions, ε_f is the residual strain after shape recovery, and N is the number of cycles. Shape fixity rates are calculated by $R_f(N) = \varepsilon_u(N) / \varepsilon_m(N) \times 100\%$, where R_f is the recovery rate, ε_u is the strain of the temporary shape after unloading [24]. Table 3-1 summaries that the recovery rates and fixity rates of pristine SMPU, PZT 60%, PZT 70% and PZT 80% in three cycles. The recovery rates and fixity rates both gradually go down with the increase of PZT particles but go up with the number of cycle. In the third cycle, even the PZT 80% performs a recovery rate of 95%. The decrease of recovery rates due to the addition of PZT particles is caused by the chain slippages induced by PZT particles. The molecular chains of SMPU in the interfaces would be bonded with PZT particles and lost the mobility even if at temperature above T_g. Therefore, if the PZT /

SMPU composites are stretched, the deformation of molecular chains in the interfaces would be different from that of their neighbors who have high mobility. In other words, the molecular chains in the interfaces and their neighbors would slip off each other resulting in chain slippages (detailed analyses and discussion are given in the section 3.3.3). Besides, the strains of molecular chains in samples with more PZT content contain more elastic strains, because more amount of interfacial bonding would restrain molecular chains from uncoiling. As a result, samples are elongated by the same stress, but the strains decrease much with the addition of PZT particles (Figure 3-2). During the cooling process with the constant stress, elastic moduli of molecular chains would increase rapidly, so elastic stains decrease quickly according to $\sigma = E\varepsilon$, where σ is the stress, E is the elastic modulus, and ε is the strain. Then the stress is unloaded, the strains further reduce because the elastic strains, which are not fixed by glass transition, would completely disappear. Therefore, PZT particles lessen fixity rates.

Table 3-1. Shape recovery performances of pristine SMPU and PZT / SMPU composites

		Pristine SMPU	PZT 60%	PZT 70%	PZT 80%
Recovery rate (%)	1st cycle	92.5	90.0	85.1	76.2
	2nd cycle	96.9	96.8	95.7	91.4
	3rd cycle	98.4	98.3	97.9	95.0
Fixity rate (%)	1st cycle	97.9	84.9	83.5	50.7
	2nd cycle	98.0	85.4	83.9	54.3
	3rd cycle	98.1	85.7	84.1	56.5

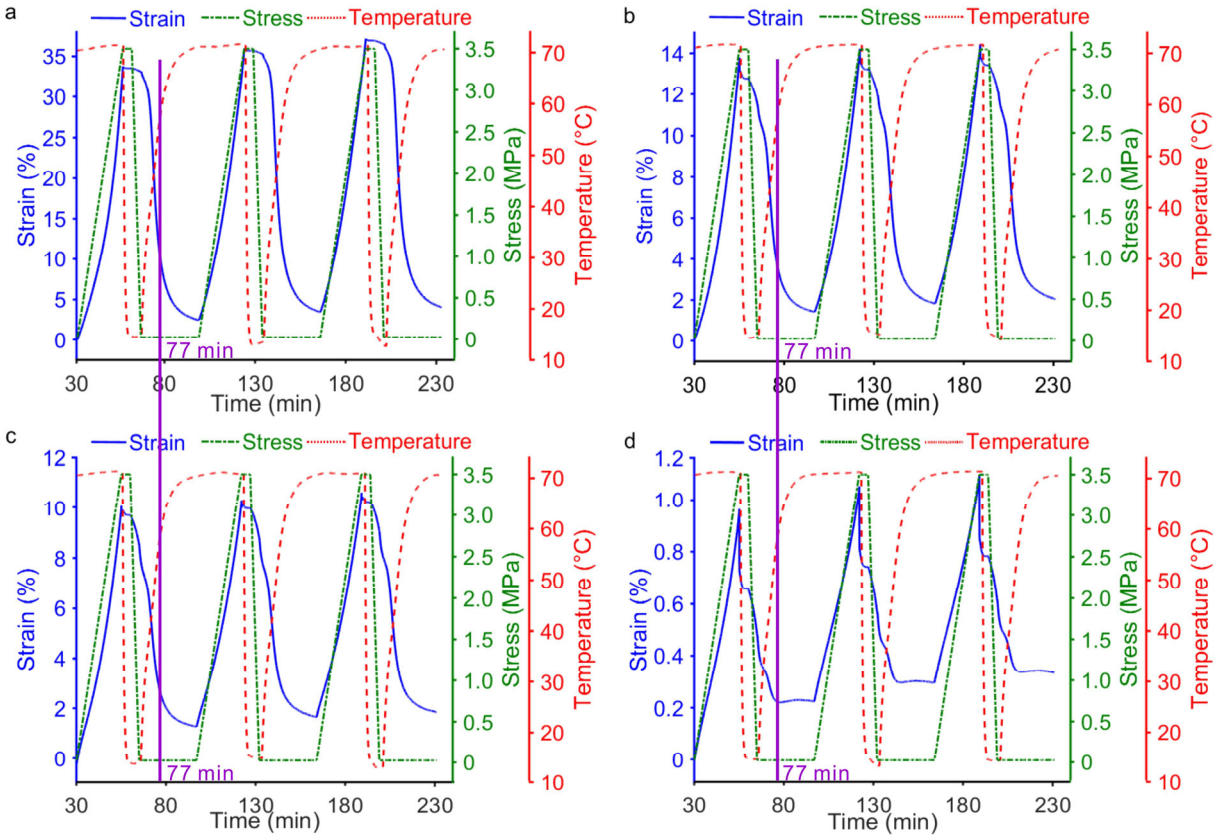

Figure 3-2. Graphs of strain, stress and temperature vs. time in the consecutive shape memory processes. (a) Pristine SMPU, (b) PZT 60%, (c) PZT 70% and (d) PZT 80%. The zero points of strain are the ones where the stresses start increasing from 0 at 71 °C.

The reason why recovery rates increase cycle by cycle is the reduction of chain slippages in the cycles. Figure 3-2 exhibits the stretching processes in the second cycle start from the end of the first cycle to the maximum strains close to the ones in the first cycle. This means that the majority of the stretching processes in the second cycle are the same as the part of those in the first cycle, except for irrecoverable strains. As a result, the irrecoverable strains in the second cycle would be less than those in the first cycle

because the strains are new produced in the second cycle, which would generate new slippages contributing to irrecoverable strains, are a minority. Similarly, the irrecoverable strains in the third cycle are less than those in the second cycle. Owing to the irrecoverable strains remaining in every cycle, fixity rates increase with the number of cycles because the percentage of elastic strains of molecular chains decreases.

Besides, PZT particles do not show an evident effect on shape recovery time, although Figure 3-2 exhibits that PZT 80% seemingly recover its shape faster than others due to lack of a slow shape recovery process (the part of strain curve after the purple line in the first cycle in Figure 3-2). In fact, the slow shape recovery process of PZT 80% disappears because thermal expansion becomes predominant due to its small strain (less than 0.24%). However, quick shape recovery processes (the part of strain curves before the purple line in the first cycle in Figure 3-2) of all samples are close. Moreover, periods of shape recovery of pristine SMPU, PZT 60% and PZT 70% are almost the same because their thermal expansion is much weaker than shape recovery. Therefore, shape recovery time is not affected evidently by PZT particles.

3.3.2 Shape recovery stresses

In opposite to the recovery rates, the PZT particles effectively improve the recovery stresses and the maximum recovery stresses are listed in Table 3-2. The maximum recovery stresses of PZT 60%, PZT 70% and PZT 80% are, respectively, 133%, 144%

and 330% higher than those of pristine SMPU. The impressive reinforcements in recovery stresses result from enhancements in elastic moduli above T_g (Table 3-2). The stretching in this study is uniaxial tension and strain energy of uniaxial tension can be calculated according to $U=V\mathrm{E}\varepsilon^2 / 2$, where U is the strain energy, V is the volume, E is the elastic modulus, ε is the strain. Apparently, the higher elastic modulus is, the more strain energy can be stored by the same strain (the volume is regarded as a constant through the whole process). In fact, the shape recovery is the process of releasing the stored strain energy [4]. In the recovery process, the material with higher elastic modulus would release more strain energy on the condition of the same strain, which would cause larger recovery stress according to $U=V\sigma\varepsilon / 2$, where σ is the stress.

Table 3-2. Shape recovery stresses of pristine SMPU and PZT / SMPU composites

Material	The average elastic moduli above T_g (MPa)	Maximum recovery stress (MPa)
Pristine SMPU	9.3	0.36
PZT 60%	23.4	0.84
PZT 70%	33.8	0.88
PZT 80%	333.8	1.55

3.3.3. Existing explanations for variations in recovery rates

Here, we explain why existing explanations for variations in recovery rates of SMCs contradict others' work. First, why recovery rates of SMCs are improved by fillers is

unable to be explained by the explanations given in the papers reporting the decrease of recovery rates. For example, the reduction of recovery rates is explained by the increase of bulk viscosity caused by carbon black (reference 29) and the lower recovery rates are attributed to the sepiolite inhibiting the movements of chain segments (reference 30). Evidently, the two above reasons are totally against the increase of recovery rates.

Second, the increased recovery rates are considered to be the result of improved crystallinity due to the nucleation effect of fillers. However, the improved crystallinity should not be the essential reason. The reference 39 shows that, compared with pristine shape memory polymer fibers, the SMC fibers with 3 wt% and 5 wt% carbon nanotubes (CNTs) exhibit lower crystallinity but perform better recovery rates. Besides, the reference 29 reports that the crystallinity of SMCs is affected very little by the addition of carbon black but recovery rates decrease dramatically. Therefore, recovery rates should be increased by other factors.

3.3.4. Molecular mechanism of SMCs

At present, the molecular mechanism of SMPs generally accepted is described as following [35-37]. The chain segments (soft segments) between netpoints (hard segments which determine the permanent shapes) could deform quite freely at temperature above the thermal transition temperature (T_{trans}). The deformation of chain segments would store strain energy. If temperature is below T_{trans}, the deformation of chain segments would be

freezing or at least partly constrained by vitrification, crystallization, or other means [40]. When temperature goes above T_{trans} again, the chain segments would be liberated and recover to their original shapes by releasing the stored strain energy. The recovery force is entropic force from changes in conformational entropy.

On the basis of the above mechanism, two obvious phenomena, which don't exist in the molecular motions of SMPs, are presented by taking the fillers into consideration:

(1) The movements and deformation of the chain segments in the interfaces are the same as that of fillers, if the interfaces are undamaged (the chain segments in the interfaces means the chain segments forming interfacial bonding).

(2) The deformation of the chain segments out of the interfaces is much greater than that of the chain segments in the interfaces at temperature above T_{trans}.

The first difference is easily understandable, because, if it is untrue, fillers and the chain segments in the interfaces would be apart (in other words, the interfaces would be broken). The second difference results from the fact that the chain segments out of the interfaces could easily generate large strains due to the chain mobility at temperature above T_{trans} [4] but the chain segments in the interfaces almost keep their initial shapes because of the first difference and the almost ignorable deformation of fillers (most of the fillers added in SMPs are usually much harder than the chain segments at temperature above T_{trans}).

According to the above two differences, the molecular mechanism of SMCs is clarified (Figure 3-3). When temperature is above T_{trans}, the chain segments out of the

interfaces (blue full lines in Figure 3-3) could freely deform but the deformation of fillers and the chain segments in the interfaces (red dashed lines in Figure 3-3) would be very few. All the deformation would store strain energy. Besides, fillers would move with the chain segments. If temperature falls below T_{trans}, all the deformation would be frozen or at least partly constrained by different means. When temperature goes above T_{trans} again, the chain segments out of the interfaces would regain the chain mobility to recover to their original shapes naturally by entropic force. With the movements of the chain segments in the interfaces, fillers would tend to go back to their former positions and, simultaneously, recover their initial shapes due to elastic recovery.

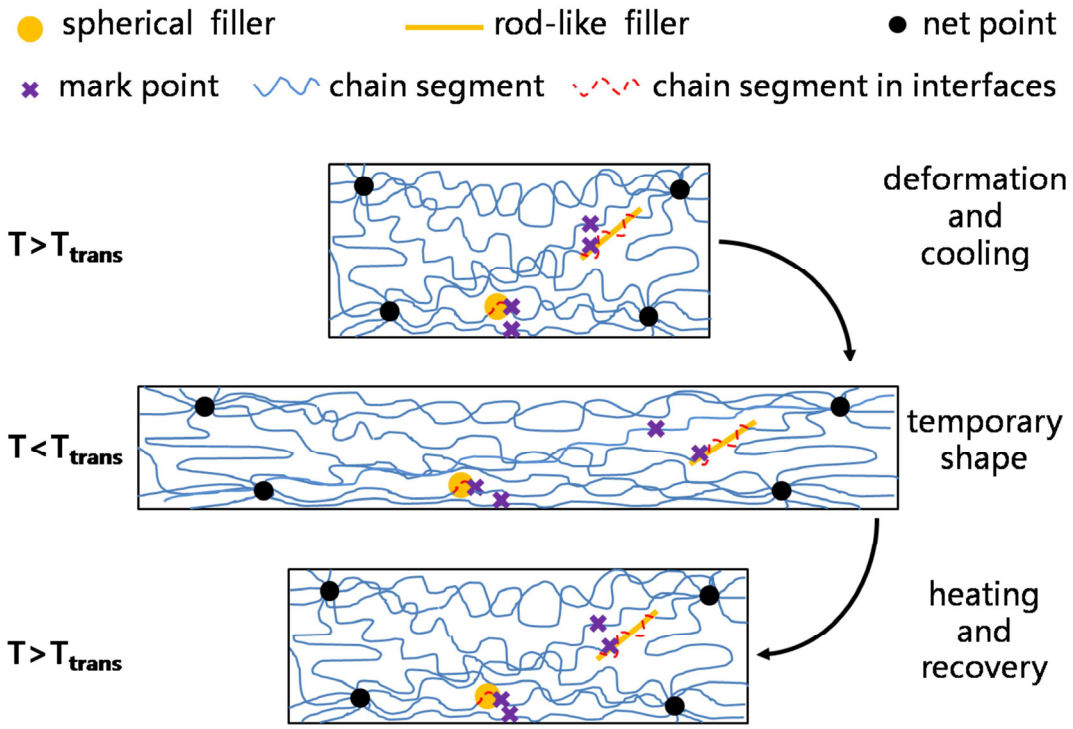

Figure 3-3. Schematic illustration of the molecular mechanism of SMCs. Because the chain segments in the interfaces are restricted by fillers, their deformation is less than that of their neighbors. This difference in deformation

(indicated by mark points) gives rise to the relative slippages between the chain segments in the interfaces and their neighbors. As a result, the relative slippages increase the final irrecoverable strains.

3.3.5. Effects induced by fillers on recovery rates

The above analyses reveal that fillers bind their neighboring chain segments together by the interfaces. Evidently, the interfaces are able to protect the chain segments bonded on the surfaces of fillers from slipping off each other. This effect of fillers would be benefit to improve recovery rates because it is similar to the role of netpoints to suppress chain slippages [4, 38, 41, 42], the main reason for irrecoverable strains [41, 42], by cross-links. Thus, the first effect of fillers is named the "cross-link" effect.

On the other hand, fillers would result in relative slippages between the chain segments in the interfaces and their neighbors. For the purpose of illustrating the relative slippages visually, some mark points are used in Figure 3-3. Because the deformation of the chain segments in the interfaces is much less than that of their neighbors at temperature above T_{trans}, the chain segments in the interfaces would slip past their neighbors during the molecular movements. In other words, fillers bring additional chain slippages. To make the chain slippages induced by fillers readily understandable, an ideal example is illustrated in Figure 3-4. It is assumed that the initial conformations of all chain segments are the same and the central points of both chain segments and fillers keep the position unchanged during the shape memory behaviors. However, Figure 3-4

exhibits that the relative slippages (shown by the mark points) still occur between the chain segments in the interfaces and their neighbors. At temperature above T_{trans}, the chain segments out of the interfaces deform largely while the chain segments in the interfaces are restricted to coiled conformations by fillers. Even though in such perfect conditions, the relative slippages cannot be avoided yet. In reality, the conformations of chain segments are random and fillers also move with the chain segments in the interfaces, so the relative slippages induced by fillers should be unavoidable. Consequently, the second effect of fillers is called "slippage" effect which is harmful to recovery rates.

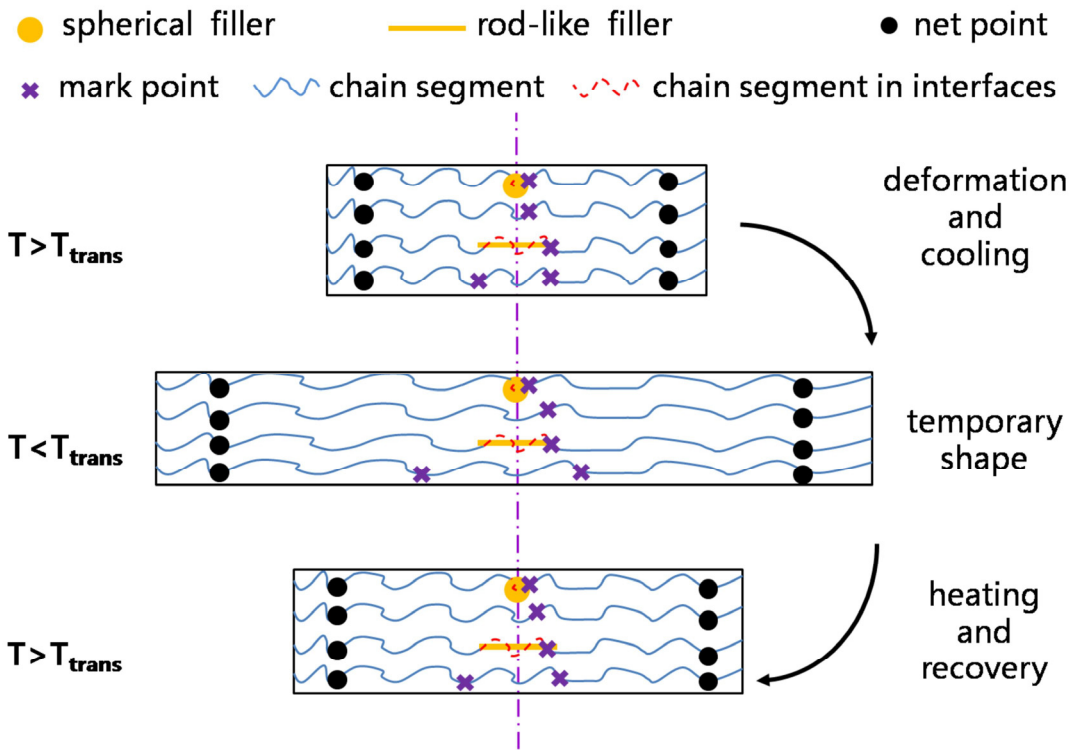

Figure 3-4. Schematic illustration of the inevitable relative slippages. Even if given the same initial conformations of chain segments and the unchanged positions of central points of fillers and chain segments, the relative slippages still occur between the chain segments in the interfaces and their neighbors. In reality,

the conformations of chain segments are random and fillers also move with the chain segments in the interfaces, so the relative slippages should be unavoidable.

At this point, the two effects, "cross-link" effect and "slippage" effect, seem to be paradoxical. This ostensible contradiction would be solved in the section 3.3.6. The analyses of the two above effects disclose that the interfaces are the direct reason for variations in recovery rates. Therefore, the two effects of fillers are exactly the ones of the interfaces.

3.3.6. Experimental evidence for "cross-link" and "slippage" effect

Here, PZT particles and TiO_2 whiskers are chosen with the intention of avoiding repeating others' work and making conclusions more general, because these two kinds of fillers are hardly doped in SMPs rather than the popular fillers like carbon nano tubes and graphene. In addition to PZT 60%, PZT 70% and PZT 80%, SMCs with different contents of TiO_2 whiskers are prepared respectively, such as TiO_2 1% (wt%), TiO_2 3% (wt%), TiO_2 5% (wt%), TiO_2 7% (wt%) and TiO_2 45% (wt%). These SMCs are divided into two groups depending on whether they are hot-pressed or not. The FE-SEM images of first group members, PZT 60% (Fig. 3-5a), PZT 70% (Fig. 3-5b), PZT 80% (Fig. 3-5c), TiO_2 1% (Fig. 3-5d), TiO_2 3% (Fig. 3-5i), TiO_2 5% (Fig. 3-5j), TiO_2 7% (Fig. 3-5k) and TiO_2 45% (Fig. 3-5l), show that PZT particles and TiO_2 whiskers are embraced tightly by SMP matrices and no gap exists between fillers and SMP matrices. In opposite, poor

interfaces of the second group members are verified by Figure 3-5e-h and Figure 3-5m-p, PZT 60%-N (Fig. 3-5e), PZT 70%-N (Fig. 3-5f), PZT 80%-N (Fig. 3-5g), TiO_2 1%-N (Fig. 3-5h), TiO_2 3%-N (Fig. 3-5m), TiO_2 5%-N (Fig. 3-5n), TiO_2 7%-N(Fig. 3-5o) and TiO_2 45%-N (Fig. 3-5p). Evident gaps exist between fillers and SMP matrices. Because the apparent distinction in the interfaces of these two groups is the only difference, the following experiment results supply strong evidence for the effects of interfaces on recovery rates.

Before the discussion on the experimental results, a principle for designing the recovery rate measurements should be explained. Recovery rates are measured with a uniaxial tension test in this study. If samples are uniaxially stretched by the same stress, their chain segments would be under the same stress condition and the strains of free chain segments (all chain segments in pristine SMP and the ones out of the interfaces in the SMCs) would be the same or very close according to $\varepsilon = \sigma / E$, where σ is the stress, E is the elastic modulus and ε is the strain. According to the molecular mechanism of SMCs, the free chain segments are the main part to perform the shape memory behaviors. That's why the designed experiments are carried out under the same stress condition, even if the macroscopic strains (total strains) of different samples are different. If samples with different fillers or different filler contents are tested under the same macroscopic strains condition, the strains of free chain segments would be different due to the almost ignorable strains and different amount of the chain segments in the interfaces. Thus, to

eliminate the factors affecting recovery rates as many as possible, the measurements are executed under the same stress condition.

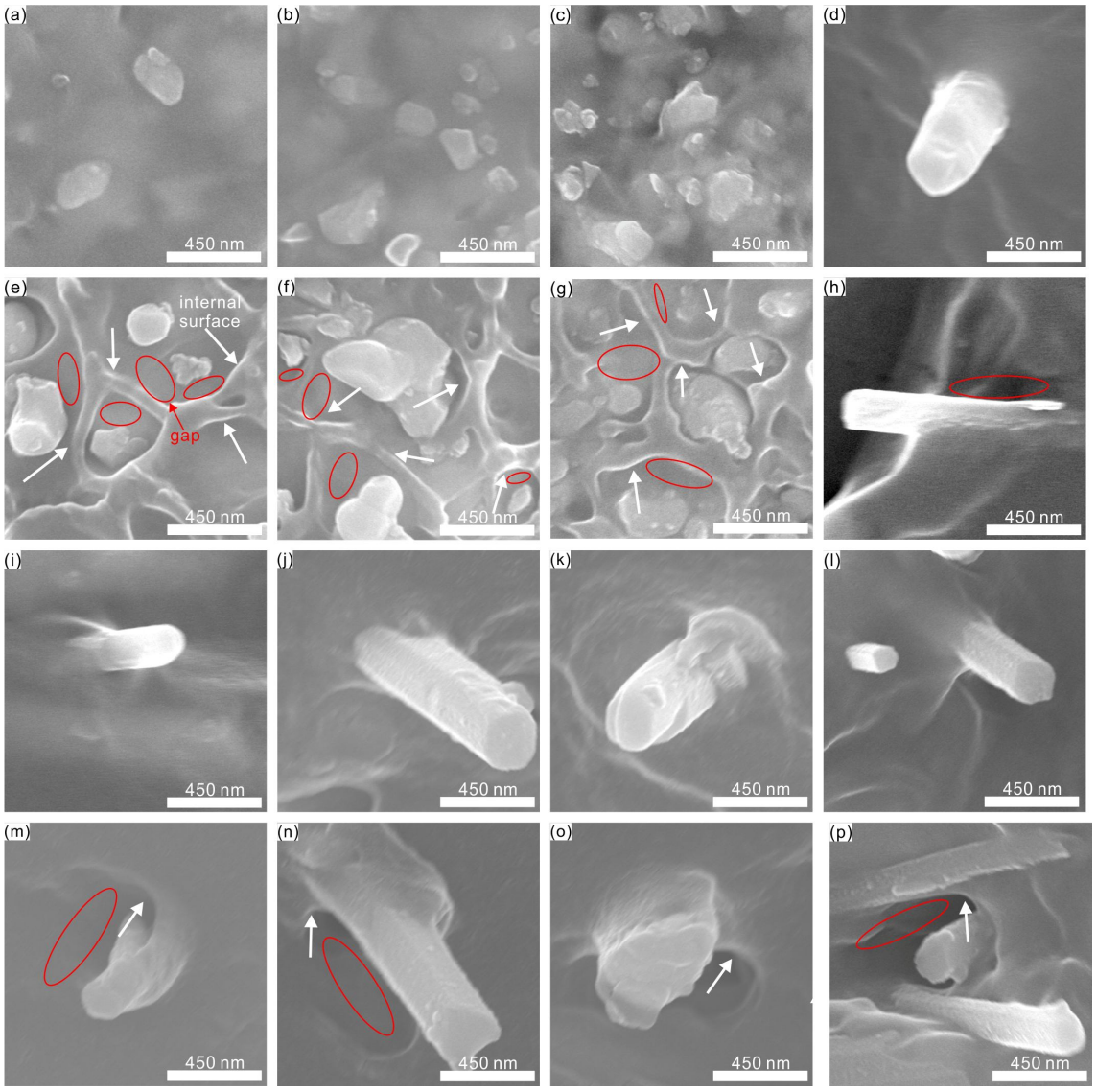

Figure 3-5. FE-SEM images of SMCs. (a) PZT 60%, (b) PZT 70%, (c) PZT 80%, (d) TiO_2 1%, (e) PZT 60%-N, (f) PZT 70%-N, (g) PZT 80%-N, (h) TiO_2 1%-N, (i) TiO_2 3%, (j) TiO_2 5%, (k) TiO_2 7%, (l) TiO_2 45%, (m) TiO_2 3%-N, (n) TiO_2 5%-N, (o) TiO_2 7%-N and (p) TiO_2 45%-N. (a-d, i-l) PZT particles and TiO_2 are embraced by SMP matrices tightly. (e-h, m-p) The gaps between fillers and matrices illustrate

the poor interfaces.

Table 3-3. Recovery rates of the pristine SMP and SMCs

	1st cycle (%)	2nd cycle (%)	3rd cycle (%)
Pristine SMP	$92.9^{+0.1}_{-0.1}$ a)	$97.1^{+0.1}_{-0.1}$	$98.1^{+0.1}_{-0.1}$
PZT 60%	$90.3^{+0.2}_{-0.4}$	$97.0^{+0.2}_{-0.1}$	$98.1^{+0.3}_{-0.2}$
PZT 70%	$84.8^{+0.3}_{-0.3}$	$95.4^{+0.3}_{-0.3}$	$97.6^{+0.3}_{-0.2}$
PZT 80%	$75.8^{+0.3}_{-0.4}$	$91.8^{+0.7}_{-0.6}$	$95.5^{+0.3}_{-0.3}$
TiO_2 1%	$93.1^{+0.1}_{-0.1}$	$97.3^{+0.1}_{-0.1}$	$98.2^{+0.1}_{-0.2}$
TiO_2 3%	$93.6^{+0.2}_{-0.1}$	$97.3^{+0.1}_{-0.1}$	98.3^{+0}_{-0}
TiO_2 5%	$93.3^{+0.2}_{-0.2}$	$97.3^{+0.1}_{-0.1}$	$98.2^{+0.1}_{-0.1}$
TiO_2 7%	$93.0^{+0.2}_{-0.1}$	$97.4^{+0.1}_{-0.1}$	$98.1^{+0.1}_{-0.0}$
TiO_2 45%	$75.2^{+0.8}_{-0.7}$	$93.0^{+0.8}_{-0.7}$	$95.9^{+0.3}_{-0.2}$
PZT 60%-N	$87.5^{+0.4}_{-0.9}$	$95.5^{+0.5}_{-0.8}$	$97.0^{+0.2}_{-0.4}$
PZT 70%-N	$80.2^{+1.3}_{-1.9}$	$93.1^{+0.6}_{-0.8}$	$96.0^{+0.3}_{-0.5}$
PZT 80%-N	$70.8^{+2.7}_{-4.8}$	$89.6^{+1.7}_{-2.1}$	$93.2^{+1.1}_{-1.9}$
TiO_2 1%-N	$92.7^{+0.1}_{-0.1}$	$97.0^{+0.2}_{-0.2}$	$97.8^{+0.1}_{-0.1}$
TiO_2 3%-N	$93.3^{+0}_{-0.1}$	$96.9^{+0.3}_{-0.3}$	$97.9^{+0.3}_{-0.2}$
TiO_2 5%-N	$92.5^{+0.5}_{-0.5}$	$96.9^{+0.1}_{-0.1}$	$98.0^{+0.1}_{-0.1}$
TiO_2 7%-N	$92.0^{+0.4}_{-0.3}$	$97.0^{+0.2}_{-0.2}$	$97.8^{+0.2}_{-0.1}$
TiO_2 45%-N	$70.6^{+0.8}_{-1.4}$	$91.5^{+0.4}_{-0.3}$	$94.8^{+0.3}_{-0.3}$

a)Main values are the average recovery rates.

Table 3-3 summarizes recovery rates which are measured in a typical three cycle method described in the section 3.2.4. In the first cycle, compared with the pristine SMP, PZT 60% shows a bit lower recovery rates, PZT 70% exhibits further decrease in recovery rates, PZT 80% and TiO_2 45% perform grave reduction in recovery rates, but

TiO_2 3% and TiO_2 5% increase a little in recovery rates (TiO_2 1% and TiO_2 7% do not display a clear change in recovery rates.). In the second cycle and third cycle, the recovery rates of the pristine SMP, PZT 60%, TiO_2 1%, TiO_2 3%, TiO_2 5% and TiO_2 7% are close to each other, but PZT 80%, PZT 70% and TiO_2 45% perform lower recovery rates. All samples show increasing recovery rates with the number of cycles on account of the programming ability of SMPs and SMCs. As it is explained in section 3.3.1, the stress in three cycles are the same and the latter two cycles are actually the repeats of the first cycle. After the main irrecoverable strains are left in the first cycle, most of the strains occurring in the second cycle are recoverable. The third cycle is similar. Therefore, the recovery rates in the first cycle are the best ones to analyze the reason for variations in recovery rates of SMCs due to the occurrence of main irrecoverable strains. To illustrate the shape recovery performances visually, bending deformation recovery of SMCs is shown in Figure 3-6.

The recovery rates of the pristine SMPU, PZT 60%, PZT 70% and PZT 80% decrease in sequence in the first cycle. It illustrates that recovery rates reduce with the increase in the amount of interfaces, because more interfaces would induce more relative displacements resulting in more chain slippages according to the "slippage" effect. On the other hand, the recovery rates of TiO_2 3% and TiO_2 5% are slightly higher than that of pristine SMP, but these are not convincing proof to support the "cross-link" effect. However, it is difficult to impressively improve the recovery rates of SMCs due to the

good recovery rates of SMP matrices and existence of the "slippage" effect. Therefore, to prove the "cross-link" effect more strongly, the samples with poor interfaces are tested in the same three cycle method. Experimental results show decreased recovery rates in the first cycle. Why do recovery rates reduce? The reason is the gaps between fillers and SMP matrices (Fig. 3-5e-h and Fig. 3-5m-p). The gaps would give rise to more chain slippages because they lead to internal surfaces (Fig. 3-5e-h and Fig. 3-5m-p) which lack cross-links. However, fillers are able to cross-link the internal surfaces by interfaces. Fig. 3-5a-d and Fig. 3-5i-l visually demonstrate the ability of fillers to bind the surrounding chain segments together.

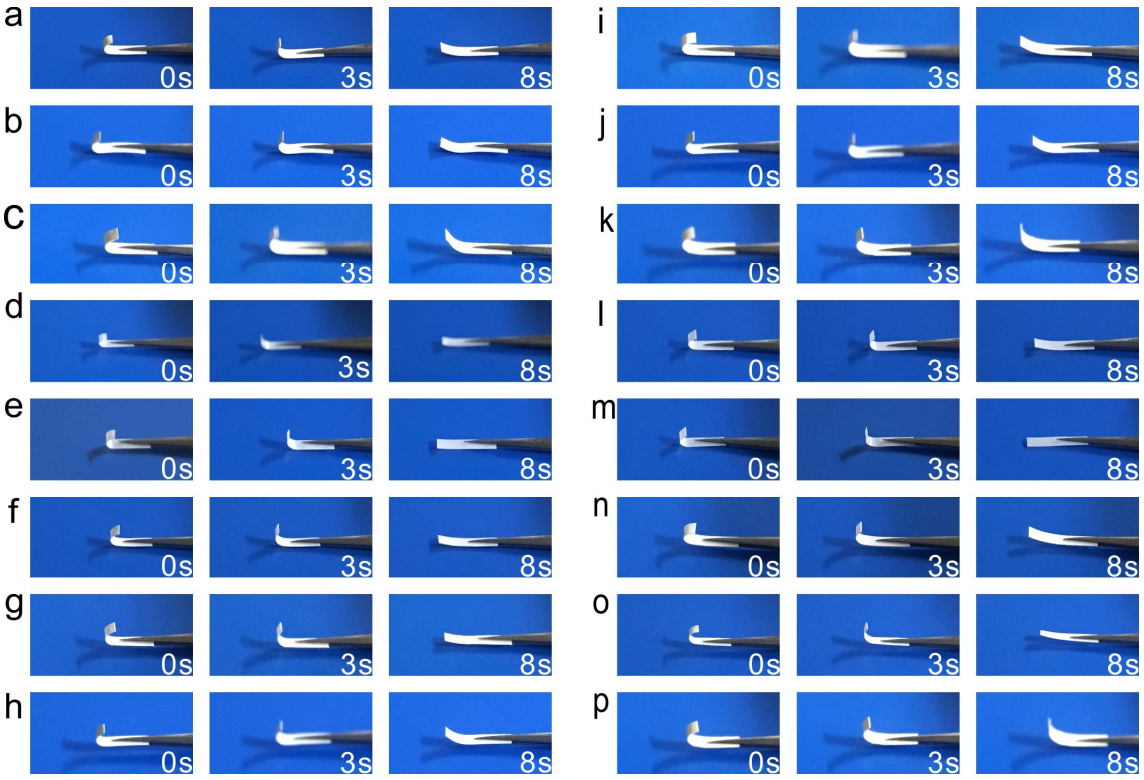

Figure 3-6. Shape recovery process of bending deformation in the first cycle. (a) PZT 60%-HP, (b) PZT 70%-HP, (c) PZT 80%-HP, (d) TiO_2 1%-HP, (e) TiO_2 3%-HP, (f) TiO_2 5%-HP, (g) TiO_2 7%-HP, (h) TiO_2 45%-HP, (i) PZT 60%-N, (j) PZT 70%-N,

(k) PZT 80%-N, (l) TiO_2 1%-N, (m) TiO_2 3%-N, (n) TiO_2 5%-N, (o) TiO_2 7%-N, and (p) TiO_2 45%-N. The samples are heated up to 70 °C after their bending deformation is fixed.

The "cross-link" effect and "slippage" effect have been demonstrated by the experimental results, but they should be uneven in most cases. Otherwise recovery rates of SMCs would be changeless. Which one is predominant? It depends on how much "pure SMP slippages" (defined in the end of this paragraph) in SMPs and SMCs before adding fillers. For easier understanding, two extremely ideal cases are given: If fillers are added into SMP matrices with recovery rates of 100% (no chain slippage), there would be total no chance for fillers to perform the "cross-link" effect; on the contrary, if fillers are added into SMP matrices with recovery rates of 0%, there would be total no chance for fillers to perform the "slippage" effect due to the impossibility of recovery rates in minus values. If there are a lot of "pure SMP slippages", the "cross-link" effect would become dominant. Compared with the samples with poor interfaces, the fillers in the hot-pressed samples mainly show the "cross-link" effect because the samples with poor interfaces contain many "pure SMP slippages" caused by the gaps or internal surfaces. The "pure SMP slippages" would be less and less with adding more fillers, while the "slippage" effect would gradually predominate. TiO_2 1% reveals the trend of TiO_2 whiskers to improve recovery rates, TiO_2 3% shows the improvement in recovery rates, but TiO_2 5% and TiO_2 7% perform the gradual reduction in recovery rates with increasing fillers due to enhanced the "slippage" effect resulting from the decrease of "pure SMP slippages". TiO_2

45% exhibits a large decline in recovery rates because of the much fewer "pure SMP slippages". The recovery rates of TiO_2 7% are very close to those of pristine SMP, because the two effects almost equal to each other. TiO_2 1% is also similar in recovery rates but it is the result of the weak "cross-link" effect due to too few fillers. After the "slippage" effect becomes the main effect, more fillers would lead to lower recovery rates. Therefore, the recovery rates of PZT 60% are less than those of PZT 70%, and the recovery rates of PZT 70% are less than those of PZT 80%. ("Pure SMP slippages" are defined as the chain slippages, excluding the ones induced by interfaces, which can be depressed by the "cross-link" effect. The chain slippages induced by interfaces are almost incapable of being depressed by adding more fillers. The chain slippages induced by interfaces occur between the chain segments in interfaces and their neighbors, so new added fillers need precisely locate between the chain segments in interfaces and their neighbors to decrease these chain slippages, according to the "cross-link" effect. However, the possibility of two fillers sharing one chain segment could be neglected in consideration of filler dispersion in the synthesis of SMCs.)

3.3.7. Unstable programming ability of SMPs and SMCs

The stability of programming ability of SMPs and SMCs are studied. The experimental results of the two groups reveal the programming ability of SMCs, whereas, if the loading stresses change, the programming ability would fail (Figure 3-7b). Hence,

programming in advance is unable to totally solve the problem that recovery rates vary in the practical usage. Here, just the experimental results of the pristine SMP, PZT 60%-HP and PZT 80%-HP are given because the shape recovery behaviors of TiO_2 1%-HP, TiO_2 3%-HP, TiO_2 5%-HP and TiO_2 7%-HP are similar to those of the pristine SMP, the shape recovery behaviors of TiO_2 45%-HP are similar to those of PZT 80%-HP, and PZT 70%-HP is just the transition from PZT 60%-HP to PZT 80%-HP. The experimental results show that recovery rates obey the programming ability form the first cycle to the second cycle and from the third cycle to forth cycle, however, a drop in recovery rates comes up from the second cycle to the third cycle due to the increase of the maximum stresses from 2.5 MPa (the second cycle) to 3.5 MPa (the third cycle). Figure 3-7a exhibits the augment of strains from the second cycle to the third cycle (even pristine SMP), as a consequence, the new incremental strains would create new chain slippages resulting in the reduce of recovery rates. The amount of drop in recovery rates (pristine SMP 1.9%, PZT60% 2.1% and PZT80% 5.8%) is proportional to the content of fillers or the amount of interfaces due to the "slippage effect" of interfaces. Therefore, the programming ability is only suitable for the repeated loads case and would be ineffective if the loads change largely enough (the amount of irrecoverable strains removed by repeating present cycle is less than that resulted from the new incremental strains).

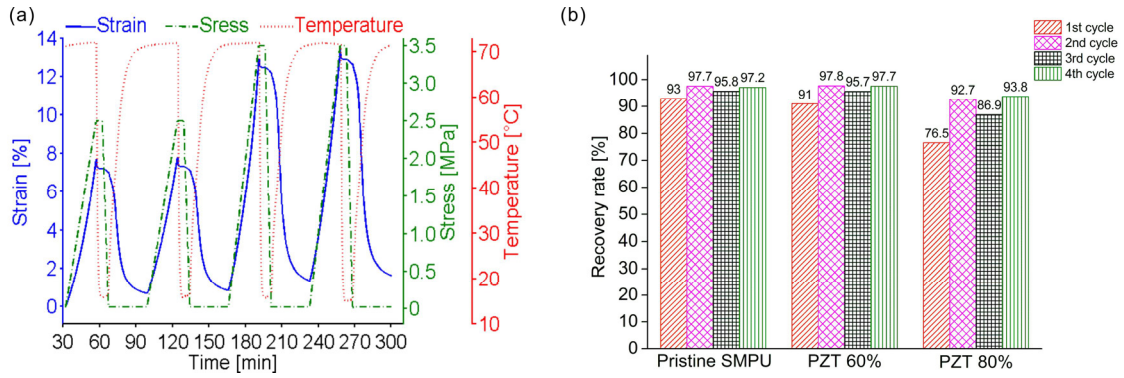

Figure 3-7. Recovery rate tested in a four cycle method. (a) The curves of strain, stress and temperature versus time in the consecutive shape memory processes of PZT 60% in four cycles. In this four cycle method, the maximum loaded stress increases from 2.5 MPa in the first two cycles to 3.5 MPa in the last two cycles. (b) The comparison in recovery rates in four cycles of pristine SMP, PZT 60% and PZT 80%.

3.3.8. Discussion and limit on molecular mechanism of SMCs

Now, we know the reason for the decrease in recovery rates of SMCs with excellent SMP matrices with good recovery rates [27-30], and the increment in recovery rates of SMCs combining SMP matrices with weak recovery rates [31, 32]. Moreover, the fluctuations in recovery rates of SMC fibers (the recovery rates of SMCs firstly go up and then go down with continuously increasing CNTs) are able to be explained too [39]. At first, considerable "pure SMP slippages" exist in the pristine SMP used in the reference 33 (the recovery rate is just 83.5%), so the "cross-link" effect reduces the "pure SMP slippages" effectively. As a result, the recovery rate of SMC fiber with 1% CNTs is improved by 7%, because the "slippage" effect is weak due to 1% CNTs. But with the

content of CNTs rising up, the "slippage" effect would be stronger and stronger while the "cross-link" effect would reach the maximum limitation. For example, if the efficacy of the two effects keep the same, the recovery rate of SMC fiber with 3% CNTs would be increased to 104.5%. Actually, that's impossible. After the "cross-link" effect reaches its limitation (the ideal case is that the "pure SMP slippages" are completely removed), the "slippage" effect would generally become predominant. Thus, the actual recovery rate of SMC fiber with 3% CNTs is 87%. In fact, the reference 39 exactly supplies evidences to support the two effects of interfaces on recovery rates, even though the given explanation contradicts the experimental results.

Finally, this study focuses on analyzing the effects of interfaces on recovery rates of SMCs, so it is unsuitable to explain shape recovery behaviors of the SMCs without interfaces such as some special SMCs synthesized by grafting the polymer chain segments onto the fillers [43-45]. I In these special SMCs, fillers are the actual netpoints and the interactions between fillers and matrices are like point connections.

3.4. Conclusions

PZT / SMPU composites show good shape memory performances even with high content of PZT particles. The addition of PZT particles give rise to the significant increase of recovery stresses because of the outstanding improvement in elastic moduli above T_g. PZT 60%, PZT 70% and PZT 80% obtain the maximum recovery stresses

which are respectively 233%, 244% and 430% as much as that of pristine SMPU. Even if the recovery rates decrease as the PZT particles increase, all of PZT / SMPU composites exhibit the recovery rates no less than 94.5% in the third cycle. These results are actually strong evidences to demonstrate the shape memory effect of PZT / SMPU composites.

Furthermore, with the purpose of understanding the shape memory behaviors of SMCs deeply, the molecular mechanism of SMCs is established upon the molecular mechanism of SMPs by taking account of the two differences between the molecular motions of SMPs and SMCs. The analyses on the molecular motion of SMCs reveal that interfaces are responsible for the decrease and increase in recovery rates of SMCs due to the "cross-link" effect and "slippage" effect of interfaces. The "cross-link" effect is benefit for recovery rates due to the ability of interfaces to bind fillers and their surrounding chain segments together, but the "slippage" effect inversely has an negative effect on recovery rates because of the relative slippages between the chain segments in the interfaces and their neighbors. The two effects are both demonstrated by the designed experiments and some conclusions are summarized as following:

(1) The "cross-link" effect and "slippage" effect of interfaces influence recovery rates at the same time.

(2) The "cross-link" effect and "slippage" effect of interfaces is proportional to the amount of interfaces (the amount of fillers in the case of same fillers).

(3) Which effect is main one that is dependent on how much the existing "pure SMP slippages".

(4) If the existing "pure SMP slippages" are quite a lot, the "cross-link" effect would be dominant and the "pure SMP slippages" would be reduced. As fillers increase, the "slippage" effect would be gradually predominant.

Moreover, the variations in recovery rates of SMCs can be predicted qualitatively. The qualitative predictions are as following:

(1) The predictions need given recovery rates of SMCs with a certain filler content (M wt%).

(2) If the SMCs with M wt% fillers (PZT 60%) perform a little decrease in recovery rates or the same recovery rates, in contrast with the pristine SMPs, SMCs with N wt% fillers (N>M, PZT 70% and PZT 80%) would perform an further reduction in recovery rates. Recovery rates would continue dropping as fillers increase.

(3) If the SMCs with M wt% fillers exhibit an improvement in recovery rates, compared with the pristine SMPs, SMCs with N wt% fillers would show two possible changes in recovery rates. The first one is that if M (TiO_2 1%) is less than the critical value at which the "cross-link" effect reaches the maximum effect, the recovery rates of SMCs with N wt% fillers (TiO_2 3%) would increase with the amount of fillers. But after N reaches the above critical value (TiO_2 3% can represent this case), the recovery rates of SMCs with N wt% fillers would reduce with increasing fillers (TiO_2 5%, TiO_2 7% and TiO_2 45%). On

the other hand, if M is no less than the above critical value (TiO_2 3% and TiO_2 5%), the recovery rates of SMCs with N wt% fillers would decline with the increase of fillers (TiO_2 7% and TiO_2 45%).

Reference

1. Lendlein, S. Kelch, Shape-memory polymers, *Angewandte Chemie International Edition*, 2002, 41: 2034-2057.

2. M. Behl, A. Lendlein, Shaper-memory polymers, *Materials Today*, 2007, 10: 20-28.

3. C. Liu, H. Qin, P. T. Mather, Review of progress in shape-memory polymers, *Journal of Materials Chemistry*, 2007, 17: 1543-1558.

4. P. T. Mather, X. Luo, I. A. Rousseau, Shape memory polymer research, *Annual Review of Materials Research*, 2009, 39: 445-471.

5. D. Ratna, J. Karger-Kocsis, Recent advances in shape memory polymers and composites: a review, *Journal of Materials Science*, 2008, 43: 254-269.

6. Y. Liu, H. Du, L. Liu, J. Leng, Shape memory polymers and their composites in aerospace applications: a review, *Smart Materials and Structures*, doi:10.1088/ 0964-1726/23/2/023001.

7. I. A. Rousseau, Challenges of shape memory polymers: a review of the progress toward overcoming SMP's limitations, *Polymer Engineering and Science*, 2008, 48: 2075-2089.

8. Y. Wang, G. Zhu, X. Cui, Electroactive shape memory effect of radiation cross-linked SBS/LLDPE composites filled with carbon black, *Colloid and Polymer Science*, doi: 10.1007/s00396-014-3266-0.

9. Z. Tang, D. Sun, D. Yang, Vapor grown carbon nanofiber reinforced bio-based polyester for electroactive shape memory performance, *Composites Science and Technology*, 2013, 75: 15-21.

10. X. Luo, P. T. Mather, Conductive shape memory nanocomposites for high speed electrical actuation, *Soft Matter*, 2010, 6: 2146-2149.

11. H. Lu, Y. Liu, J. Leng, Carbon Nanopaper Enabled Shape Memory Polymer Composites for Electrical Actuation and Multifunctionalization, *Macromolecular Materials and Engineering*, 2012, 297: 1138-1147.

12. S. M. Oh, K. M. Oh, T. D. Dao, The modification of graphene with alcohols and its use in shape memory polyurethane composites, *Polymer International*, 2013, 62: 54-63.

13. J. T. Choi, T. D. Dao, K. M. Oh, Shape memory polyurethane nanocomposites with functionalized graphene, *Smart Materials and Structures*, doi:10.1088/0964-1726/21/7/075017.

14. J. W. Cho, J. W. Kim, C. J. Yong, Electroactive shape-memory polyurethane composites incorporating carbon nanotubes, *Macromolecular Rapid Communications*, 2005, 26: 412-416.

15. N. G. Sahoo, Y. C. Jung, H. J. Yoo, Influence of carbon nanotubes and polypyrrole on

the thermal, mechanical and electroactive shape-memory properties of polyurethane nanocomposites, *Composites Science and Technology*, 2007, 67: 1920-1929.

16. F.-P. Du, E.-Z. Ye, W. Yang, Electroactive Shape memory polymer based on optimized multi-walled carbon nanotubes/polyvinyl alcohol nanocomposites, *Composites Part B*, 2015, 68: 170-175.

17. M. Raja, S. H. Ryu, A. M. Shanmugharaj, Influence of surface modified multiwalled carbon nanotubes on the mechanical and electroactive shape memory properties of polyurethane (PU)/poly(vinylidene diflouride) (PVDF) composites, *Colloids and Surfaces A*, 2014, 450: 59-66.

18. H. Koerner, G. Price, N. A. Pearce, Remotely actuated polymer nanocomposites—stress-recovery of carbon-nanotube-filled thermoplastic elastomers, *Nature Materials*, 2004, 3: 115-120.

19. K. Yu, Y. Liu, J. Len, Shape memory polymer/CNT composites and their microwave induced shape memory behaviors, *RSC Advances*, 2014, 4: 2961-2968.

20. J. Liang, Y. Xu, Y. Huang, Infrared-triggered actuators from graphene-based nanocomposites, *The Journal of Physical Chemistry C*, 2009, 113: 9921-9927.

21. Z. He , N. Satarkar , T. Xie, Remote controlled multishape polymer nanocomposites with selective radiofrequency actuations, *Advanced Materials*, 2011, 23: 3192-3196.

22. Q. Peng, H. Wei, Y. Qin, Shape-memory polymer nanocomposites with a 3D conductive network for bidirectional actuation and locomotion application, *Nanoscale*,

2016, 8: 18042-18049.

23. X. Liu, H. Li, Q. Zeng, Y, Electro-active shape memory composites enhanced by flexible carbon nanotube / graphene aerogels, *Journal of Materials Chemistry A*, 2015, 3: 11641-11649.

24. G. Yu, H. Chen, W. Wang, Influence of sepiolite on crystallinity of soft segments and shape memory properties of polyurethane nanocomposites, *Polymer Composites*, doi :10.1002/pc.24115.

25. Y. Sun, Y. Luo, Y. Dong, Shape memory and mechanical properties of silk fibroin/poly(ε-caprolactone) composites, *Materials Letters*, 2017, 193: 26-29.

26. X. Xiao, T. Xie and Y.-T. Cheng, Self-healable graphene polymer composites, *Journal of Materials Chemistry*, 2010, 20: 3508-3514.

27. K. Galla, , M. L. Dunn, Y. Liu, Shape memory polymer nanocomposites, *Acta Materialia*, 2002, 50: 5115-5126.

28. F. Cao, S. C. Jana, Nanoclay-tethered shape memory polyurethane nanocomposites, *Polymer*, 2007, 48: 3790-3800.

29. F. Li, L. Qi, J. Yang, Polyurethane/conducting carbon black composites: structure, electric conductivity, strain recovery behavior, and their relationships, *Journal of Applied Polymer Science*, 2000, 75: 68-77.

30. G. Yu, H. Chen, W. Wang, Influence of sepiolite on crystallinity of soft segments and shape memory properties of polyurethane nanocomposites, *Polymer Composites*,

doi:10.1002 pc.24115.

31. A. Saralegi, S. C. M. Fernandes, A. Alonso-Varona, Shape-memory bionanocomposites based on chitin nanocrystals and thermoplastic polyurethane with a highly crystalline soft segment, *Biomacromolecules*, 2013, 14: 4475-4482.

32. M. Yoonessi, Y. Shi, D. A. Scheiman, graphene polyimide nanocomposites; thermal, mechanical, and high-temperature shape memory effects, *ACS Nano*, 2012, 6: 7644-7655.

33. Y. Zare, Determination of polymer–nanoparticles interfacial adhesion and its role in shape memory behavior of shape memory polymer nanocomposites, *International Journal of Adhesion & Adhesives*, 2014, 54: 67-71.

34. T. Qiao, L. Liu, Y. Liu, Thermal mechanical constitutive model of fiber reinforced shape memory polymer composite: based on bridging model, *Composites: Part A*, 2014, 64: 132-138.

35. M. Behl, A. Lendlein, Shape memory polymers, *Materials Today*, 2017, 10: 20-28.

36. A. Lendlein, S. Kelch, Shape memory effect, *Angewandte Chemie International Edition*, 2002, 41: 2034-2057.

37. C. Liu, H. Qin, P. T. Mather, Review of progress in shape-memory polymers, *Journal of Materials Chemistry*, 2007, 17: 1543-1558.

38. X. Feng, G. Zhang, S. Zhuo, Dual responsive shape memory polymer/clay nanocomposites, *Composites Science and Technoogy*, 2016, 129: 53-60.

39. Q. Meng, J. Hu, Y. Zhu, Shape-memory polyurethane/multiwalled carbon nanotube fibers, *Journal of Applied Polymer Science*, 2007, 106: 837-848.

40. I. A. Rousseau, P. T. Mather, Shape memory effect exhibited by smectic-C liquid crystalline elastomers, *Journal of American Chemistry Society*, 2003, 125: 15300-15301.

41. Y. S. Wong, Y. Xiong, S. S. Venkatraman, Shape memory in un-cross-linked biodegradable polymers, *Journal of Biomaterials Science, Polymer Edition*, 2008, 19: 175-191.

42. T. Xie, Recent advances in polymer shape memory, *Polymer*, 2011, 52: 4985-5000.

43. J. Xu, W. Shi, W. Pang, Synthesis and shape memory effects of Si–O–Si cross-linked hybrid polyurethanes, *Polymer*, 2006, 47: 457-465.

44. Y. Zhang, Q. Wang, C. Wang, High-strain shape memory polymer networks crosslinked by SiO_2 *Journal of Materials Chemistry*, 2011, 21: 9073-9078.

45. L. Bombalski, H. Dong, J. Listak, Null-scattering hybrid particles using controlled radical polymerization, *Advanced Materials*, 2007, 19: 4486-4490.

Chapter 4

Piezoelectric performances and nanopositioning in the common environment

Chapter 4: Piezoelectric performances and nanopositioning in the common environment

4.1. Introduction

PZT is a kind of piezoelectric material which has been widely used in aerospace, medical device, microelectromechanical system, health monitoring, nanomachining and many other industries. The nanogenerators made from PZT have been even presented over recent years [1]. But the brittleness still critically limits its applications. Thus, PZT composites are proposed to overcome this weakness. Active fiber composite (AFC) [2,3] and micro fiber composite (MFC) [4] should be the most famous. However, the actual applications of AFC and MFC suggest that the interfaces between PZT fibers and matrices are too weak. Therefore, PZT particulate composites start to attract more attentions [5,6]. To improve piezoelectric constant, different kinds of conductive fillers are added for more effective polarization. Graphene [7], CNTs [7-11], graphite [12-14] and carbon black [15] are employed to synthesize PZT composites to improve the permittivity and conductivity. Surface modification on PZT particles is also used to disperse PZT particles better and reinforce the interfaces of fillers and matrices [16]. But the researches about PZT particulate composites mostly focus on the sensing properties,

dielectric properties and mechanical properties. The actuation performances of PZT particulate composites are hardly reported.

Here, PZT / SMPU composites we prepared show the promising potential in nanopositioning. The composite film actuators can achieve the displacements of 1 nm resolution with the positioning errors no more than ±5 nm without any control method and any controlled experimental environment. It implies the possibility of the PZT / SMPU composites to reduce the costs of nanopositioning. What is more, these film actuators can generate larger displacements with the same positioning errors by deforming them into designed shapes owing to the benefit from the combination of piezoelectricity and shape memory property. Besides, the piezoelectric effect of PZT / SMPU composites without hot-pressing is studied as well with the aim to classify the role of interfaces on piezoelectric effect.

4.2. Materials and methods

4.2.1. Actuators fabrication

P_b-P_t alloy electrodes were sputtered (E-1030, Hitachi Co., Ltd, Japan) on the surfaces of PZT / SMPU composite films. Then the films were polarized at 80 °C for 2h in a silicone oil bath under the electric field of 10 kV/mm supplied by a high voltage power supply (ES30, Gamma High Voltage Research Inc., U.S.A.). The "U" type actuator and "Z" type actuator were simply deformed at 75 °C by hand and fixed the shapes by

cool down to room temperature.

4.2.2. Nanoscale displacement Measurements

The nanoscale displacements were measured by a laser interferometer (SI-F01, Keyence Corp., Japan) with a moving average filter (the mean of 256 points) when the actuators and the laser sensor were fixed with simply designed fixtures (Fig. 1). First, the actuators were fixed on glass slides with glue (a small glass slide with a metal layer on the upper surface was stuck to the top of the "U" type actuator to reflect the laser, but the electrodes on the surfaces of the other actuators were able to reflect the laser). Second, the glass slides with actuators were put into the groove in the designed fixture 1 made of steel and fixed with two magnets (magnet 1 was placed on the upper surface of the hole and magnet 2 was placed on the bottom of the glass slide) by attractive force. The laser sensor was fixed with the designed fixture 2 by a bolted connection (the designed fixtures 1 and 2 were made by the authors). Then designed fixture 1 was fixed in designed fixture 2 by a bolted connection. The applied step voltage signals were generated by a high voltage power supply (HJPQ-30P1, Matsusada Precision Inc., Japan). The data of nanoscale displacements were recorded by the software, SI-Navigator, in a personal computer (PC) that was connected to a control laser sensor through a USB connection. These measurements were implemented without any control on the environmental parameters.

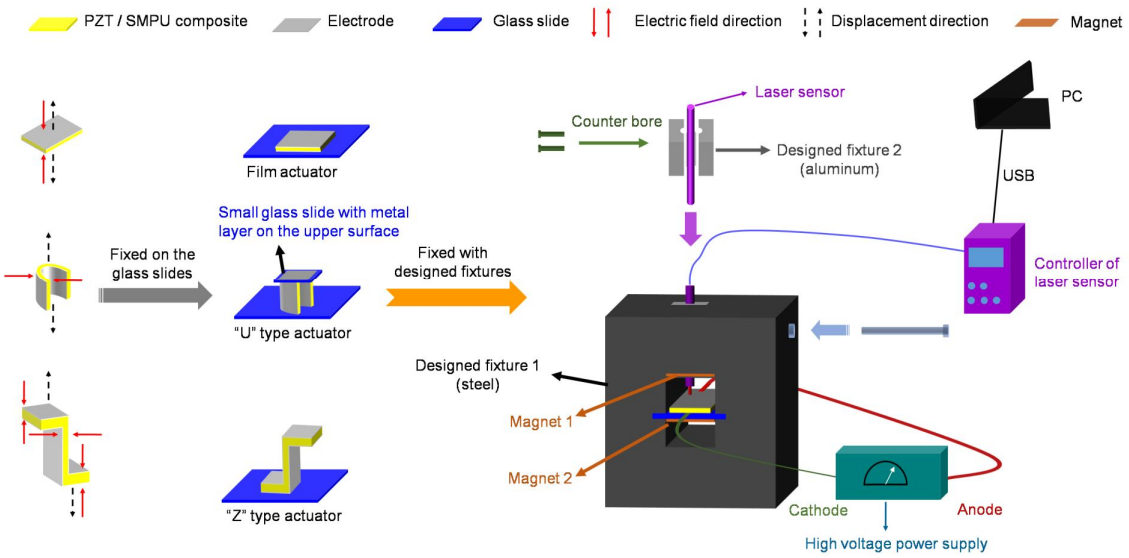

Figure 4-1. Schematic illustration of the displacement measurement system in a common experimental environment.

4.2.3. Relative permittivity

Circular samples with the diameter of 10 mm were measured by a SI 1260 Impedance / Gain-Phase Analyzer (AMETEK Inc., U.S.A.) and 1296A Dielectric Interface System (AMETEK Inc., U.S.A.). The DC voltages (averagely divided into 30 points) from 100 to 500 V were supplied by a high voltage power supply system (High Voltage Interface HVI-1000, TOYO Corp., Japan and Bipolar Operational Power Supply / Amplifier Model BOP 1000M, TOYO Corp., Japan).

4.3. Results and discussion

4.3.1. Piezoelectric Performances and Nanopositioning

The actuation performances of PZT / SMPU composites are measured at a common

laboratory environment without any control on environmental parameters (the measurement system is shown as Figure 4-1). The driving signals are the step signals without any control method and the produced nanoscale displacements are shown in Figure 4-2, PZT 60% (Figure 4-2a,d), PZT 70% (Figure 4-2b,e) and PZT 80% (Figure 4-2c,f) are all able to generate the displacements with the resolution of 1 nm and the positioning errors (measured displacement - desired displacement) are no more than ±5 nm after noise reduction by a moving average filter (the mean of 256 points).The positioning errors are caused by the variations of the environmental parameters (temperature, humidity, air pressure, noise and vibration) and the measurement errors of the laser interferometer mainly as a consequence of the thermal fluctuation [17]. At present, it is generally considered that a controlled environment in closed space [18] or in high vacuum [19] is necessary for the nanopositioning to improve the positioning accuracy by reducing the influence from the ambient disturbances. Actually, the harsh operating environment of nanopositioning further raise the costs up. The high costs of nanopositioning is one of the main reasons for which the industry process is much slower than the process of research. These PZT / SMPU composites demonstrate the possibility to reduce the costs of nanopositioning, even no requirement for a high accuracy controller.

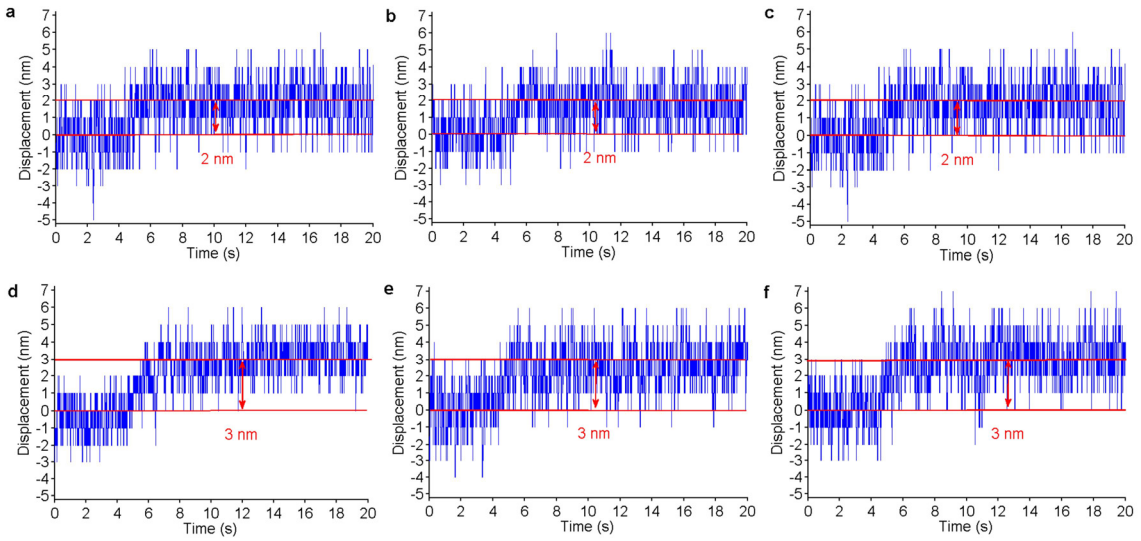

Figure 4-2. Displacement responses of PZT / SMPU composites under step voltage signals. (a) PZT 60% applied a step voltage of 600V. (b) PZT 70% applied a step voltage of 540V. (c) PZT 80% applied a step voltage of 400V. (d) PZT 60% applied a step voltage of 800V. (e) PZT 70% applied a step voltage of 720V. (f) PZT 80% applied a step voltage of 500V. All the displacements are measured under a common experimental environment and the positioning errors are within ±5 nm.

Figure 4-3 illustrates the linear relations of displacements of PZT / SMPU composites and applied voltages. The piezoelectric charge constants (d) of PZT 60%, PZT 70% and PZT 80% are respectively 5 pm/V, 5.6 pm/V and 10 pm/V calculated by piezoelectric charge constant = $\Delta D/\Delta V$, where ΔD is the displacement increment, and ΔV is the voltage increment. In comparison to PZT 60%, PZT 70% increases by only 12% in the piezoelectric charge constant, but PZT 80% shows enhancement by 100% with the addition of more 10% PZT particles in weight. In view of this, PZT 70% is not deformed into a designed shape in the 4.3.2 section.

Besides, the average relative permittivity of PZT 60%, PZT 70% and PZT 80% is 5.4, 6.8 and 7.7 in sequence. The piezoelectric voltage constants (g) of PZT 60%, PZT 70% and PZT 80% are respectively 104.6 mV·m/N, 93.1 mV·m/N and 146.7 mV·m/N, according to piezoelectric voltage constant = piezoelectric charge constant/k_0k [20, 21], where k_0 is the vacuum permittivity, and k is the relative permittivity. The piezoelectric voltage constant of PZT 70% is less than that of PZT 60%, because PZT 70% performs an increase of 12% in the piezoelectric charge constant but an increment of 26% in the relative permittivity.

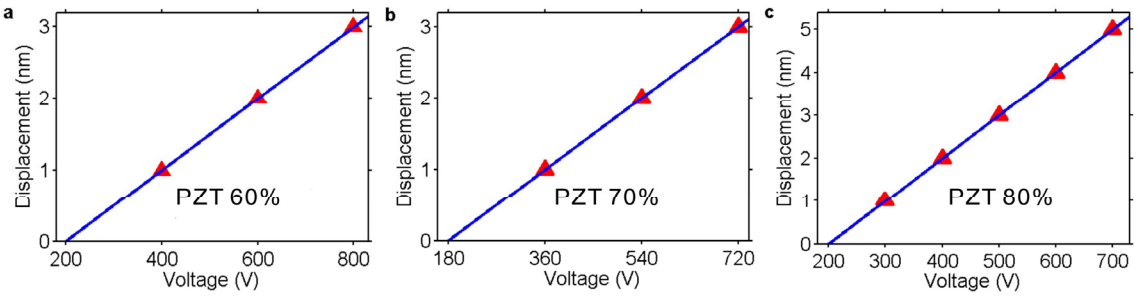

Figure 4-3. Displacements vs. applied voltages. (a) PZT 60%, (b) PZT 70% and (c) PZT 80%. The lines are linear fittings.

4.3.2. Advantages of combining piezoelectric and shape memory effect

The film actuators (Figure 4-4a) just can produce very limited displacements. Generally, for the sake of larger displacements, many layers of actuating materials are stacked together to obtain a stack-like actuator by connecting all anodes together, connecting all cathodes together and then packaging the components [22, 23]. Actually, the difficulty of manufacturing a stack actuator is how to use wires or other mediums for

connecting electrodes on every layer together while achieving a compact structure. The wires or other mediums fixed between layers would result in gaps between layers, which gravely do harm to the performances of the stack actuator. However, PZT / SMPU composite films possess a much more convenient method of achieving larger displacements. Merely taking advantage of the shape memory property, it is easy to deform the films into the designed shapes and the shaped films could generate more displacements as actuators. A "U" type actuator (Figure 4-4b) and a "Z" type actuator (Figure 4-4e) are made of PZT 60% and PZT 80%, respectively. The "U" type actuator generates a displacement of 18 nm under the step signal of 840 V (Figure 4-4d) and the "Z" type actuator produces a displacement of 75 nm under the step signal of 600 V (Figure 4-4g). The average piezoelectric charge constants of the "U" type actuator and the "Z" type actuator are, respectively, about 23.5 pm/V (Figure 4-4c, the slope of linear fitting line) and 133.1 pm/V (Figure 4-4f, the slope of linear fitting line). Simple deformations succeed in improving the piezoelectric charge constant of PZT 60% by about 3.7 times and increasing that of PZT 80% to more than 13.3 times. Moreover, the positioning errors of the "U" type actuator (Figure 4-4d) and "Z" type actuator (Figure 4-4g) are still within ±5 nm. The enlargement of the displacement ranges would not magnify the positioning errors.

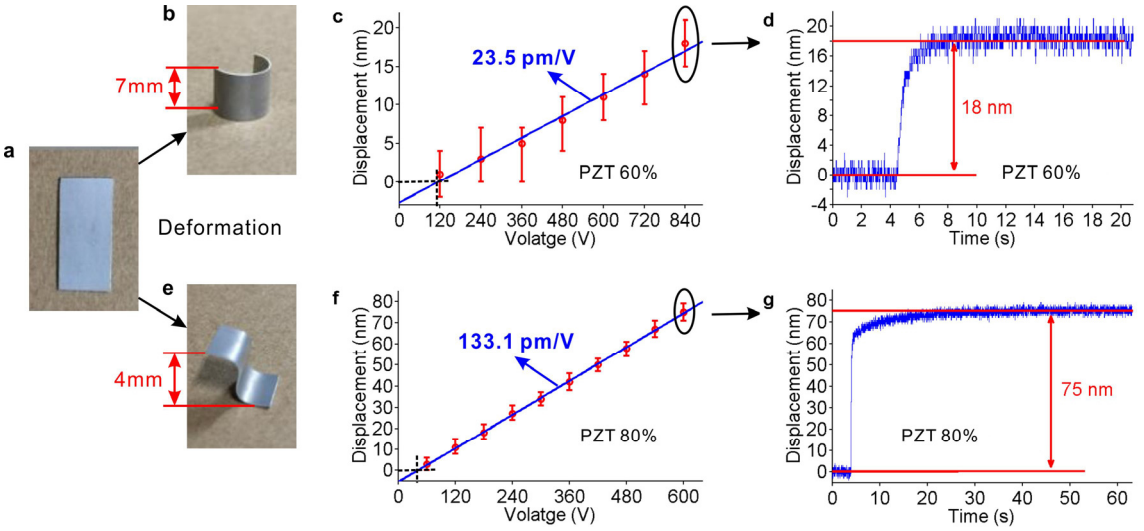

Figure 4-4. PZT / SMPU composite actuators and their nanoscale displacements. (a) A film actuator. (b) "U" type actuator of PZT 60%. (c) Displacements of the "U" type actuator vs. applied voltages with a linear fitting line. (d) Displacement response of the "U" type actuator corresponding to a step voltage of 840V. (e) "Z" type actuator of PZT 80%. (f) Displacements of the "Z" type actuator vs. applied voltages with a linear fitting line. (g) Displacement response of the "Z" type actuator corresponding to a step voltage of 600V. All the measurements are carried out under common experimental conditions and the positioning errors are no more than ±5 nm.

It should be noted that, in contrast with the film actuators, which generate displacements in d_{33} mode (the electric field is parallel to the strains [24, 25]), the "U" type actuator outputs displacements in d_{31} mode (the electric field is perpendicular to the strains [24, 25]) and the "Z" type actuator outputs displacement both in d_{33} and d_{31} modes, but mainly in d_{31} mode (the directions of electric fields and output strains are shown in Figure 4-1). Hence, the displacements of the two shaped actuators are shrink, which is opposite to the elongation of film actuators. In addition, there is one difference from the

actuators made of PZT / SMPU composites to common actuators that the SMPU matrices would "absorb" some displacements. The linear fitting lines (Figure 4-4c and f) show the zero points of displacements corresponding to certain critical voltages rather than 0 V. The film actuators of PZT 60%, PZT 70% and PZT 80% are similar (Figure 4-3). In fact, all the actuators are unable to output measurable displacement until the applied voltages are increased to a high enough value. It seems that the SMPU matrices "absorb" the displacements generated by PZT particles below the critical values. This phenomenon also can be concluded from the displacement-voltage graphs in Figure 4-3 and 4-4. If the SMPU matrices do not "absorb" displacements, the film actuators of PZT 60%, PZT 70% and PZT 80% should output the displacements of 3 nm under, respectively, the step voltages of 600 V, 540 V and 400 V according to their piezoelectric charge constants, but the actual output displacements are 2 nm. Similarly, the "U" type and "Z" type actuators should output the displacements of 3 nm and 8 nm, respectively, at the applied step voltages of 120 V and 60 V, but the actual output displacements are, respectively, 1 nm and 3 nm. Although the output displacements of actuators may be not completely linear with the applied step voltages, the SMPU matrices actually "absorb" the output displacements of PZT particles. The microscopic mechanism of actuation (Figure 4-5, one basic unit of PZT / SMPU composites) is able to account for this lost displacement. When driving voltage signals are applied on PZT / SMPU composites, PZT particles immediately output displacements by deformation. Whereas the SMPU matrices

surrounding PZT particles just encounter local deformations in the areas near interfaces, the displacements would not be delivered (step 1 in Figure 4-5) until the output stresses of PZT particles reach a threshold value to move the matrices (step 2 in Figure 4-5). As Hooke's law described ($\sigma = E\varepsilon$), enough strains are necessary for the threshold stresses and these strains would not be transmitted by the SMPU matrices. Thus, they seem to be "absorbed" or lost. Just because the SMPU matrices have the ability to "absorb" displacements, the disturbances from ambient noise also would be "absorbed". In actuation behaviors, the SMPU matrices actually act as the inbuilt isolators. This is why the actuators made of PZT / SMPU composites are capable of producing displacements within ±5 nm errors without controlling the environmental parameters.

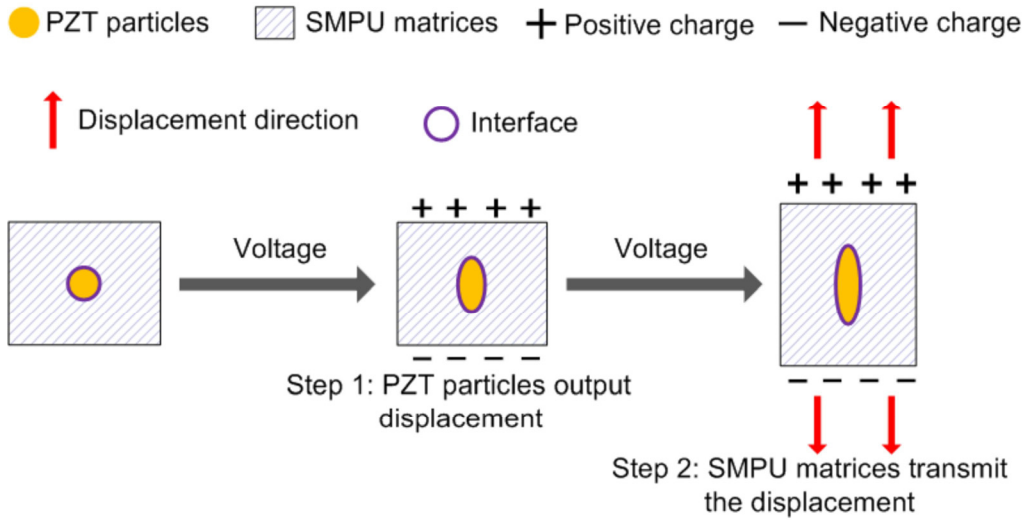

Fig 4-5. Schematic illustration of microscopic actuation mechanism of one basic unit. When voltage signals are applied on the unit, PZT particles would output displacements immediately but SMPU matrices would not transmit the displacements until the output stresses of PZT particles are strong enough to move the matrices.

The shape memory effect brings another advantage, adaptability to various structures (the "U" and "Z" type actuators are simple examples). This advantage would make it easier to integrate PZT / SMPU composite actuators into specific structures to fabricate nanopositioning devices, even nanomachining devices.

4.3.3. Effect of interfaces on relative permittivity

Figure 4-6 is the relative permittivity of two groups of PZT / SMPU composites measured under DC voltages. Why do we test the DC relative permittivity? The PZT / SMPU composites are polarized under DC voltages, so the DC relative permittivity, in contrast with the alternating current (AC) relative permittivity, implies the polarization efficiency of PZT / SMPU composites (exactly, PZT particles) more accurately. The polarization mainly determines the piezoelectric effect of PZT / SMPU composites. The data in Fig. 3 are the average values of relative permittivity measured at 30 voltage values from 100 V to 390 V with the voltage interval of 10 V (The error bars are not given in Fig. 3 because of their too small numerical values, but all the data are in Table 4-1). The relative permittivity of PZT / SMPU composites with good interfaces is proportional to the content of PZT particles. That is because the relative permittivity of PZT particles (1500) is much greater than that of SMPU matrices (2.8). Thus, more PZT particles would give rise to higher relative permittivity. Compared with the first group members, the second group members display lower relative permittivity on account of free spaces

between PZT particles and SMPU matrices (Figure 4-7d-f). The relative permittivity of free spaces should be close to 1 (the relative permittivity of vacuum) which is less than 2.8 (the relative permittivity of SMPU matrices). For easier understanding, the PZT / SMPU composites with poor interfaces could be considered as the composites containing PZT particles and a kind of polymer matrices whose relative permittivity (the equivalent relative permittivity of SMPU matrices and free spaces) is lower than that of SMPU matrices. Hence, the relative permittivity of the first group is higher than that of the second group.

Moreover, Using this relative permittivity difference is capable of estimating whether the interfaces of composites are good or not (the composites should be still dielectric materials). For example, if the relative permittivity of PZT 70% is lower than that of PZT 60%, it implies the poor interfaces in PZT 70%

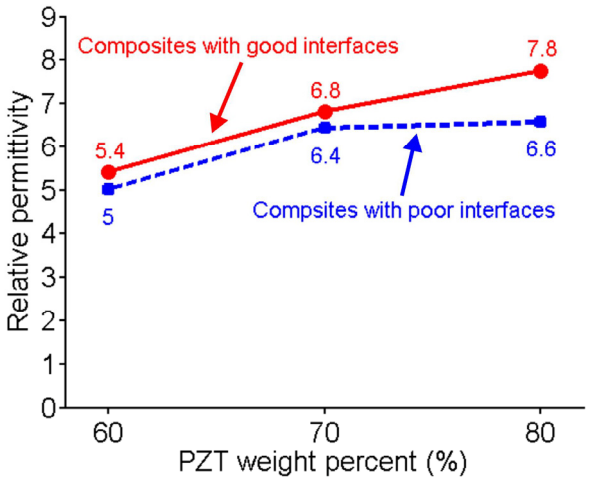

Figure 4-6. Relative permittivity (static permittivity) of PZT / SMPU composites.

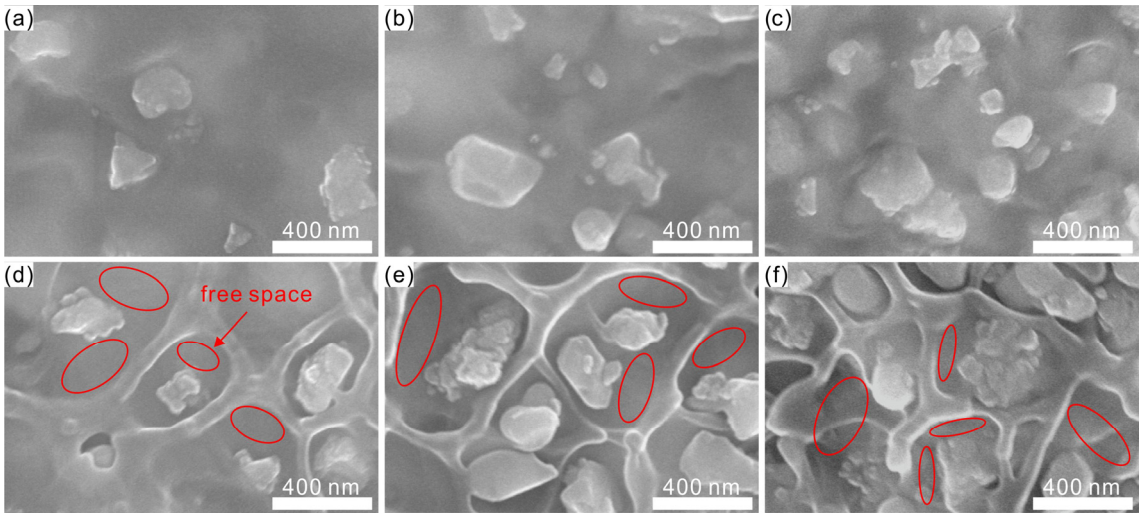

Figure 4-7. Microscopic morphology of PZT / SMPU composites. (a-c) The FE-SEM images of composites with good interfaces: PZT 60% (a), PZT 70% (b) and PZT 80% (c). (d-f) The FE-SEM images of composites with poor interfaces: PZT 60%-N (d), PZT 70%-N (e) and PZT 80%-N (f). The free spaces between fillers and matrices illustrate the poor interfaces visually.

Table 4-1. DC relative permittivity of PZT / SMPU composites

Voltage	PZT 60%	PZT 60%-N	PZT 70%	PZT 70%-N	PZT 80%	PZT 80%-N
100 V	5.40	5.00	6.82	6.42	7.69	6.57
110 V	5.40	4.99	6.82	6.43	7.70	6.55
120 V	5.41	5.02	6.83	6.43	7.72	6.57
130 V	5.40	5.01	6.79	6.45	7.72	6.57
140 V	5.40	5.01	6.80	6.43	7.73	6.56
150 V	5.40	5.02	6.82	6.44	7.72	6.57
160 V	5.40	4.99	6.82	6.43	7.74	6.55
170 V	5.42	4.99	6.83	6.44	7.72	6.55

180 V	5.41	4.99	6.82	6.43	7.74	6.56
190 V	5.43	5.01	6.82	6.42	7.74	6.57
200 V	5.41	5.03	6.82	6.43	7.72	6.58
210 V	5.39	5.03	6.82	6.43	7.75	6.58
220 V	5.41	5.01	6.83	6.42	7.74	6.59
230 V	5.39	5.01	6.82	6.45	7.76	6.56
240 V	5.39	4.98	6.82	6.44	7.76	6.56
250 V	5.40	5.01	6.82	6.45	7.77	6.56
260 V	5.39	5.02	6.83	6.45	7.71	6.57
270 V	5.41	5.02	6.82	6.44	7.75	6.57
280 V	5.40	5.02	6.82	6.42	7.72	6.60
290 V	5.41	5.02	6.83	6.46	7.73	6.59
300 V	5.41	5.01	6.83	6.45	7.74	6.59
310 V	5.40	5.00	6.82	6.42	7.76	6.58
320 V	5.41	4.99	6.82	6.43	7.75	6.56
330 V	5.41	5.02	6.83	6.43	7.78	6.57
340 V	5.41	5.02	6.81	6.45	7.81	6.58
350 V	5.41	5.01	6.82	6.45	7.78	6.55
360 V	5.41	5.02	6.83	6.47	7.79	6.59
370 V	5.42	5.03	6.82	6.44	7.75	6.60

380 V	5.41	5.03	6.81	6.43	7.74	6.59
390 V	5.40	5.02	6.83	6.44	7.84	6.59

4.3.4. Effect of interfaces on piezoelectric effect

The piezoelectric charge constant (d) of PZT / SMPU composites is calculated by $d_{33} = \Delta D/\Delta V$, where ΔD is the displacement increment, ΔV is the voltage increment. Table 1 presents the nanoscale displacements of PZT 60%, PZT 70% and PZT 80%. The d_{33} values of PZT 60%, PZT 70% and PZT 80% are, respectively, 5 pm/V, 5.6 pm/V and 10 pm/V.

Figure 4-8a-f reveal the importance of interfaces for the piezoelectric effect. Figure 4-8a-c are the displacement responses of PZT / SMPU composites with good interfaces and Figure 4-8d-f are the displacement responses of PZT / SMPU composites with poor interfaces. Obviously, the second group of PZT / SMPU composites are incapable of producing measurable displacements while the first group of PZT / SMPU composites are able to generate stable displacements. Figure 4-8g schematically illustrates the reason for the inability of PZT / SMPU composites with poor interfaces to output displacements from the perspective of microscopic interactions between PZT particles and SMPU matrices. The FE-SEM images (Figure 4-7d-f) have demonstrated the existence of free spaces between PZT particles and SMPU matrices. If voltages are applied on the PZT / SMPU composites with poor interfaces, the PZT particles would output displacements by

changing their shapes but the free spaces prevent PZT particles from transferring displacements to SMPU matrices. Because the displacement of single PZT particle is so tiny that the displacement could not pass through the free spaces to reach SMPU matrices. Besides, PZT 70%, compared with PZT 60%, shows a slight improvement in d_{33}.The possible reason is that more 10% PZT particles are not enough to reach in reach the value resulting in effective enhancement in the piezoelectric performances.

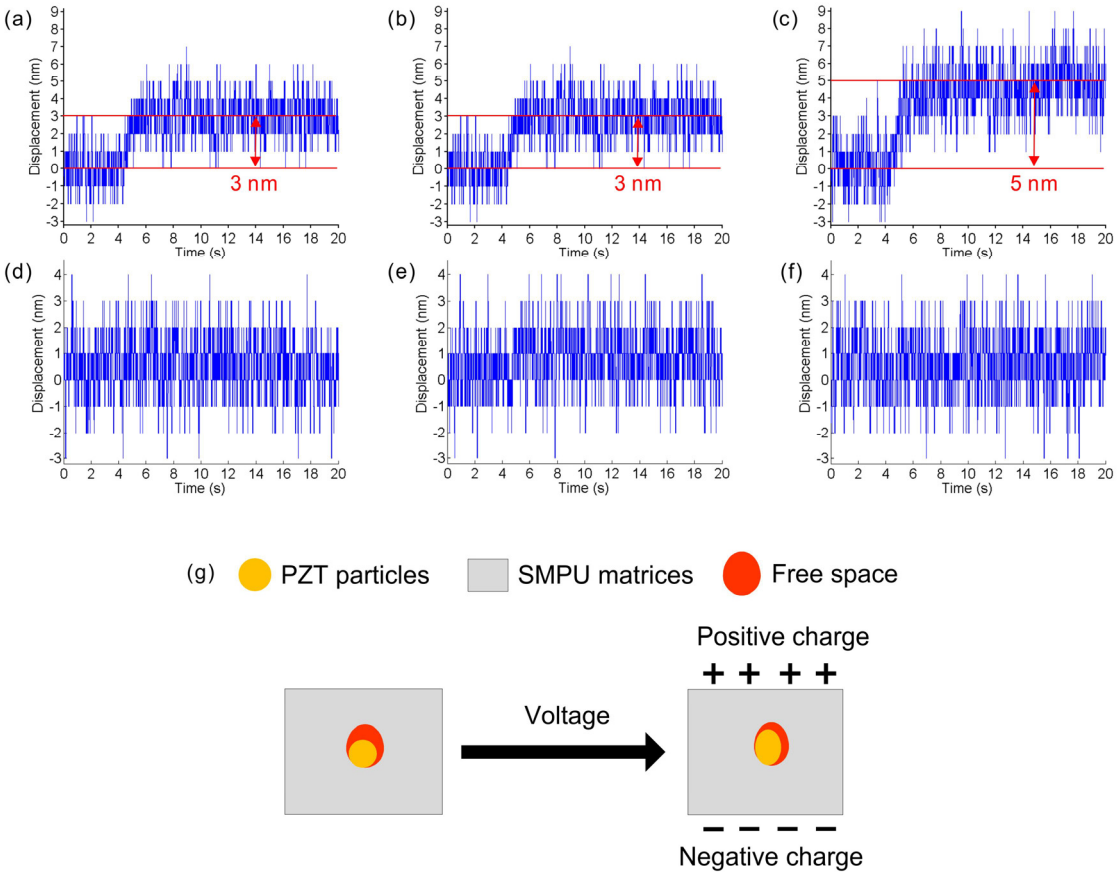

Figure 4-8. (a-f) The comparison in displacements of PZT / SMPU composites. (a) PZT 60% under a step voltage of 800V, (b) PZT 70% under a step voltage of 720V, (c) PZT 80% under a step voltage of 700V, (d) PZT 60%-N under a step voltage of 800V, (e) PZT 70%-N under a step voltage of 720V and (f) PZT 80% under a step voltage of 800V. The positioning errors are within ±5 nm. (g)

Schematic illustration of microscopic actuation behaviors of PZT / SMPU composites with poor interfaces.

4.4. Conclusions

This chapter not only certify the piezoelectric effect of PZT / SMPU composites, but also reveal the promising potential in nanopositioning because of the built in isolators, SMPU matrices, which have the capacity to reduce the disturbance from ambient noise. The actuators made of these composites are able to output 1 nm resolution displacements with positioning errors within ±5 nm in a common experimental environment. Owing to the combination of two smart effects, the actuators can generate more displacements by deformation. The piezoelectric charge constants of the "U" type actuator and the "Z" type actuator are, respectively, about 3.7 and 12.3 times more than those of their film actuators, but the positioning errors are still within ±5 nm. The ability of carrying out nanopositioning at lower cost is testified, and it is helpful to reduce the cost of mechanical. Besides, the actuators can be built into the integrated nanopositioning and even nanomachining devices due to the easiness of being shaped. In the future work, we will make efforts to improve the piezoelectric effect further and develop more applications of these composites.

Moreover, the interfaces play a important role in the relative permittivity and piezoelectric actuation behaviors. The poor interfaces would reduce the relative permittivity on the account of the lower relative permittivity of the free spaces between

PZT particles and SMPU matrices. But, in some case, this reduction in relative permittivity resulting from poor interfaces could estimate whether the interfaces of the composites are good or not. What is more worse is that the poor interfaces would destroy the actuation ability of PZT / SMPU composites, because, microscopically, the output displacements of PZT particles are too few to pass through the free spaces and reach the SMPU matrices. As a result, PZT particles are incapable of transferring the output displacement to SMPU matrices.

Reference

1. X. Chen, S. Xu, N. Yao, 1.6 V nanogenerator for mechanical energy harvesting using PZT nanofibers, *Nano Letters*, 2010,10: 2133-2137.

2. V. K. Wickramasinghe, W. N. Hagoo, Material characterization of active fiber composites for integral twist-actuated rotor blade application, *Smart Materials and Structures*, 2004, 13: 1155-1165.

3. V. K. Wickramasinghe, W. N. Hagoo, Durability characterization of active fiber composite actuators for helicopter rotor blade applications, *Journal of aircraft*, 2004, 41: 931-937.

4. H. A. Sodano, G. Park, D. J. Inman, An investigation into the performance of macro-fiber composites for sensing and structural vibration applications, *Mechanical Systems and Signal Processing*, 2004, 18: 683-697.

5. I. Babu, G. de. With, Highly flexible piezoelectric 0–3 PZT–PDMS composites with high filler content, *Composites Science and Technology*, 2014, 91: 91-97.

6. K. S. Lam, Y. W. Wong, L.S. Tai, Dielectric and pyroelectric properties of lead zirconate titanate / polyurethane composites, *Journal of Applied Physics*, 2004, 96: 3896-3899.

7. N. Saber, S. Araby, Q. Meng, Superior piezoelectric composite films: taking advantage of carbon nanomaterials, *Nanotechnology*, doi:10.1088/0957-4484/25/4/045501.

8. D. Carponcin, E. Dantras, J. Dandurand Electrical and piezoelectric behavior of polyamide/PZT/CNT multifunctional nanocomposites, *Advanced Engineering Materials*, doi: 10.1002/adem.201300519.

9. H. Gong, Y. Zhang, J. Quan, Preparation and properties of cement based piezoelectric composites modified by CNTs, *Current Applied Physics*, 2011, 11: 653-656.

10. S. Tian, F. Cui, X. Wang, New type of piezo-damping epoxy-matrix composites with multi-walled carbon nanotubes and lead zirconate titanate, *Materials Letters*, 2008, 62: 3859-3861.

11. X. Guan, Y. Zhang, H. Li, PZT / PVDF composites doped with carbon nanotubes, *Sensors and Actuators A: Physical*, 2013, 194: 228-231.

12. W. K. Sakamoto, P. Marin-Franch, D.K. Das-Gupta, Characterization and application of PZT / PU and graphite doped PZT / PU composite, *Sensors and Actuators A: Physical*, 2004, 100: 165-174.

13. X.-F. Liu, C.-X. Xiong, H.-J. Sun, Piezoelectric and dielectric properties of PZT /

PVC and graphite doped with PZT / PVC composites, *Materials Science and Engineering B*, 2006, 127: 261-266.

14. S. Moharana, R. N. Mahaling, Novel three phase polyvinyl alcohol (PVA)-nanographite (GNP) -$Pb(ZrTi)O_3$ (PZT) composites with high dielectric permittivity, *Materials Research Innovations*, doi: 10.1080/14328917.2017.1304858.

15. I. Babu, G. de. With, Enhanced electromechanical properties of piezoelectric thin flexible films, *Composites Science and Technology*, 2014, 104: 74-80.

16. N. Saber, Q. Meng, H.-Y. Hsu, Smart thin-film piezoelectric composite sensors based on high lead zirconate titanate content, *Structural Health Monitoring*, 2015, 14 : 214-227.

17. E. Manske, G. Jäger, T. Hausotte, Recent developments and challenges of nanopositioning and nanomeasuring technology, *Measurement Science and Technology*, doi:10.1088/0957-0233/23/7/074001.

18. H. C. Yeh, W. T. Ni, S. S. Pan, Digital closed-loop nanopositioning using rectilinear flexure stage and laser interferometry, *Control Engineering Practice*, 2005, 13: 559-566.

19. D. J. Lee, S. K. Lee, W. S. Kim, Precise contour motion of XY stage driven by ultrasonic linear motors in a high vacuum environment. *International Journal of Precision Engineering and Manufacturing*, 2016, 17: 293-301.

20. N. K. James, D. van den Ende, U. Lafont, S. van der Zwaag, W. A. Groen. Piezoelectric and mechanical properties of structured PZT–epoxy composites. *Journal of*

Materials Research, 2013,28: 635–641.

21. E. Venkatragavaraj, B. Satish, P. R. Vinod, M. S. Vijaya. Piezoelectric properties of ferroelectric PZT–polymer composites. *Journal of Physics D: Applied Physics*, 2001,34: 487–492.

22. E. Flint, L. Chen, C. A. Rogers, Electromechanical analysis of piezoelectric stack active member power consumption, *Journal of Intelligent Material Systems and Structures*, 1995, 6: 117-124.

23. A. K. Yi, J. R. Veillette, A charge controller for linear operation of a piezoelectric stack actuator, *IEEE Transactions on Control Systems Technology*, 2005, 13: 517-526.

24. S.-G. Kim, S. Priya, I. Kanno, Piezoelectric MEMS for energy harvesting, *MRS Bulletin*, 2012, 37: 1039-1050.

25. Y. B. Jeon, R. Sood, J. h. Jeong, MEMS power generator with transverse mode thin film PZT, *Sensors and Actuators A Physical*, 2005, 122: 16-22.

Chapter 5

Mechanical properties

Chapter 5: Mechanical properties

5.1. Introduction

The better mechanical properties are always one of the main purposes to develop composite materials. Up to now, a variety of fillers have been employed to prepare composites so as to reinforce the mechanical properties. The addition of 40% SiC increases the elastic modulus and hardness of SiC / SMP composites to about 3times as much as the pristine SMPs [1]. The tensile strength of silica/epoxy composites is significantly improved by adding just 1.5% silica nanoparticles [2]. 0.3% CNTs are utilized to enhance the flexural strength and flexural modulus of CNT / epoxy composites [3]. 0.2% well dispersed graphene bring 52% improvement in quasi-static fracture toughness in graphene / epoxy composites [4]. Various natural fibers are compounded into composites for the enhancement of mechanical properties [5].

Mechanical properties mainly including, static mechanical properties and dynamic mechanical properties, are an important indicator for the materials performances of composites. Generally, the static mechanical properties of composites are measured by tensile experiments and the dynamic mechanical properties of composites are tested by the device s of dynamic mechanical analysis (DMA). A series of static mechanical parameters are able to be quantitatively measured by the tensile testing, such as elastic

modulus, yield stress, tensile strength and the strain of breakage. The tensile testing is not only limit to macro materials, micro materials are also tested by making use of special equipments [6] or common precision instruments like atomic force microscope (AFM) and scanning probe microscope (SPM) [7]. Moreover, the elastic modulus and yield stress are able to indicate the interfacial adhesion of fillers and matrices [8, 9].

DMA is an quantitative estimation for viscoelastic behaviors of polymers and polymeric composites. The storage modulus typically related to the elastic modulus represents the elastic behaviors, the loss modulus associated with "internal friction" stands for the viscous behaviors [10], and the temperature of tan σ_{max} or maximum loss modulus is usually defined as T_g [11, 12]. The capability of DMA is more than the value of simple parameters, an quantitative relation between the stored entropic energy density as well as the maximum strain and the stress at maximum strain is established by DMA experiments [13].

Hence, in addition to piezoelectric effect and shape memory effect, mechanical properties are analyzed too. PZT / SMPU composites exhibit remarkable increase in elastic modulus, yield stress and storage modulus with the increasing content of PZT particles. Besides, PZT particles have little effect on T_g.

5.2. Materials and methods

5.2.1. Tensile Experiments

The dumbbell specimens made according to the standard of JIS K-6251-7 (Figure

5-1) were stretched at the speed of 1 mm/min at the room temperature by a tensile testing machine (RTC1250A, A&D Co., Ltd, Japan).

Figure 5-1. A dumbbell specimen for tensile testing (JIS K-6251-7)

5.2.2. Dynamic mechanical analysis

The DMA of pristine SMPU and hot-pressed PZT / SMPU composites was performed on a DVA-225 instrument (IT Keisoku Seigyo Co., Ltd., Japan). The rectangular samples, with the width of 2 mm, length of 10 mm and thickness from 100 to 175 μm, were tested under force track 200%, 10 Hz, and 5 °C/min (from 30 °C to 100 °C).

5.3. Results and discussion

5.3.1. Static mechanical properties

Table 5-1 summarizes the mechanical performances. The main numerical values are not the average values but the mechanical properties of the strain-stress curves in Figure 5-2, and the scatter ranges are also given. Compared with pristine SMPU, the elastic moduli of PZT 80%, PZT 70% and PZT 60% are enhanced by about 164%, 69% and 66% (calculated by the main numerical values), respectively. The yield stresses (defined by the

0.2%-strain offset method) of PZT 60% and PZT 70% are, respectively, increased by about 32% and 33% (calculated by the main numerical values). The fracture of PZT 80% occurs before the plastic deformation due to excessive high concentration of PZT particles and local aggregations of small particles; however, the yield stress must be higher than 65.3 MPa, which is almost two times as high as that of pristine SMPU. The increase in yield stresses, in contrast with the improvement of the elastic moduli, is stronger evidence for good interfaces. Because the yield stresses, taking place at the larger deformation, are more dependent on interfacial adhesion than the elastic moduli that are measured at the smaller deformation [8, 9]. The good interfaces are the essential reason for the enhancement in recovery stresses, because the higher elastic moduli above T_g are the results of good interfacial adhesion.

Table 5-1. Static mechanical properties of pristine SMPU and PZT / SMPU composites

Material	Yield stress[a)] (MPa)	Elastic modulus (GPa)	Tensile strength (MPa)	Break strain (%)
Pristine SMPU	$32.7^{+1.3}_{-0.5}$	$0.705^{+0.34}_{-0}$	$58.5^{+1.5}_{-0.2}$	$419.7^{+15.7}_{-11.7}$
PZT 60 %	$43.3^{+0.6}_{-2.2}$	$1.174^{+0.095}_{-0.087}$	$56.5^{+0.6}_{-2.6}$	$32.3^{+4.9}_{-2.8}$
PZT 70%	$43.6^{+2}_{-0.1}$	$1.196^{+0.311}_{0}$	$56.9^{+1.7}_{0}$	$6.3^{+0.3}_{-1.1}$
PZT 80%	$>65.3^{+1.2}_{0}$ b)	$1.862^{+0.024}_{-0.173}$	$65.3^{+1.2}_{0}$	$3.5^{+0.4}_{0}$

a)Yield stresses are defined by the 0.2%-strain offset method.

b)PZT 80 wt% composite rupture before plastic deformation occurred.

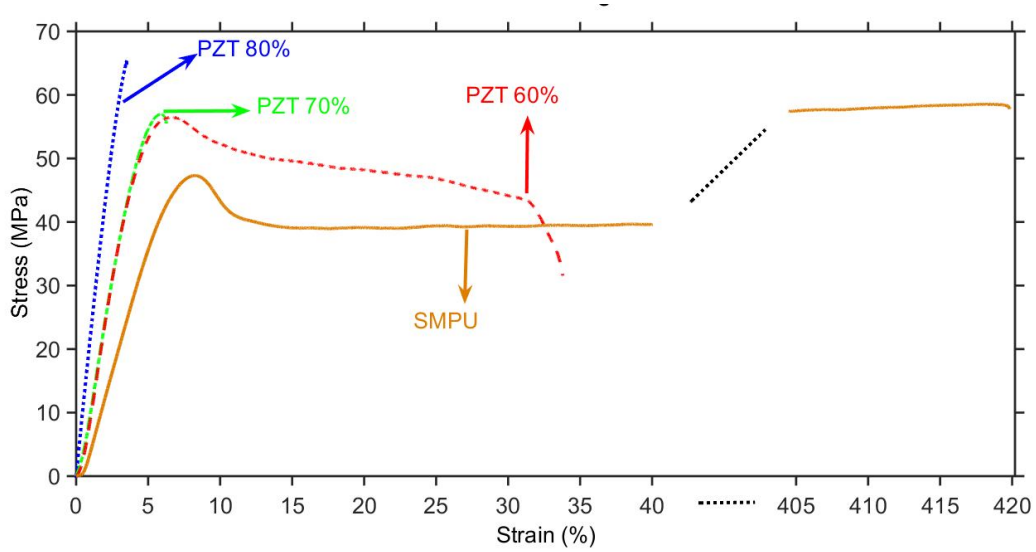

Figure 5-2. Comparison of strain-stress curves of pristine SMPU, PZT 60t%, PZT 70% and PZT 80%. The part without characteristic values in the strain-stress curve of pristine SMPU is ignored to show the key parts clearly.

However, PZT 70%, in contrast with PZT 60% and PZT 80%, performs very little reinforcement in the elastic modulus, piezoelectric charge constant, piezoelectric voltage constant and recovery stress. To confirm whether or not there are a larger number of defects inside the PZT 70%, the density of PZT / SMPU composites is measured by using the buoyancy effect and the results are summarized in Table 5-2. The density of PZT / SMPU composites is calculated by $\rho_c = m_a\rho_w/(m_a - m_w)$, where ρ_c is the density of PZT / SMPU composites, ρ_w is the density of water, m_a is the mass of PZT / SMPU composites in air, and m_w is the mass of PZT / SMPU composites in water. The density of PZT 60%, PZT 70% and PZT 80% closely follows the rule of mixture. The density of the mixture is defined by $\rho_m = 1/((\chi_a/\rho_a)+(\chi_b/\rho_b))$, where ρ_m is the density of the mixture, ρ_a is the density of phase A (the density of SMPU is 1.25 g/cm^3), ρ_b is the density of phase B (the

density of PZT is 7.9 g/cm^3), χ_a is the weight percent of phase A, and χ_b is the weight percent of phase B. Therefore, the PZT 70% should not contain many defects inside. The content of PZT in PZT 70% may not reach the value that would result in obvious improvement in material performances. It is similar that multiwall carbon nanotubes (MWNTs) enhance the dielectric constant dramatically at a volume fraction of 0. 02 [10] and carbon black (CB) increases the positive temperature coefficient by several orders of magnitude at the critical value [11].

Table 5-2. Density of PZT / SMPU composites

Material	m_a (g)	m_w (g)	ρ_c (g/cm^3)[a)]	ρ_m (g/cm^3)
PZT 60 wt%	0.073	0.044	2.52	2.53
PZT 70 wt%	0.100	0.067	3.03	3.04
PZT 80 wt%	0.103	0.076	3.81	3.83

a) The density of water (ρ_w) is 1 g/cm^3.

5.3.2. Dynamic mechanical analysis

Figure 5-3 is the results of DMA performed on pristine SMPU, PZT 60%, PZT 70% and PZT 80%. Figure 5-3a shows that the storage modulus increases with the PZT particle content in PZT / SMPU composites, and the reinforced effect of PZT particles on the storage modulus become stronger when the temperature goes up. This storage modulus improvement is benefit from the good interfaces between PZT particles and SMPU matrices. Similar enhancements are also discovered in the loss modulus, because interfaces are in effect on both elastic part and viscous part. The storage modulus and loss

modulus respectively represent elastic part (stored energy) and viscous part (energy lost as heat) [12]. Besides, the data of DMA also exhibit the variations of T_g. Usually, the temperature of tan σ_{max} or maximum loss modulus is defined as T_g [13, 14], although the glass transition occurs in a certain temperature range. Figure 5-3b and 5-3c respectively illustrate the temperature corresponding to maximum loss modulus and tan σ_{max}, and reveal that the T_g of two definitions both change very little, considering the high content of PZT particles. Mostly, the variations of T_g result from the changes of cross-link density [15], crystallinity of polymers [16], free volumes at the interfaces [17] and other effects on the interactions of fillers and matrices [18]. However, PZT / SMPU composites are synthesized by a kind of amorphous SMPU and the interaction between fillers and matrices is physical adhesion. Moreover, the interfaces of hot-pressed PZT / SMPU composites are good, so no free volume (free space) at the interfaces. That's why the T_g of hot-pressed PZT / SMPU composites vary so little even though the PZT content is high.

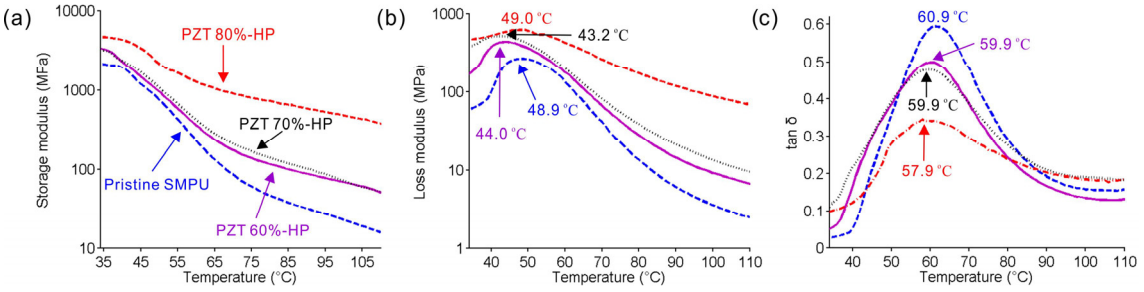

Figure 5-3. Dynamic mechanical analysis of PZT / SMPU with good interfaces. (a) Comparison of the storage modulus, (b) Comparison of the loss modulus, (c) Comparison of the values of tan σ.

5.4. Conclusions

PZT 60%, PZT 70% and PZT 80% all show strong improvements in both static and dynamic mechanical properties, benefit from the good interfaces between PZT particles and SMPU matrices. The elastic moduli are enhanced by at least 60% and the yield stresses are improved to more than 133%. The storage moduli are improved effectively while the loss moduli are increased likewise. But PZT particles change the T_g very little even if the content of PZT particles are high because no chemical agents and surface modifications are induced in PZT /SMPU. The physical interfacial bonding would keep the T_g close to pristine SMPU.

Reference

1. K. Gall, M. L. Dunn, Y. Liu, Shape memory polymer nanocomposites, *Acta Materialia*, 2002, 50: 5115-5126.

2. Y. Dong, Q.-Q. Ni, Y. Fu, Preparation and characterization of water-borne epoxy shape memory composites containing silica, *Composites: Part A*, 2015, 72:1-10.

3. B. P. Singh, K. Saini, V. Choudhary, Effect of length of carbon nanotubes on electromagnetic interference shielding and mechanical properties of their reinforced epoxy composites, *Journal of Nanoparticle Research*, doi: 10.1007/s11051-013-2161-9.

4. L.-C. Tang, Y.-J. Wan, D. Yan, The effect of graphene dispersion on the mechanical properties of graphene/epoxy composites, *Carbon*, 2013, 60: 16-27.

5. N. Saba, M. Jawaid, O. Y. Alothman, A review on dynamic mechanical properties of

natural fibre reinforced polymer composites, *Construction and Building Materials*, 2016, 106: 149-159.

6. A. Reichardt, M. Ionescu, J. Davis, *In situ* micro tensile testing of He^{+2} ion irradiated and implanted single crystal nickel film, *Acta Materialia*, 2015, 100: 147-154.

7. D.S. Gianola, C. Eberl, Micro- and nanoscale tensile testing of materials, *The Journal of The Minerals, Metals & Materials Society*, 2009, 61: 25-35.

8. I. Švab, V. Musil, M. Leskovac, The adhesion phenomena in polypropylene/wollastonite composites, *Acta Chimica Slovenica*, 2005, 52: 264-271.

9. F. Stricker, M. Bruch, R. MLilhaupt, Mechanical and thermal properties of syndiotactic polypropene filled with glass beads and talcum, *Polymer*, 1997, 38: 5347-5353.

10. L. Wang, Z.-M. Dang. Carbon nanotube composites with high dielectric constant at low percolation threshold. *Applied Physics Letter*, 2005, doi: 10.1063/1.1996842.

11. H. Tang, J. Piao, X. Chen, Y. Luo, S. Li. The Positive temperature coefficient phenomenon of vinyl polymer / CB composites. *Journal of Applied Polymer Science*, 1993, 48: 1795-1800.

12. M. A. Meyers, K. K. Chawla, Mechanical Behavior of Materials 2nd edn, Cambridge University Press, 2009, Cambridge.

13. J. Rieger, The glass transition temperature T_g of polymers-comparison of the values from differential thermal analysis (DTA, DSC) and dynamic mechanical measurements (torsion pendulum), *Polymer Testing*, 2001, 20: 199-204.

14. W. K. Goertzen, M. R. Kessler, Dynamic mechanical analysis of fumed silica/cyanate ester nanocomposites, *Composites: Part A*, 2008, 39: 761-768.

15. H. Miyagawa, M. J. Rich, L. T. Drzal, Thermo-physical properties of epoxy nanocomposites reinforced by carbon nanotubes and vapor grown carbon fibers, *Thermochimica Acta*, 2006, 442: 67-73.

16. T. Ryynänen, A. Nykänen, J. V. Seppälä, Poly(CL/DLLA-b-CL) multiblock copolymers as biodegradable thermoplastic elastomers, *Polymer Letters*, 2008, 2: 184-193.

17. Y. Sun, Z. Zhang, K.-S. Moon, Glass transition and relaxation Behavior of epoxy nanocomposites, *Journal of Polymer Science: Part B: Polymer Physics*, 2004, 42: 3849-3858.

18. A. Hartwig, M. Sebald, M. Kleemeier, Cross-linking of cationically polymerised epoxides by nanoparticles, *Polymer*, 2005, 46: 2029-2039.

Chapter 6

Actuators with interdigitated electrodes

Chapter 6: Actuators with interdigitated electrodes and energy harvesting

6.1. Introduction

Interdigitated electrodes (IDTs) were proposed to generate and detect surface elastic waves piezoelectrically by R. M. White and F. W. Voltmer in 1965 [1]. Since 1990s, IDTs have been employed as electrodes on the surfaces of piezoceramic fiber composites, because the IDTs are able to improve the ability of actuation and sensing by using the piezoelectric effect along the longitudinal direction of fibers [2-6]. Taking advantage of the capability induced by IDTs, piezoceramic fiber composites have been applied in different fields as actuators and sensors [7-10]. Besides, due to the benefit of planar sensing and actuation, IDTs are made into nanoscale level [11] and utilized in biochemical sensors [12], capacitive immunosensors [13], bio-affinity sensors [14], glucose sensor [15], nanosensors [16] and nanogenerators [17].

In this chapter, IDTs are made on the PZT / SMPU composites with the purpose to generate bending displacements and harvest energy by utilizing the piezoelectric effect along the longitudinal direction. The experiment results exhibit that PZT 60% IDTs on one surface can produce bending displacements in response to applied electric voltages, and are able to generate electric voltages resulting from applied mechanical vibrations.

6.2. Materials and methods

6.2.1. Fabrication of interdigitated electrodes

The IDTs (Figure 6-1) were sputtered on the surfaces of actuations made from PZT / SMPU actuators by a magnetron sputtering coater (E-1030, Hitachi Co., Ltd, Japan). Then the actuators with IDTs were polarized at 80 °C for 2h in a silicone oil bath under the electric field of 9 kV/mm supplied by a high voltage power supply (ES30, Gamma High Voltage Research Inc., U.S.A.).

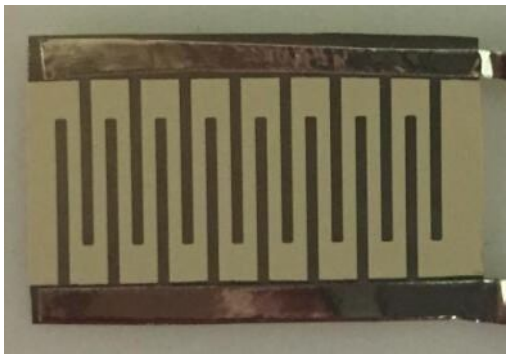

Figure 6-1. A actuator with interdigitated electrodes

6.2.2. Bending displacement measurement

One end of PZT / SMPU composites with IDTs was fixed on a steel block by a magnet (figure 6-2) and the bending displacements of another free end was measured by a laser sensor (LK-80G, Keyence Corp., Japan) with a moving average filter (the mean of 256 points). The applied step voltage signals were generated by a high voltage power supply (HJPQ-30P1, Matsusada Precision Inc., Japan).

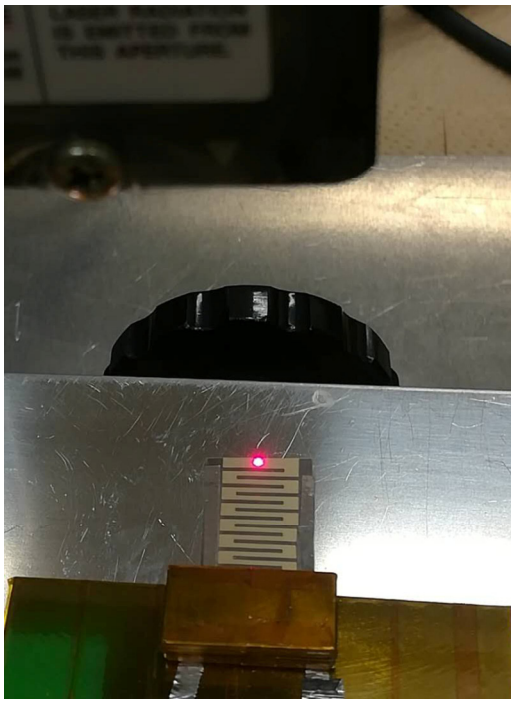

Figure 6-2. Bending displacement measurement system.

6.2.3. Energy harvesting test

PZT / SMPU composites with IDTs were fixed at one end and another end was free where vibrations were applied by a actuator made in our group. Output voltages were measured by a digital oscilloscope (DS-5414A, IWATSU ELECTRIC Co., Ltd, Japan).

6.3. Results and discussion

6.3.1. Bending displacements

Figure 6-2 exhibits that PZT 60% with IDTs are able to generate displacements of several microns resulting from applied step electric voltages. The produced bending displacements are approximately linear with the applied electric voltages (Figure 6-4b), and reach to 2.4 μm at 2100V (Figure 6-4a). The actuator of PZT 60% with IDTs can

produce bending displacements because the IDTs only on one surface result in inhomogeneous polarization which decreases with the increase of distance away from the IDTs along the direction of thickness. Thus, elongation of the upper surface (figure 6-2) is the largest and that of the lower surface is the smallest, and this difference in elongation gives rise to bending displacements.

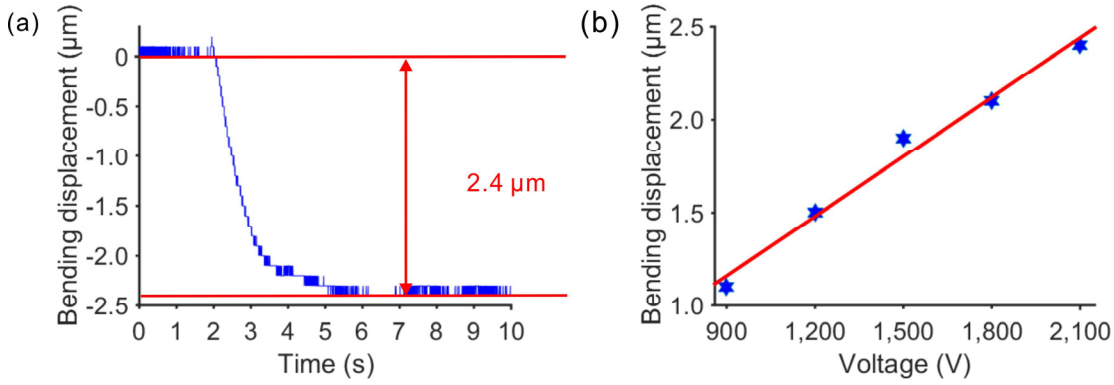

Figure 6-3. Bending displacements of PZT 60% with IDTs in response to applied step voltages. (a) Bending displacement at 2100V. (b) Bending displacements vs. applied voltages, the red line is the linear fitting line.

6.3.2. Energy harvesting

Figure 6-4a shows peak-to-peak values of output voltages generated by PZT 60% with IDTs in response to applied mechanical vibrations at the frequency from 10 to 2000Hz (the frequency interval is 10 Hz from 10 to 200Hz and the frequency interval is 50 Hz from 200 to 2000Hz). The peak-to-peak values gradually increase with the growth of frequency of applied vibration and reach to about 2.36V at 2000Hz, because higher frequency usually provides higher accelerated which gives rise to larger force or stress on

PZT 60% accord to $F = ma$, where F is the force, m is the mass and a is the accelerated speed. Besides, the relation between output voltages and frequency seems to be linear at some frequency ranges, such as frequency from 10 to 50Hz and from 250 to 450Hz, but nonlinear at other frequency ranges. The possible reason is that the applied vibrations are produced by a gel actuator fabricated by our group members and its frequency response characteristic is not stable.

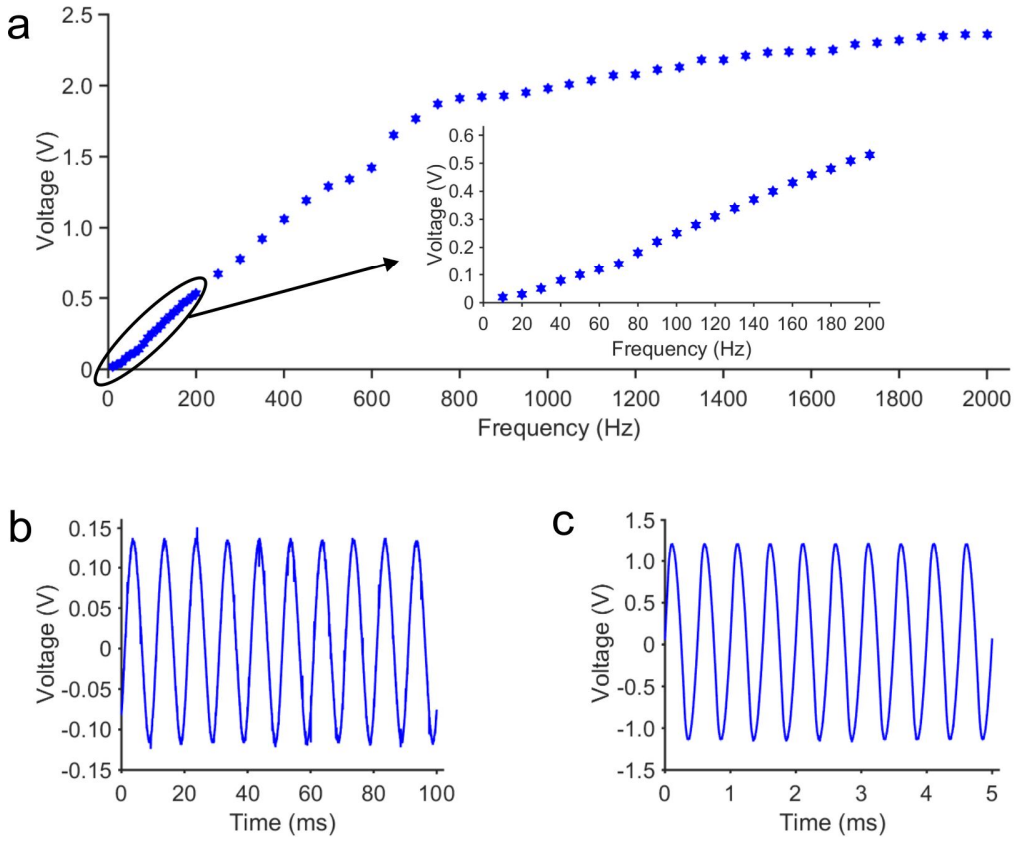

Figure 6-4. Output voltages of PZT 60% with IDTs in response to applied sinusoidal vibrations. (a) Peak-to-peak values of output voltages at the frequency from 10 to 2000Hz, (b) Sine wave output voltage at 100Hz, (c) Sine wave output voltage at 2000Hz.

Figure 6-4b and Figure 6-4c reveal that PZT 60% with IDTs is able to produce sine

wave voltages, indicating the ability to track the stimuli and harvest energy continuously. Moreover, it also implies the potential for supplying electric energy sustainably to power electric devices. It should be noticed that the generated voltages contain induced voltages resulted from surrounding electromagnetic waves, because IDTs likewise act as antennas.

6.4. Conclusions

PZT 60% with IDTs shows the ability to generate bending displacements of several microns and the relation between generated bending displacements and applied step electric voltages is approximately linear. Besides, PZT 60% with IDTs can also harvest energy from external stimuli, and output voltages go up bit by bit with the increasing frequency of applied vibrations. The continuous output voltages also imply the promising potential for powering electric devices sustainably. In the future, we will test the energy harvesting performances resulting from controllable and stable vibrations to analyse the reason for the variations of output voltages.

Reference

1. R. M. White, F. W. Voltmer, Direct piezoelectric coupling to surface elastic waves, *Applied Physics Letters*, 1965, 7: 314-316.

2. N. Hagood, R. Kindel, K. Ghandi, Improving transverse actuation of piezoceramics using interdigitated surface electrodes, *Proceedings SPIE 1917, Smart Structures and*

Materials 1993: Smart Structures and Intelligent Systems, doi: 10.1117/12.152766.

3. H.Y. Zhang, Y.P. Shen, Vibration suppression of laminated plates with 1–3 piezoelectric fiber-reinforced composite layers equipped with interdigitated electrodes, *Composite Structures*, 2007, 79: 220–228.

4. R. B. Williams, Nonlinear mechanical and actuation characterization of piezoceramic fiber composites, PhD Thesis, Virginia Polytechnic Institute and State University, Virginia, USA, 2004.

5. A. A. Bent, N. W. Hagood, J. P. Rodgers, Anisotropic actuation with piezoelectric fiber composites, *Journal of Intelligent Material Systems and Structures*, 1995, 6: 338-349.

6. A. A. Bent, N. W. Hagood, Piezoelectric fiber composites with interdigitated electrodes, *Journal of Intelligent Material Systems and Structures*, 1997, 8: 903-919.

7. V. K. Wickramasinghe, N. W. Hagood, Material characterization of active fiber composites for integral twist-actuated rotor blade application, *Smart Materials and Structures*, 2004, 13: 1155-1165.

8. V. K. Wickramasinghe, N. W. Hagood, Durability characterization of active fiber composite actuators for helicopter rotor blade applications, *Journal of Aircraft*, 2004, 41: 931-937.

9. H. A. Sodano, G. Park, D. J. Inman, An investigation into the performance of macro-fiber composites for sensing and structural vibration applications, *Mechanical Systems and Signal Processing*, 2004, 18: 683–697.

10. C. Mo, S. Kim, W. W. Clark, Theoretical analysis of energy harvesting performance for unimorph piezoelectric benders with interdigitated electrodes, *Smart Materials and Structures*, doi:10.1088/0964-1726/18/5/055017.

11. L. H. D. Skjolding, C. Spegel, A. Ribayrol, Characterisation of nano-interdigitated electrodes, *Journal of Physics: Conference Series*, doi:10.1088/1742-6596/100/5/052045.

12. P. V. Gerwen, W. Laureyn, W. Laureys, Nanoscaled interdigitated electrode arrays for biochemical sensors, *Sensors and Actuators B*, 1998, 49: 73-80.

13. A. Qureshi, J. H. Niazi, S. Kallempudi, Label-free capacitive biosensor for sensitive detection of multiple biomarkers using gold interdigitated capacitor arrays, *Biosensors and Bioelectronics*, 2010, 25: 2318-2323.

14. Z. Zou, J. Kai, M. J. Rust, Functionalized nano interdigitated electrodes arrays on polymer with integrated microfluidics for direct bio-affinity sensing using impedimetric measurement, *Sensors and Actuators A*, 2007, 136: 518-526.

15. O. Korostynska, A. Arshak, P. Creedon, Glucose monitoring using electromagnetic waves and microsensor with interdigitated electrodes, *2009 IEEE Sensors Application Symposium*, doi: 10.1109/SAS.2009.4801772.

16. J. Huang, S. Virji, B. H. Weiller, Nanostructured polyaniline sensors, *Chemistry-A European Journal*, 2004, 10: 1314-1319.

17. X. Chen, S. Xu, N. Yao, 1.6 V nanogenerator for mechanical energy harvesting using PZT nanofibers, *Nano Letters*, 2010, 10: 2133-2137.

Chapter 7

Ag / PZT / SMPU composites

Chapter 7: Ag / PZT / SMPU composites

7.1. Introduction

As shown in Figure 5-3, the piezoelectric charge constants of film actuators are relative low. In fact, the weak piezoelectric effect results from the gravely low relative permittivity of SMPU matrices (only 2.8) which greatly weaken the polarization effect. Because the electric field acting on PZT particles are mainly depend on the relative permittivity of polymer matrices [1-3]. The main route for improving the dielectric permittivity of piezoelectric composites is to introduce conductive particles into the polymer matrices (CNTs [4, 5], graphene [6]). Moreover, some researchers have demonstrated the possibility for conductive fillers to promote the piezoelectric constant. Nasser Saber et al. improve the piezoelectric effect by the addition of graphene [7], Xiao-fang Liu et al. increase the d_{33} from 16 to 22 pC/N by adding graphite [8], Hongyu Gong et al. successfully use CNTs to enhance the d_{33} [9] and Indu Babu et al. put CNTs and carbon black into PZT/PDMS (poly dimethyl siloxane) composites resulting in augment of piezoelectric constant [10].

However, CNTs, graphite, graphene, carbon black are all the fillers that have one or two dimensions in the size much larger than nanoscale. According to the mechanism of SMCs we proposed in the section 3.3.4, the above fillers would affect recovery rates

negatively. With the consideration of depressing the negative effect on recovery rates, silver nanoparticles are selected as conductive fillers to improve the piezoelectric effect of PZT / SMPU composites. The resultant three phase composites (Ag / PZT / SMPU) display that the d_{33} is increased by at least 100%.

7.2. Materials and methods

7.2.1. Preparation of sliver nanoparticles

The preparation method of sliver nanoparticles refers to the reference 11 and 12. 1.0g polyvinylpyrrolidone (PVP) (P0471, Tokyo Chemical Industry Co., Ltd., Japan) was dissolved in deionized water (20 ml) by stirring for 10 min at room temperature. 0.50 g (2.94 mmol) $AgNO_3$ (196-00831, Wako Pure Chemicals Industries, Ltd., Japan) was added and the solution was stirred for 10 min to dissolve the $AgNO_3$. An aqueous solution that 0.88 g (2.94 mmol) trisodium citrate dihydrate (Na_3Ct) (199-01781, Wako Pure Chemicals Industries, Ltd., Japan) in deionized water (20 ml) was added dropwise. After adding all of the Na_3Ct solution, another aqueous solution of 0.5 ml deionized water and 0.027 g (0.294 mmol) dimethylaminoethanol (DMAE) (049-02693, Wako Pure Chemicals Industries, Ltd., Japan) was added to the reaction mixture. Then the mixture was stirred at room temperature for one hour. Until the color of the solution gradually changed from white to pale brown, the silver particles were separated from the solution by centrifugation at the speed of 5000 rpm (H-27F, Kokusan Chemical Co. Ltd., Japan) and washed several times with deionized water and ethanol. Finally, a oven

was employed to dry the sliver nanoparticles.

7.2.2. Synthesis of Ag / PZT / SMPU composites

It is similar to the synthetic method of PZT / SMP composites. First, Silver nanoparticles were put into THF and dispersed by an ultrasonic device (Sonifier 250, Branson Ultrasonics Corp., U.S.A.) for 15 min at the level 3. Then, PZT particles were poured into the mixture and the ultrasonic device was employed to disperse PZT particles for 15 min at the level 3 again. After dispersion, shape memory polyurethane pellets (the weight was one seventh of THF), were dissolved in the Ag / PZT / THF suspension and the mixture was stirred magnetically for 48 h at a speed of 400 r/min. Then THF evaporated naturally when the mixture was still stirred until the weight ratio of shape memory polyurethane and THF became 1:5. After the mixture was put statically for 48 h to remove air bubbles, it was casted on a teflon film with an auto film applicator (PI-1210, Tester Sangyo Co., Ltd., Japan). The resulting films cured after evaporating THF again for 3 days in nature. The obtained Ag / PZT / SMPU composite films were further dried at 65 ^{o}C for 3 days and then pressed for 8h under the pressure of 6 MPa at 80 ^{o}C by a hot-press machine (SA-303, Tester Sangyo Co., Ltd., Japan).

7.2.3. Polarization

P_b-P_t alloy electrodes were sputtered (E-1030, Hitachi Co., Ltd, Japan) on the surfaces of Ag / PZT / SMPU composite films. Then the films were polarized at 80 °C for

2h in a silicone oil bath under the electric field of 10 kV/mm supplied by a high voltage power supply (ES30, Gamma High Voltage Research Inc., U.S.A.).

7.3. Results and discussion

7.3.1 Microscopic morphology

Figure 7-1 is the FE-SEM images of Ag / PZT / SMPU composites which contain PZT 60%+Ag 3% (wt%), PZT 70%+Ag 3% (wt%), PZT 80%+Ag 3% (wt%). It is clear that no free space or voids between PZT particles and SMPU matrices. The interfaces of all Ag / PZT / SMPU composites are good. As for sliver nanoparticles, their sizes are about 5 nm according to the reference 11 and 12. Thus, FE-SEM images are difficult to show silver nanoparticles, and they are also very hard to be found among PZT particles (averagely 400 nm).

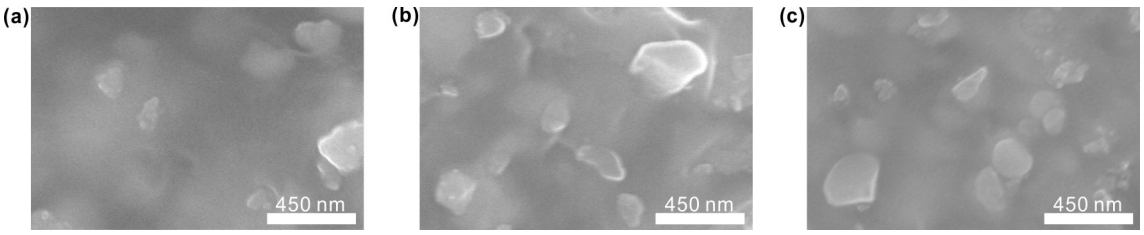

Figure 7-1. FE-SEM images of Ag / PZT / SMPU composites. (a) PZT 60%+Ag 3%, (b) PZT 70%+Ag 3%, (c) PZT 80%+Ag 3%.

7.3.2. Piezoelectric performances

The nanoscale displacements of PZT 60%+Ag 3% (Figure 7-2), PZT 70%+Ag 3% (Figure 7-3) and PZT 80%+Ag 3% (Figure 7-4) show that, as expected, the piezoelectric effect is enhanced impressively. The d_{33} of PZT 60%+Ag 3%, PZT

70%+Ag 3% and PZT 80%+Ag 3% is respectively increased by about 134%, 137% and 100%, which is the result of more effective polarization of PZT particles. Because the relative permittivity of matrices is improved by extreme excellent conductivity of silver nanoparticles, the electric field acting on PZT particles would be increased so that the effect of polarization become better. However, Ag / PZT / SMPU composites with sliver nanoparticles below 3 weight percent do not show effective improvement in the d_{33}.

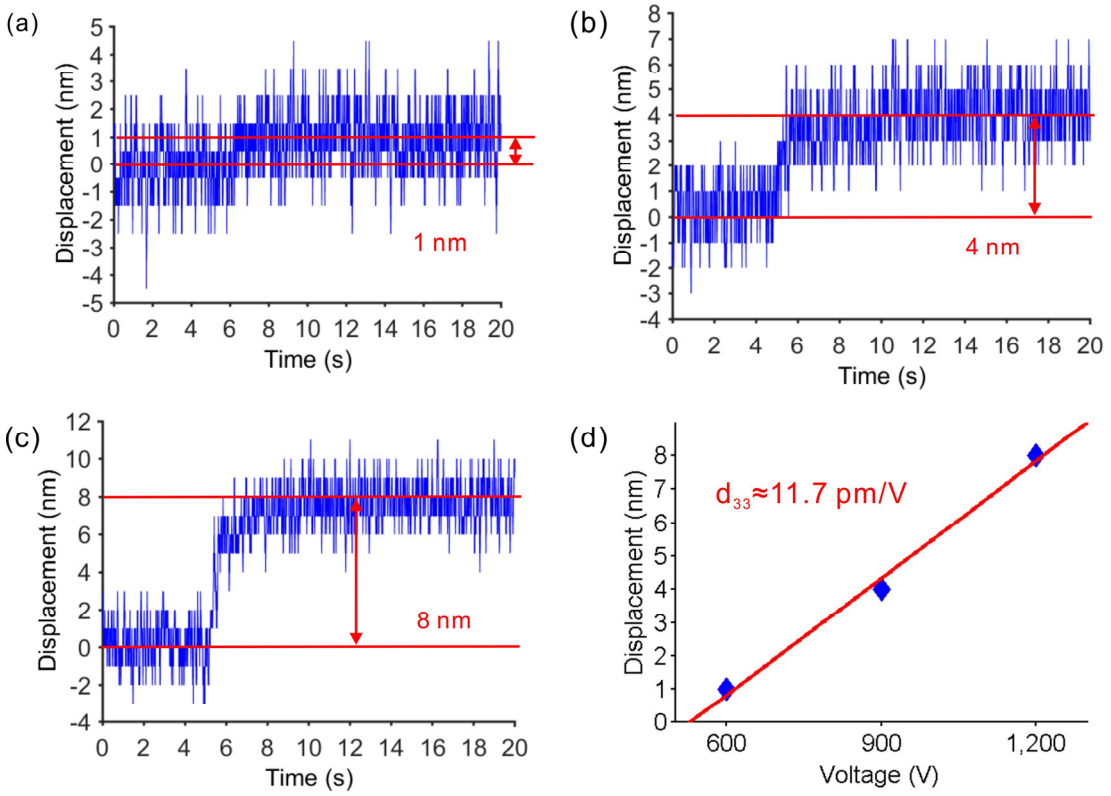

Figure 7-2. Displacements and Linear fitting of displacements and applied voltages of PZT 60%+Ag 3%. (a) Displacement under 600V. (b) Displacement under 900V. (c) Displacement under 1200V. (d) Displacements vs. applied voltages, the red line is the linear fitting line.

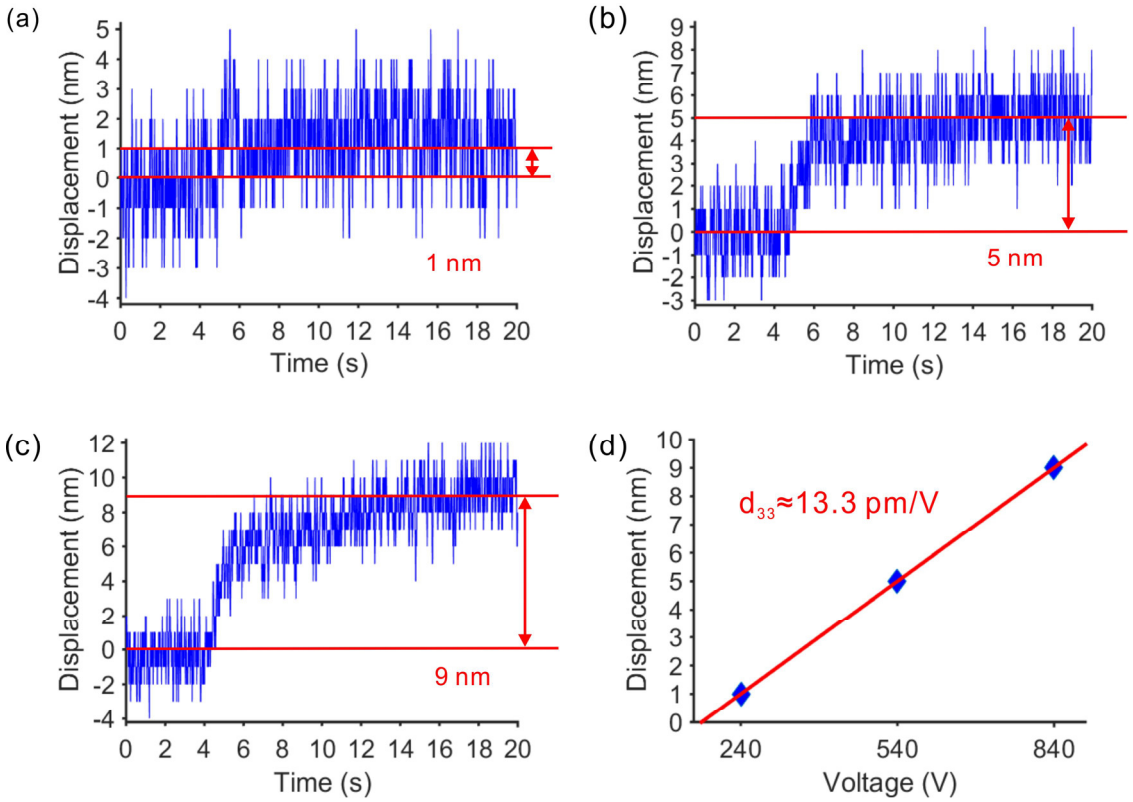

Figure 7-3. Displacements and Linear fitting of displacements and applied voltages of PZT 70%+Ag 3%. (a) Displacement under 240V. (b) Displacement under 540V. (c) Displacement under 840V. (d) Displacements vs. applied voltages, the red line is the linear fitting line.

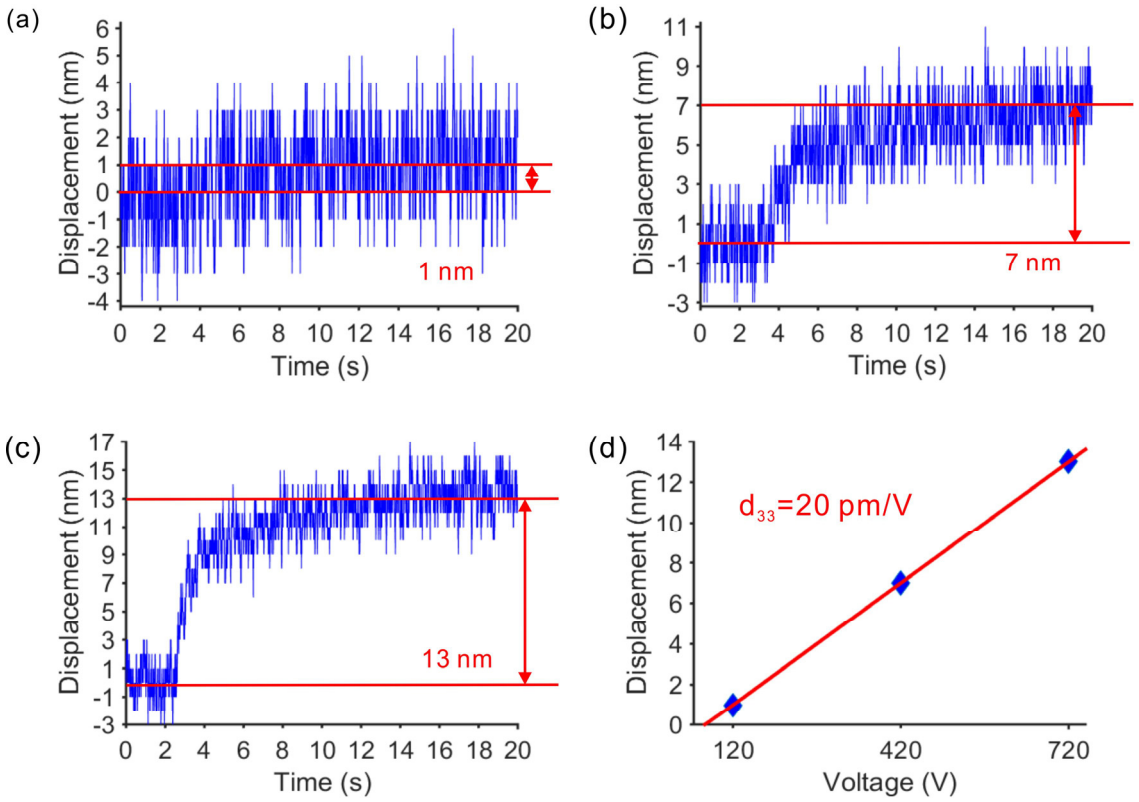

Figure 7-4. Displacements and Linear fitting of displacements and applied voltages of PZT 80%+Ag 3%. (a) Displacement under 120V. (b) Displacement under 420V. (c) Displacement under 720V. (d) Displacements vs. applied voltages, the red line is the linear fitting line.

7.4. Conclusions

PZT / SMPU composites perform a strong improvement in piezoelectric effect because of the addition of silver nanoparticles of 3 weight percent. The d_{33} of Ag / PZT / SMPU composites is at least 100% higher than that of PZT / SMPU composites with the same content of PZT particles. The significant improvement in d_{33} should be caused by the more efficient polarization due to the larger electric field acting on PZT particles.

Reference

1. W. K. Sakamoto, P. Marin-Franch, D.K. Das-Gupta, Characterization and application of PZT / PU and graphite doped PZT / PU composite, *Sensors and Actuators A: Physical*, 2004, 100: 165-174.

2. D. Sinha, P. K. C. PiHai, The conductivity behavior in lead zirconate titanate polyvinylidene fluoride composites, *Journal of Applied Physics*, 1988, 2571-2574.

3. D. J. Mickish, Effects of interfacial polarization and loading factor in dielectricloss measurements of composites, *Journal of Applied Physics*, 1979, 50: 5923-5929.

4. D. Carponcin, E. Dantras, J. Dandurand Electrical and piezoelectric behavior of polyamide/PZT/CNT multifunctional nanocomposites, *Advanced Engineering Materials*, doi: 10.1002/adem.201300519.

5. X. Guan, Y. Zhang, H. Li, PZT / PVDF composites doped with carbon nanotubes, *Sensors and Actuators A: Physical*, 2013, 194: 228-231.

6. S. Moharana, R. N. Mahaling, Novel three phase polyvinyl alcohol (PVA)-nanographite (GNP) -$Pb(ZrTi)O_3$ (PZT) composites with high dielectric permittivity, *Materials Research Innovations*, doi: 10.1080/14328917.2017.1304858.

7. N. Saber, S. Araby, Q. Meng, Superior piezoelectric composite films: taking advantage of carbon nanomaterials, *Nanotechnology*, doi:10.1088/0957-4484/25/4/045501.

8. X.-F. Liu C.-X. Xiong, H.-J. Sun, Piezoelectric and dielectric properties of PZT/PVC and

graphite doped with PZT/PVC composites, *Materials Science and Engineering B*, 2006,

127: 261-266.

9. H. Gong, Y. Zhang, J. Quan, Preparation and properties of cement based piezoelectric composites modified by CNTs, *Current Applied Physics*, 2011, 11: 653-656.

10 I. Babu, G. de. With, Enhanced electromechanical properties of piezoelectric thin flexible films, *Composites Science and Technology*, 2014, 104: 74-80.

11. J. Natsuki, T. Abe, Synthesis of pure colloidal silver nanoparticles with high electroconductivity for printed electronic circuits: The effect of amines on their formation in aqueous media, *Journal of Colloid and Interface Science*, 2011, 359: 19-23.

12. J Natsuki, T. Natsuki, T. Abe, Low molecular weight compounds as effective dispersing agents in the formation of colloidal silver nanoparticles, *Journal of Nanoparticle Research*, 2013, doi: 10.1007/s11051-013-1483-y.

Chapter 8

General conclusions

Chapter 8: General conclusions

PZT / SMPU composites are proposed with the purpose to combine two smart effects (piezoelectric effect and shape memory effect) which have been widely used in different areas into one kind of composites by compounding PZT particles with the average diameter of 400 nm and SMPU matrices. The resultant composites exhibit not only decent shape memory effect but also promising potential in nanopositioning resulting from the combination of the two smart effects. The possibility of carrying out nanopositioning in a common experimental condition, not a controlled environment, is revealed by the nanoscale displacement measurements. This would be helpful to development of the nanomachining and nanofabrication at low cost. The main conclusions of our work are given as below.

The process of seeking the optimal method to prepare PZT / SMPU composites are shown in chapter 2. The results show that the solution of SMPU / THF with the weight ratio of 1 : 7 is helpful for preparation by reason of the effective dispersion of PZT particles and the protection of PZT particles from deposition, meanwhile able to shorten the time for evaporating THF. Besides, the hot-pressing and enough mobility of SMPU chain segments are necessary for PZT / SMPU composites to form good interfaces and usable piezoelectric effect requires at least 60 weight percent of PZT particles.

The good shape memory performances of PZT / SMPU composites are displayed and the molecular mechanism of SMCs is proposed in chapter 3. PZT particles give rise to the outstanding improvement in recovery stresses because of the outstanding improvement in elastic moduli above T_g. PZT 60%, PZT 70% and PZT 80%, compared with the pristine SMPU, obtain the augment of 133%, 144% and 330%, respectively, in maximum recovery stresses. Even though the recovery rates of PZT / SMPU composites decrease with the increase of PZT particles, all of PZT / SMPU composites exhibit the recovery rates higher than 94.5% in the third cycle. Furthermore, the mechanism of SMCs are built up based on the molecular mechanism of SMPs, aiming to understand the shape memory behaviors of SMCs deeply. The molecular mechanism of SMCs is established by taking account of the two differences between the molecular motions of SMPs and SMCs and both the negative effect and positive ("cross-link" effect and "slippage" effect) The relations between the interfaces and recovery rates are summarized as following:

(1) The "cross-link" effect and "slippage" effect of interfaces influence recovery rates at the same time.

(2) The "cross-link" effect and "slippage" effect of interfaces is proportional to the amount of interfaces (the amount of fillers in the case of same fillers).

(3) Which effect is main one that is dependent on how much the existing "pure SMP slippages".

(4) If the existing "pure SMP slippages" are quite a lot, the "cross-link" effect would be

dominant and the "pure SMP slippages" would be reduced. As fillers increase, the "slippage" effect would be gradually predominant.

Moreover, the variations in recovery rates of SMCs can be predicted qualitatively. The qualitative predictions are as following:

(1) The predictions need given recovery rates of SMCs with a certain filler content (M wt%).

(2) If the SMCs with M wt% fillers (PZT 60%-HP) perform a little decrease in recovery rates, in contrast with the pristine SMPs, SMCs with N wt% fillers (N>M, PZT 70% and PZT 80%) would perform an further reduction in recovery rates. Recovery rates would continue dropping as fillers increase.

(3) If the SMCs with M wt% fillers exhibit an improvement in recovery rates, compared with the pristine SMPs, SMCs with N wt% fillers would show two possible changes in recovery rates. The first one is that if M (TiO_2 1%) is less than the critical value at which the "cross-link" effect reaches the maximum effect, the recovery rates of SMCs with N wt% fillers (TiO_2 3%) would increase with the amount of fillers. But after N reaches the above critical value (TiO_2 3% can represent this case), the recovery rates of SMCs with N wt% fillers would reduce with increasing fillers (TiO_2 5%, TiO_2 7% and TiO_2 45%). On the other hand, if M is no less than the above critical value (TiO_2 3% and TiO_2 5%), the recovery rates of SMCs with N wt% fillers would decline with the increase of fillers (TiO_2 7% and TiO_2 45%).

Besides the piezoelectric effect of PZT / SMPU composites, more further

advantages of combining shape memory effect and piezoelectric effect is presented in chapter 4 as well. The film actuators made of PZT / SMPU composites are able to output 1 nm resolution displacements with positioning errors within ±5 nm in a common experimental environment because of the built in isolators, SMPU matrices, which have the capacity to reduce the disturbance from ambient noise according the microscopic actuation mechanism of PZT / SMPU composites. It implies a promising potential in nanopositioning because the cost could be reduced. Moreover, the displacements can be enlarged by deforming the PZT / SMPU composite films into designed shapes. The "U" type actuator and the "Z" type actuator, respectively, output displacements about 3.7 and 12.3 times more than those of their film actuators, while the positioning errors are still within ±5 nm. The actuators are able to be built into the integrated nanopositioning and even nanomachining devices due to the easiness of being shaped. Besides, Interfaces play a critical role in the effects of interfaces on relative permittivity and piezoelectric actuation behaviors. Poor interfaces destroy the actuation ability of PZT / SMPU composites because, microscopically, the output displacements of PZT particles are too few to pass through the free spaces and reach the SMPU matrices. Poor interfaces also reduce the relative permittivity on the account of the lower relative permittivity of the free spaces between PZT particles and SMPU matrices. But, in some case, this reduction in relative permittivity resulting from poor interfaces could estimate whether the interfaces of the composites are good or not.

Mechanical properties, including static and dynamic mechanical properties, are

exhibited in chapter 5. The PZT / SMPU composites all show strong enhancements in elastic moduli, yield stresses and storage moduli due to the good interfaces between PZT particles and SMPU matrices while PZT particles change the T_g very little even if the content of PZT particles are high. Because no chemical agents and surface modifications are induced in PZT /SMPU, the simple physical interfacial bonding would keep the T_g close to pristine SMPU.

The bending behaviors and energy harvesting application of PZT / SMPU composites with IDTs are studied in chapter 6. PZT 60% with IDTs shows the ability to generate bending displacements of several microns and produce continuous electric voltages under applied vibrations. also imply the promising potential for powering electric devices sustainably.

Ag / PZT / SMPU composites, which are PZT / SMPU composites added with silver nanoparticles, are synthesized in chapter 7 in order to increase the piezoelectric charge constants. The d_{33} of Ag / PZT / SMPU composites is at least 100% higher than that of PZT / SMPU composites with the same content of PZT particles, because the polarization is more efficient due to the larger electric field acting on PZT particles resulting from the higher local conductivity induced by silver nanoparticles.

In summary, PZT / SMPU composites are a kind of multifunctional composite materials. Based on the proven techniques of abroad usage of shape memory and piezoelectric materials, PZT / SMPU composites are easy to be applied in various areas. We will make efforts to develop more applications of these composites in the future.

List of Publications

1. **Hairong Chen**, Hong Xia, Yiping Qiu, Zhenzhen Xu, and Qing-Qing Ni, Smart Composites of Piezoelectric Particles and Shape Memory Polymers for Actuation and Nanopositioning, *Composites Science and Technology*, 2018, 163: 123-132.
2. **Hairong Chen**, Hong Xia and Qing-Qing Ni, Study on Material Performances of Lead Zirconate Titanate / Shape Memory Polyurethane Composites Combining Shape Memory and Piezoelectric Effect, *Composites Part A: Applied Science and Manufacturing*, 2018, 110: 183-189.
3. **Hairong Chen**, Hong Xia, Yiping Qiu and Qing-Qing Ni, Analyzing Effects of Interfaces on Recovery Rates of Shape Memory Composites from the Perspective of Molecular Motions, *Composites Science and Technology*, 2018, 163: 105-115.
4. Wanwan Liu, **Hairong Chen**, Mingqiao Ge, Qing-Qing Ni, and Qiang Gao, Electroactive shape memory composites with TiO 2 whiskers for switching an electrical circuit, *Materials and Design*, 2018, 143: 196-203.

Scientific Presentation

◆ **International conference**

1. **Hairong Chen**, Hong Xia, Qing-Qing Ni, Nano Composite Film With Two Smart Properties, 5th International Conference on Nano and Materials Science, 2017, San Diego, USA.
2. **Hairong Chen**, Hong Xia, Qing-Qing Ni, Functional Nanocomposites for Nanopositioning, Workshop of Advanced Composites, 2017, Ueda, Japan.

◆ **Domestic conference**

1. **Hairong Chen**, Hong Xia, Qing-Qing Ni, A New kind of Nanocomposite Combining Piezoelectricity and Shape-memory Property, 日本機械学会 北陸信越支部 第 53 期総会・講演会, 2016, Nagano.
2. **Hairong Chen**, Hong Xia, Qing-Qing Ni, A New Kind of Flexible Nanopositioning Actuator with Shape-Memory Property and Piezoelectricity, The 8th Japan Conference on Composite Materials, 2017, Tokyo.
3. **Hairong Chen**, Hong Xia, Qing-Qing Ni, Development of multi-functional composites with piezoelectric and shape memory effect, The 9th Japan Conference on Composite Materials, 2018, Kyoto.

Acknowledgements

It is my great pleasure to discuss and co-work with the persons who give me help and advice. Here, I want to give my most sincere gratitude to them.

First, I have to thank my supervisor Prof. Qing-Qing Ni. He gives me the most important supports for my research and living and also encourages me to do some innovate work. His advice helps me to overcome several key problems in my work and teaches me how to write a scientific paper in a strict manner. Thanks to his guidance, I can complete my PhD.

I also want to express my thanks to Prof. Toshiaki Natsuki for his help for my research and living. We always have good discussion related to my work and his advice is pretty helpful.

The researcher in our group, Hong Xia, gives me a lot of help and assistance in experiments and Japanese language learning. She helps me to make progress in my research quickly.

I want to express my gratitude to Interdisciplinary Graduate School of Science and Technology (Shinshu University) for the financial support, and the members of Ueda Rokumonsen Rotary Club especially my counselor, Hisao Nishizawa, for supplying my scholarship and helping me learn about more Japanese culture.

I want to thank the technicians in our group, Nakamura, and other technicians in our campus, especially Nishida, for their kindness and help.

The same to my kind friends in Japan: Ran Li, Juhong Yu, Xiaoyu Guan, Wanwan Liu, Zhe Yang, Fangtao Ruan, Zhong Wang, Xiangdong Xiong, Yongjie Yan, Jun Hong, Ke Ma, Jing Hui, Yinan Jing, Yajun Liu, Xiaojuan Li and Yican Huang. Thanks to their help for my living and PhD.

Finally, I need to thanks my parents. They always support me completely so that I have the opportunity to go all out for what I desired without any hesitation.